



CAPE PENINSULA
UNIVERSITY OF TECHNOLOGY



Faculty of Engineering

Fiber Optic Sensors Ensuring Structural Integrity

by

Frumence E. Utou

Under the supervision of

Prof. Bohua Sun

Prof. J. Gryzagoridis

**Thesis submitted in fulfillment of the requirement of the Doctor of Technology:
Mechanical Engineering (DTECHME) in the Faculty of Engineering at the Cape Peninsula
University of Technology.**

Cape Town, December 2005

Declaration of Originality

This thesis has been successfully carried out in the Faculty of Engineering, Department of Mechanical Engineering at the Cape Peninsula University of Technology (CPUT), South Africa.

I declare that this is essentially my own work, and any other work done by others is acknowledged.

I also declare that to the best of my knowledge, there are no copied materials or paraphrased form of work published by any other person, except where duly acknowledge in the text.

Specific acknowledgement from other Institutions and Organizations


Acknowledgement is made to the former Head of the Mechanical Engineering Department of University of Cape Town Prof J. Gryzagoridis, who gave me insight into optical technology during the six month training at UCT under the course content "Non-Destructive Test Methods".

The manufacturing of the standard specimen, tool and jigs were also done under his supervision.

I also give thanks for the advice and the supply of optical materials from companies such as Net-Connect, Communica, Thorlabs, AMT Composites, and RS components, who were extremely helpful.

My last thanks goes to the Department of Electrical Engineering at CPUT for providing me with specialized fusion equipment and assistance in fabricating of opto- electrical unit.

I, Frumence Ernest Utou , submit this thesis in fulfillment of the requirement for the award of the degree of Doctorate in Mechanical Engineering of the Cape Peninsula University of Technology. I declare that this is essentially my own work and that it has not been submitted in this or a similar form for a degree at any other University.



.....

Frumence E. Utou (Msc Mech. Eng. Kirovograd Institute of Machine Building Technology –Ukraine)

Cape Town, South Africa

December 2005

Acknowledgements

It is my obligation to present this acknowledgement to all individuals or group(s) who, in one way or another supported me in executing this work.

First and foremost, I thank His Almighty God for providing me with extra strength during the entire period of my studies. Thanks for standing on my side.

Secondly, my thanks goes to my Supervisor Prof. Dr B. Sun, who was the founder of the idea of my project, and who constantly took care of the administrative issues.

I would also like to thank my External Supervisor, Emeritus Prof.J.Gryzagoridis of UCT who was very close in supervision of my thesis. His inputs and critiques were remarkably appreciated. Thank you very much.

Thirdly, to the HOD–Mech. Eng. at CPUT Mr Keith Jacobs; and Departmental Secretary Ms Elvina Moosa, who constantly contributed their best towards my studies. I highly recognize their support.

Fourthly, my special thanks should go to my lovely wife Sarah P Utou and our daughters Irene and Lorine who always stood on my side and gave me encouragement throughout of my studies. Thank you and I love you.

To my Parents Ernest and Anastazia, you have been so wonderful to me. Thank you very much.

Fifthly, I would like to extend my vote of thanks to the administration of the CPUT former Deputy Vice Chancellor Prof. Brian Figaji; Prof.A. Staak, Dr Franks and Ms V.Tanga for providing warmth condition for my study and stay at CPUT.

To the Staff of Mechanical and Electrical Engineering Departments, especially Prof G.J.Oliver; Dr O.Philander; Mr P.Simelane, Mr Kassim, Mr I. Omar, Mr W.Kholifer, Ms Nicole Titus, Dr T. Khan, Mr Adonis , Mr Matasane and all that I haven't be able to mentioned them here

To my colleagues Mr A.Mtawa, and N.Mbonde for their closest support.

I would like to thank the National Research Foundation (NRF) of South Africa for providing me with financial support towards my studies and for facilitating my visit to the SPIE Conference in Perth -Australia.

Lastly, I would like to extend my gratitude to the Dar-es-salaam Institute of Technology (DIT), in Tanzania especially to Prof J.W. Kondoro the Principal, and Dr R.Masika the Director of Studies for allowing me to pursue my studies and who supported me both morally and materially.

As it is not possible to mention each and everyone who contributed towards this work, therefore,I would like to apologize for any one whose name hasn't been mentioned, but I thank them all.

Dedication

To my children

“... My aspiration is to see you achieve the best of your ambitions through learning. May this work be your reference to your future dreams...”

Abstract

Among the issues that are taken into consideration for many years by Engineers and Technologists is the integrity of the servicing elements in structures and mechanisms. It is a documented phenomenon that after a certain period of time, in service, engineering components tend to change their original state, and begin to develop faults and defects. This includes the original shape distortion due to effects such as bending, twisting, and cracks. The above-sited effects may be caused by the sudden or accumulative effect of overloading, thermal shocks, corrosion etc, which eventually lead to malfunction of these engineering components.

The occurrence of the cracks may be as a result of stress variation in excess of different or similar materials; thermal shocks, vibration, etc.

A system of structural health monitoring using optical fiber sensors to track down a crack occurrence and its propagation is considered to be a promising method in warning of catastrophic events.

Taking advantage of optical fibers' properties and behavior, such as easy interaction with other materials, small size, low weight, corrosion resistance, geometrical flexibility and an inherent immunity to electromagnetic interference, there is potential in adopting the Fiber Optic Sensors (FOS) for structural health monitoring systems.

Structural integrity does not confine itself to crack detection only. For example there are many instances where unwanted or excessive displacement may occur.

Optical fibers play an important role in proximity sensing as evidenced in the literature [49] to [54] and available commercial systems.

However it is felt that FOS displacement sensors may suffer in measurement accuracy due to in situ conditions. For example the texture and reflectivity of the sensor's target surface, the angularity that may exist between the sensor's tip and target etc.

The work performed on the above-mentioned aspects has been mainly of experimental nature and has been benchmarked by presenting it in an International Conference and its publication in an International Journal.[55]

In summary, the information that this work has yielded is useful as guidelines or criteria to experimenters attempting measurement of displacement, motion or speed using FOS's.

This thesis in addition to pertinent information regarding FOS's for displacement measurement mainly presents the successful development of a crack sensing system utilizing three optical fibers laid equally spaced across a host specimens' intended crack propagation path.

The sensor was fabricated and tested under laboratory conditions at the Bellville Campus of the Cape Peninsula University of Technology.

The three optical fibers were placed about 2 mm apart and firmly supported on both ends, thus being subjected to elongation during the crack opening.

As the crack propagated along the x-axis, at the same time it opened along the y-axis, which coincided with the elongation of the optical fiber.

As a result of the fibers elongation, the light passing through the fibers, suffered a loss of intensity.

The experimental results, shows that the crack propagates within 0.8 mm away from each fiber optic sensor before the effect of the crack opening begins to elongate the fiber and affect the intensity of the light being transmitted through it.

We were able to develop the governing sensor equation, which basically consists of the physical parameters, which affect the change of state of both the host specimen and the optical fibers.

In summary, the sensor equation has integrated parameters such as stress intensity factor, host specimen geometry, optical fiber gauge length, strain and diameter etc.

Experiments validate the sensor equation.

Contents

Declaration of Originality	i
Acknowledgments	iii
Dedication	v
Abstract	vi
Contents	ix
List of Figures	xv
List of Tables	xix
Chapter 1 Smart Structure Materials and Device	1
1.1 Introduction	1
1.2 Crack propagation in material	2
1.3 Aim and Scope of Investigation	3
1.4 Overview of Fiber Optical Sensors	4
1.4.1 Sensor classification	6
1.4.2 FOS Basic components	7

1.4.2.1	Illumination Sources	7
1.4.2.2	Detectors or Receivers	8
1.4.3	Fiber optic sensor for crack propagation measurement	9
1.4.4	Fiber optic sensors for displacement measurement	10
1.5	Integrity and material compatibility for embedded sensors	10
Chapter 2	Crack propagation theory and mechanisms	13
2.1	Introduction	13
2.1.1	Modes of crack propagation	14
2.1.2	Singular stress and displacement fields	16
2.1.3	Crack Propagation Using an Open Mode I Type	17
2.1.4	Plane stress versus plane strain	18
2.1.5	Plastic zone shape and size	20
2.1.6	Crack tip opening displacement (CTOD)	22
2.1.7	Crack length value	24
2.1.8	Stress concentration	26
2.1.9	Energy release rate	27
2.2	Optical fiber mechanical deformation response under extension	29
2.2.1	Introduction	29
2.2.2	Variability of individual optical fiber strength	31
2.3	Mechanical deformation of the embedded Optical Fiber within a host material under tension loading.	32
2.3.1	Introduction	32
2.4	Mechanism of interaction between optic fibers with host material	34
2.4.1	Mechanisms of optical fiber attenuation due to micro and macro bending	35
2.5	Change of optical light intensity influenced by physical deformation on the optical fiber.	35
2.5.1	Introduction	35

2.6 Mechanisms of optical fiber attenuation due to micro-extension	41
Chapter 3 Designs and Manufacture of Effective Terminals for the Transmission of the Optical Beam	44
3.1 Introduction	44
3.2 Preparation Introduction on and manufacture of the fiber optic connections	45
3.2.1 Equipments and tools for termination	45
3.3 Fabrication of optical fiber with connectors	48
3.3.1 Inspection and observation of optical fiber end surfaces through macroscopic magnifications.	49
3.3.2 Terminating and splicing of optical fibers	51
Chapter 4. Fiber Optic Sensor for Crack Propagation and Detection	52
4.1 Introduction	52
4.2 Sensor system component specification and design aspects	53
4.2.1 Photo diode laser source.	53
4.2.2 Photo detectors	55
4.2.3 Design of the crack propagation detection instrument	57
4.2.4 Fiber optical cables	57
4.2.5 Signal output, amplification and displays	58
4.3 Component requirements in setting-up the integrated crack detection system	59
4.3.1 Performance analysis and assessment of the crack detection warning system	61
Chapter 5 Experimental Results of Crack Propagation due to Mechanical Deformation	63
5.1 Introduction	63
5.1.1 Assumption	64

5.2 Test requirements	64
5.2.1 Compact Specimen Configuration	65
5.2.2 Specimen Selection and manufacturing	65
5.3 Experimental Procedure	66
5.3.1 Apparatus	67
5.3.2 Analytical Procedure	68
5.4 Test results and discussion	70
5.4.1 Fatigue Test	70
5.4.2 Determining the values of crack tip size $r_p(\theta)$ under the plane stress conditions	75
5.4.3 Determining the value of crack tip size $r_p(\theta)$ under plane strain conditions	75
5.4.4 Determining the value of crack opening displacement (δ)	77
5.4.5 Determining the crack length value (a_i)	78
Chapter 6. The Effect of Optical Fiber Elongation to its Performance as a Light Conduit	83
6.1 Introduction	83
6.1.1 Influencing factors on the optical fiber output	84
6.1.2 Experimental Procedures	84
6.2 Preparing a failure warning sensor	86
6.3 Discussion	88
6.3.1 Optical fiber extension due to loading	88
6.3.2 Voltage output (light intensity) versus optical fiber elongation	88
6.3.3 Voltage output of the OF due to tensile loading	88
6.3.4 Interdependence of the applied tensile load, light intensity output and elongation of the OF	89
6.3.5 Determination of the light intensity output value relative to the crack opening	89
6.4 Experimental results	90

Chapter 7	Influencing Parameters in Formulating the Sensor Equation	99
7.1	Introduction	99
7.2	The area common around the deformation of the work piece and the embedded fiber (Mechanical).	100
7.3	Mechano-opto relations	101
7.4	Development of the sensor equation	101
7.4.1	Formulation of the sensor equation.	101
7.4.1.1	Deformation of the optical fiber.	101
7.4.1.2	Relationship between the host specimen deformation and the optical fiber elongation.	103
7.4.1.3	Relationship between optical fiber diameter change and the optical output power.	104
7.4.2	Output power transmitted in the optical fiber versus its deformation	106
7.4.3	Development of the OF crack detection sensor model	106
7.5.	Discussion on theoretical –experimental comparison results	109
7.5.1	Comparison of Theoretical- Experimental results for the individual OF due to Load versus elongation.	109
7.5.2	Comparison of Theoretical- Experimental results for the fatigue loading versus CTOD.	109
7.5.3	Comparison results of the theoretical- experimental between the optical fiber elongation and crack opening of the host specimen	109
7.5.4	Comparison of Experimental- Theoretical of voltage output against elongation	110
7.5.5	Comparison of Experimental- Theoretical Voltage output against tensile loading for “stand alone” OF	110
7.6	Validation of Experimental- Theoretical results	111

Chapter 8	116
8.0 The Performance of Fiber Optics as Displacement Sensors	116
8.1 Introduction	116
8.2 Experiments	117
8.2.1 Calibration procedure	118
8.2.2 Reflectivity	119
8.2.3 The effect of thickness of transparent material	120
8.2.4 The effect of slight angularity on a moving target	122
8.2.5 The effect of angularity (target to sensor inclination)	124
Chapter 9 Conclusions and Recommendation	125
9.1 Introductory comments.	125
9.1.1 Experimental outcomes	127
9.1.1.1 Fatigue test on a stand-alone host specimen	127
9.1.1.2 Experimental results on the embedded optical fiber with host specimen	127
9.1.1.3 Experiments on the performance of the FOS as a displacement sensor	127
9.2 Theoretical approach	128
9.3 Recommendation	128
References	129
Appendix A Crack Propagation using Fatigue Test	135
Appendix B List of Auxiliary Apparatus, and Tools employed for the Sensor Making. as discussed in chapters 3 and 4	142
Appendix C Opto-Electrical circuitry	144

List of figures

Chapter 1

- Figure 1.1:** Illustration of “confusing” signal to the photo detector. 5
- Figure 1.2:** Schematic diagram of FOS system for deformation detection set up 8
- Figure 1.3:** Embedded of optical fibers into the test piece 9
- Figure 1.4:** Scheme of filler shape (a) and reinforcements (b, c and d) for composite Materials 11
- Figure 1.5:** Schematic representation of coated optical fiber embedded in an infinitely large isotropic composite host 12

Chapter 2

- Figure 2.1:** A crack length $2a$ in infinite plate subjected to a uniform stress σ_1 , radius ρ at near infinity 14
- Figure 2.2:** Three Modes of crack tip deformation 15
- Figure 2.3:** Stress component at crack tip in an elastic material for the mode 16
- Figure 2.4:** crack dimensional changes influenced by plane strain. 21
- Figure 2.5:** Stress influence on crack dimensional changes. 22
- Figure 2.6:** Compliance Correction for Specimen Rotation 25

Figure 2.7: Features of the participation of the optical fiber strain on crack propagation	30
Figure 2.8: Load transfer in a fiber /matrix composite material and variation of tensile stress (σ_f) in the fiber and interfacial shear stress (τ) with distance along the interface.	33
Figure 2.9: (a) Ray path transmission in a step-index fiber (b) Step index profile	36
Figure 2.10: (a): Effect of the light configuration on a multimode graded index and their path as measured by the NA	38
Figure 2.10 (b): Micro-bend effects of the light beam cause little diffraction	38
Figure 2.10 (c): Macro-bend effects of the light beam causes large amount of diffraction	38
Figure 2.11: Absorption and scattering as function of wavelength. (reprinted from AMP Inc.)	39
Figure 2.12: Propagation modes of optical light beam on a fiber at deformation due to tension.	41
 Chapter 3	
Figure 3.1(a): Tools and accessories for splicing and terminating process	
(b): X100 magnification microscope for the ferrule ends observation	47
 Figure 3.2: Schematic of the OF on Compact Fusion Device aligned for the fusion process.	48
 Figure 3.3: Optical fiber cable end product before polishing	48
Figure 3.4: Samples of the 100X magnification of the end ferrule.	50
 Chapter 4	
Figure 4.1: Schematic layout of the test specimen with a two-fiber sensor, for example, and respective light beam emitting and receiving components	54

Figure 4.2: CPDS set up during the mechanical deformation test. 61

Chapter 5

Figure 5.1: Specimen Geometry according to ASTM International Standards E 399-81, E-1820 and BS 7448 66

Figure 5.2: Schematic diagram of Specimen mounted on the Universal Fatigue Test Machine. 68

Figure 5.3: Load-displacement record for K_{Ic} determination 69

Figure 5.4: Critical fracture toughness G_c (or K_{Ic}^2) versus plate thickness B 70

Figure 5.5: Mode I fracture of a standard compact specimen before and post fatigue induced fracture. 72

Figure 5.6: Typical Load –Displacement curve as obtained from the fatigue tests 73

Figure 5.7: Effect of incline θ angle caused by the compliance Load to the plastic zone size r_p 77

Figure 5.8: Stress distribution related to the crack tip size under plane stress conditions 77

Figure 5.9: Yield stress and plane strain as they affect the value of plastic zone size 80

Figure 5.10: Influence of load on the COD and the crack length. 81

Figure 5.11: The effect of released energy rate to the crack growth 81

Figure 5.12: Values of Compressive and tensile loading for a number of cycles (N). 82

Figures 5.13: Tension/compression under fatigue loading 82

Chapter 6

Figure 6.1: Schematic diagram of the gripping of optical fiber during the elongation test. 85

Figure.6.2: Schematic diagram of optical fibers embedded within the test

specimen.	87
Figure 6.3: Typical results from individual optical fiber elongation under tension	90
Figure 6.4: Decrease of light intensity through the optical fiber versus fiber elongation	91
Figure 6.5: Voltage drop manifesting light intensity through the OF versus applied load in stretching the OF.	92
Figure 6.6: Light intensity through the OF as a function of tensile load and fiber elongation	93
Figure 6.7: Fiber light intensity output versus crack opening	94
Figure 6.8: Fiber light intensity output versus crack travel	95
Figure 6.9: Relationship between the crack travel and opening for the positions I, II; and III of the optical fibers.	96
Figure 6.10: Schematic diagram indicating the crack travel trend versus crack opening for the three positioned optical fiber.	97
Figure 6.11: Overall-crack travel versus crack opening	98
 Chapter 7	
Figure 7.1: Area of sensing	100
Figure 7.2: Optical fiber crack detection sensor model (CDSM)	107
Figure 7.3: Theoretical optical power versus light, input-output ratio	108
Figure 7.4 Theoretical/experimental comparison results for the Load versus elongation of the OF	111
Figure 7.5: Theoretical-experimental comparison results for the fatigue load versus crack opening	112
Figure 7.6: Theoretical-experimental comparison of OF elongation versus CTOD	113
Figure 7.7: Comparison results of theoretical- experimental for the light intensity out put versus the optical fiber extension	114
Figure 7.8 Optical fiber diameter change due to tensile loading and fiber elongation (as from equations (7.3)).	115

List of Tables

Chapter 2

Table 2.1: Selected mechanical properties of the S_iO_2 fiber.	31
Table 2.2 : Typical properties of various Fiber Types	40

Chapter 4

Table 4.1: Characteristics of the fiber optic LED model OPF 692	55
Table 4.2: Characteristics of the PIN Photo diode model OPF 792	55
Table 4.3: Characteristics of the high-speed photo detector model SUV7-4.2.2	56
Table 4.4: General characteristics of the CPDI-01	57
Table 4.5: Fiber optic characteristics and design profiles	58

Chapter 5

Table 5.1: Specimen Dimensions	66
Table 5.2: Tabulated values for the ratio $\frac{a}{W}$	71
Table 5.3. Summary of experimental results from the standard fatigue test.	74
Table 5.4: Summary table representing the experimental values pertaining to the crack plastic zone, size, and stress and strain.	78

Chapter 1

1.0 Fiber Optic Sensors and Devices

1.1 Introduction

In the past few decades, we have been witnessing drastic changes in materials technology. Latest developments such as the use of materials with embedded devices have changed the way of thinking in modern design and manufacturing. The incorporated devices such as sensors, actuators and the algorithms into the structure, form a system, which is called a Smart Materials System (SMS) or Smart Structure System (SSS) and sometimes, the Intelligent Response Materials (IRM) [1], [2].

All the above terminologies express an extra ordinary performance of such structures. The system has the ability to feel, think, act, correct and inform the status of the structure, by monitoring its health condition. With the aid of the adaptive devices, it is possible to measure parameters such as displacement, speed, vibration, noise and others. In the advanced systems, the change of physical or mechanical quantities can be detected, measured and later used as feedback information to provide remote or self-correction modes.

The importance of ensuring the monitoring of the health condition of the structure is due to the current demand in safety for various applications in the

fields such as aerospace and aviation industries; military applications, machine tools; construction industries; mining and many others. Most of the above-mentioned areas have specific structures, which experience dynamic and/or static loadings in specific points, which cause mechanical deformation and later failure during their lifetime of service.

1.2 Crack propagation in material

Crack propagation in materials is considered as a mechanical fault that needs attention. This is due to the consequences in case of failure during service, which may be catastrophic. The crack may develop as a result of internal stresses caused by mechanical deformation, and other influencing factors such as temperature variation, degradation due to corrosion and other changes within the environmental conditions.

On the other hand, some researchers consider the crack to serve a positive role as a stress relief mechanism (residual stress) [3], [4].

Mechanical deformation from fatigue loading has been taken as a major influencing factor in crack creation and propagation.

B.S Jeon et al [5], have shown that for composite structures, the analysis on crack propagation is complex mainly due to the non-homogeneous properties within the layers of composite materials. Delaminating of layers in composites is regarded as a contributing factor that can cause further complication in analysing the behaviour of crack development.

Due to the fact that cracks sometimes develop from the inner side (core) of the material, it is difficult to detect or visualize their occurrence, and in most cases to locate their propagation path. The tendency of crack growth may be developed in a form of mixed kind of behaviour such as multi-directional propagation, shape and configuration; therefore it is difficult to predict its critical mode failure in real time [6].

Crack occurrence and its orientation can be detected by several existing non-destructive tests (NDT) such as magnetic particles detection, acoustic emission, ultrasonic, electronic speckle pattern interferometric (ESPI), as well

as physical visualization [7]. In the years 2001 and 2002, researchers such as Z.L Yang, G R Liu, K Y Lam, Y.C Liang and C Hwu, have been attempting to detect crack orientation using strain measured by optical fibers [8]; [9].

In 1992, D. Rees, W. Chiu and R. Jones published their work titled Numerical study of crack monitoring in patched structures, using piezoelectric sensors [10].

In 2002, Yoji Okabe, Shigeki Yashiro, Tatsuro Kosaka, and Nabuo Takeda published their work Detection of transverse cracks in CFRP composites using embedded fiber Bragg grating sensors [11].

1.3 Aims and Scope of this work.

In this work, the main focus has been on detecting the onset of a crack and its propagation characteristics. The research aims to develop a system that can detect and give warning of the presence of a crack. In the process of detecting and monitoring crack propagation, the optical fibers are embedded (as part of the host material) to form a sensor. Upon detection, the sensor is able to capture the state of material change and produce a signal, which informs on the status of the crack presence, in real time. This work incorporates numerous activities including the preparation of the specimens; mechanical tests; embedding technique; fiber optic and opto-electronic knowledge; mechanics of materials as well as other non-destructive test methods for verifications, such as electronic speckle pattern interferometry (ESPI), magnetic particles detection, acoustic emission ultra sonic method, and physical observations.

The following activities were planned for execution to form a system reliable in providing sensing ability within the structure due to the action of deformation and crack initiation and detection of its propagation on the structure, using the Fiber Optical Sensor (FOS) technology.

a) To build models of embedded critical components using materials such as wood, metal, composites and alloys, which can accommodate the Fibre Optical Sensor to form the Smart Structure System.

In this regard, the selection of the material to model the critical components is regarded a prime factor. Proper selection of the embedding process is also an important factor.

The technique of preparing the fiber optical terminals, the design and development of sensory network is considered to be a crucial aspect.

b) To investigate the influence of the presence of the optical fibres in the composite materials. Factors such as mechanical strain, loading, and localization of fibers are investigated.

In performing this work, reference is made to the existing theories of mechanics and properties of materials and results from various previously reported investigations.

c) To verify the practicability and workability of the crack detection warning system (CDWS) by using the available equipments in our laboratory. On this aspect, much attention focuses on the performance of all the incorporated equipments so as to have a functioning system.

d) To develop the existing theories and results from various experiments, into viable application.

Selection of the manufacturing process will obviously be based on the review of the previously employed manufacturing process.

e) Work consists of various experiments to verify the effect of parameters that might possibly have an effect on the accuracy of commercial FOS displacement or deformation measurement equipment.

1.4 Overview of Fiber Optic Sensors

Optical fiber, being a physical medium, when subjected to a perturbation, it experiences geometrical and optical changes to a larger or lesser extent depending upon the nature and the magnitude of the perturbation. In communication applications one tries to minimize any perturbations so that signal transmission and reception is reliable. On the other hand in fiber optic

sensing, the response to external influence is deliberately enhanced so that the resulting change in optical radiation can be used as a measure of the external perturbation. In communication, the signal passing through a fiber is already modulated, while in sensing, the fiber acts as a modulator. It also serves as a transducer and converts perturbations like temperature, stress, strain, rotation or electric and magnetic currents into a corresponding change in the optical radiation. Since light is characterized by amplitude (intensity), phase, frequency and polarization, any one or more of these parameters may undergo a change. The usefulness of the fiber optic sensor therefore depends upon the magnitude of these changes and our ability to measure and quantify the same reliably and accurately.

For example, consider a fiber optic sensor that could be used as a proximity-measuring device. Figure 1.1 illustrates that our ability to measure accurately depends very much in recognizing the physical system and parameters that affect it. In this case the fact that there are two reflections captured by the photo detector should be indicative of a dubious result.

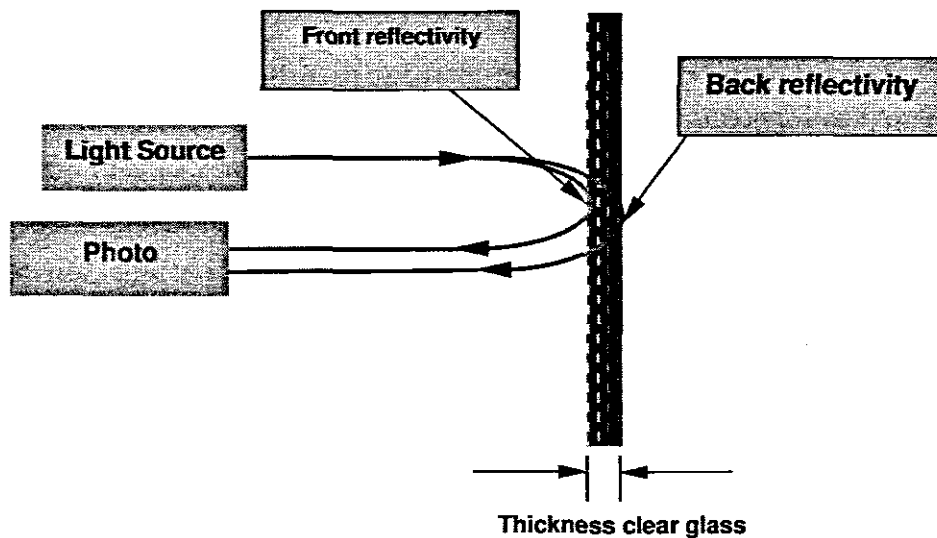


Figure 1.1: Illustration of “confusing” signal to the photo detector.

Some of the advantages of fiber optic sensors are that they are free from electro-magnetic Induction (EMI), have wide bandwidth capability, compactable, possess geometrical versatility and are fairly economical. In

general, FOS is characterized by high sensitivity when compared to other types of sensors. They are passive in nature due to the dielectric construction. Specially prepared fibers can withstand high temperature and other harsh environments. In telemetry and remote sensing applications it is possible to use a segment of the fiber as a sensor gauge while a long length of the same or another fiber can convey the information to a remote station. Deployment of distributed and array sensors covering extensive structures and their geographical locations are also feasible. Many signal processing devices (splitter, combiner, multiplexer, filter, delay line etc.) can also be made of fiber elements thus enabling the realization of an all-fiber measuring system. Recently photonic circuits (Integrated Optics) have been proposed as a single chip optical device or signal-processing element, which enables miniaturization, batch production, economy and enhanced capabilities. [20].

1.4.1 Sensor classification

The sensors are classified depending on their range of applications as discussed below.

Based on the modulation and demodulation process, a sensor can be called as intensity (amplitude), a phase, a frequency, or a polarization sensor. Since detection of phase or frequency in optics calls for interferometric techniques, the latter are also termed as interferometric sensors. From the detection point of view the interferometric technique implies heterodyne detection/coherent detection. On the other hand intensity sensors are basically incoherent in nature. Intensity or incoherent sensors are simple in construction, while coherent detection (interferometric) sensors are more complex in design but offer better sensitivity and resolution [21].

Fiber optic sensors can also be classified on the basis of their application: physical sensors (e.g. measurement of temperature, stress, etc.); chemical sensors (e.g. measurement of pH content, gas analysis, spectroscopic studies, etc.); bio-medical sensors (inserted via catheters or endoscopes which measure blood flow, glucose content and so on). Both the intensity types and the interferometric types of sensors can be considered in any of the

above applications.

Extrinsic or intrinsic sensors are another classification scheme. In the former, sensing takes place in a region outside of the fiber and the fiber essentially serves as a conduit for the to-and-fro transmission of light to the sensing region *efficiently and in a desired form*. On the other hand, in an intrinsic sensor one or more of the physical properties of the fiber undergo a change as mentioned above [22].

1.4.2 FOS Basic components

A fiber optic sensor in general will consist of a source of light, a length of sensing (and transmission) fiber, a photodetector, demodulator, processing and display optics and the required electronics.

1.4.2.1 Illumination Sources:

In FOS semiconductor based light sources offer the best advantages in terms of size, cost, power consumption and reliability. Light emitting diodes (LEDs) and laser diodes (LDs) are the type of sources used with FOS although in laboratory experiments the He-Ne laser is frequently used. Features of LED include very low coherence length, broad spectral width, low sensitivity to back reflected light and high reliability. They are useful in intensity type of sensors only. LDs on the other hand exhibit high coherence, narrow linewidth and high optical output power, all of which are essential in interferometric sensors. Single mode diode lasers are made using distributed feedback or external cavity schemes. High performance Mach-Zehnder and Fabry-Perot type sensors need single mode lasers. LDs in general are susceptible to reflected (feedback) light and temperature changes. They are also less reliable and more expensive. Coupling of light from source to fiber is an important aspect and may call for special optical devices. The use of a pigtailed source can alleviate this problem but such devices are expensive.

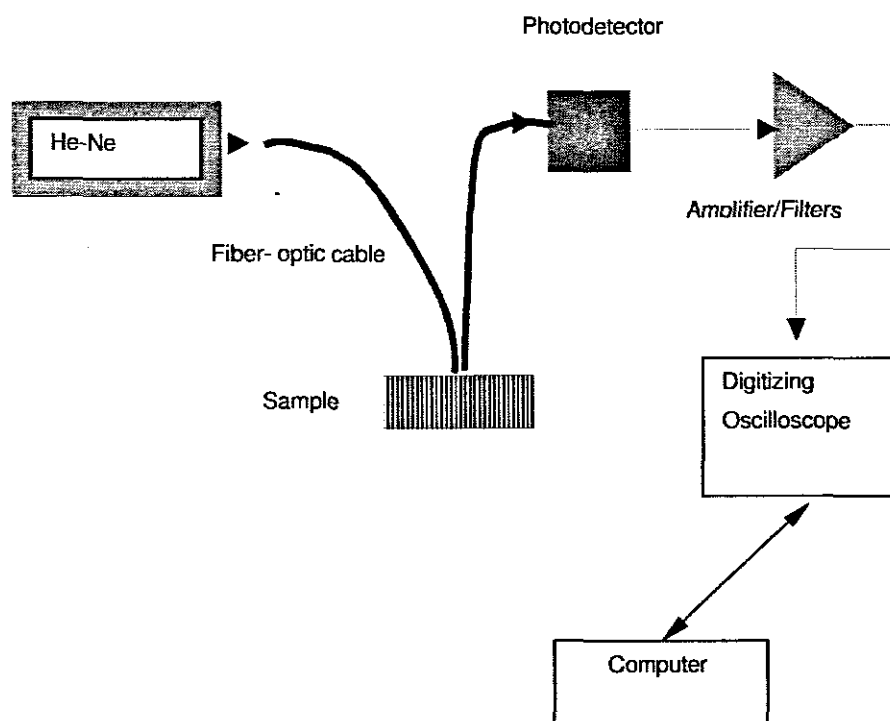


Figure 1.2: Schematic diagram of FOS system for deformation detection set up

1.4.2.2 Detectors or Receivers:

Semiconductor photodiodes (PDs) and avalanche photodiodes (APDs) are the most suitable detectors in FOS. APDs can sense low light levels due to the inherent gain because of avalanche multiplication, but need large supply voltage typically about 100 V. The various noise mechanisms associated with the detector and electronic circuitry limit their detection capability. Thermal and shot noise are two main noise sources and need to be minimized for good sensor performance. Detector response varies as a function of wavelength. Silicon PD is good for visible and near IR wavelengths. Generally there is no

bandwidth limitation due to the detector as such, although the associated electronic circuits can pose some limitations.

1.4.3 Fiber optic sensor for crack propagation measurement.

As it was stated earlier in this chapter optical fiber sensors can play the role of ensuring the health condition of structures, including the detection of crack propagation.

Fiber optical sensor measurement of the crack propagation system consists of a typical set-up as indicated in the figure 1.2 above. The test piece is equipped with three optical fibers embedded at 1mm depth, and about 2mm apart. In order for the embedded optical fiber to withstand the tension during the pull out action, a strong bonding agent is applied. The embedded fibers on the specimen are shown on figure 1.3 below.

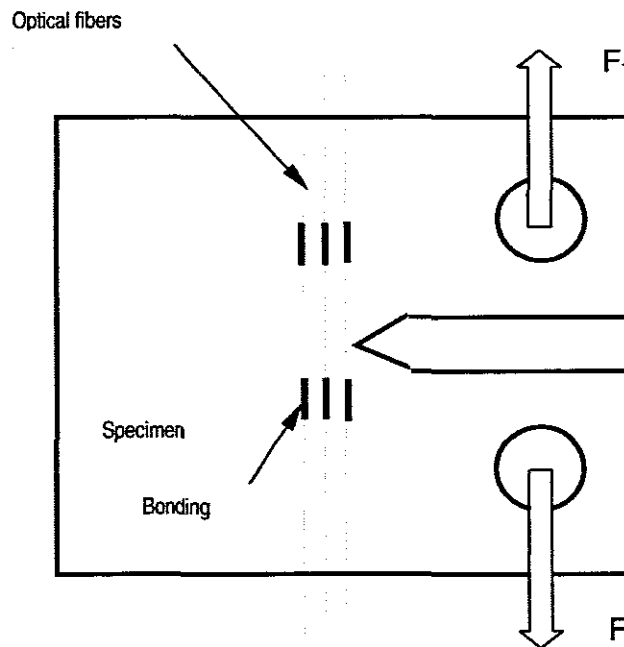


Figure 1.3: Embedded optical fibers into the test piece

1.4.4 Fiber optic sensors for displacement measurement

In some instances unwanted deflection or displacements may occur without crack formation and propagation. In such a case, using the principles of phase shifting due to variation in reflection, a fiber optic displacement sensor can be used, *affording the possibility of measuring slight deformations that might affect structural integrity.*

The work reported here consists of various experiments that were conducted in order to ascertain the effect of parameters that might affect the accuracy of FOS displacement measurements using a commercially available system. It is expected that texture and reflectivity of the surface will affect the sensor's input of the reflecting surface. Similarly the angular orientation of the sensor with respect to the normal to the surface or the induced angularity by a curving displacement of the surface relative to the sensor are parameters that might affect the sensor's accuracy.

1.5 Integrity and material compatibility for embedded sensors

A composite material is a mixture or combination of two or more micro constituents that differ in form and chemical composition and are essentially insoluble in each other.

A composite material has superiority to all other structure materials in specific strength and other properties such as light weight, toughness and suitability for bonding with other materials. In order to acquire optimum properties in composite materials, their components are chosen to have sharply different, but complementary properties. The composite materials consist of the matrix and fillers, essential components for binding, shaping and strengthening. The components above determine the operating characteristics such as the working temperatures, fatigue strength, resistance to environmental effects, density and specific strength.

Studies have shown that embedding a fiber optic sensor in composite materials, can be easily accommodated. The orientation of the fiber in the

composite materials facilitates the process. Figure 1.6 shows the 3-D arrangement of the fiber orientation and its reinforcement. Studies by Udd E [14] and David Krohn [15] reveal the extensive work on material's compatibility during embedment of fiber optics in composite fibers.

strength This work has gone as far as identifying individual fiber optical properties by determining their tensile as well as their extension/bending effects during the period of service [16]. The study also investigated the bonding mechanism, which is associated with the stress field in the effective area of the composite material. Since the optical fiber is meant to serve as a strain gauge, it is important to know the extent of strain on the composite before and at the state of embedment.

The optical fiber is to be laid in an isotropic material. Both the optical fiber and its coating are assumed to have isotropic mechanical properties and the bonding between the three materials is assumed to be perfect. Figure 1.6 represents the coordinate system of the embedded fiber into the composite

.The long axis of the fiber is parallel to the x_3 -axis, where r_f and r_j are the radii of the fiber and the coating or cladding respectively.

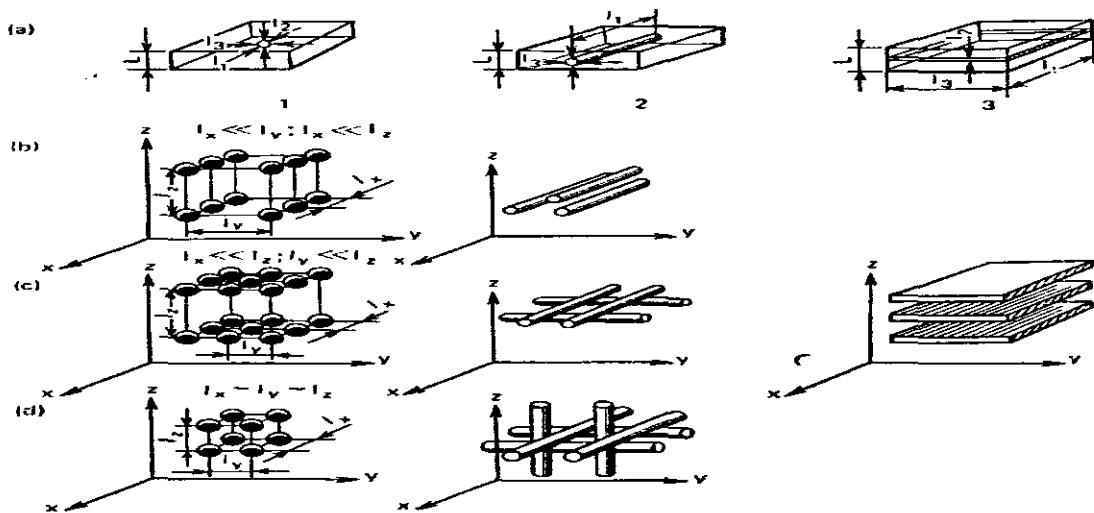


Figure 1.4: Scheme of filler shape (a) and reinforcements (b, c and d) for composite materials.

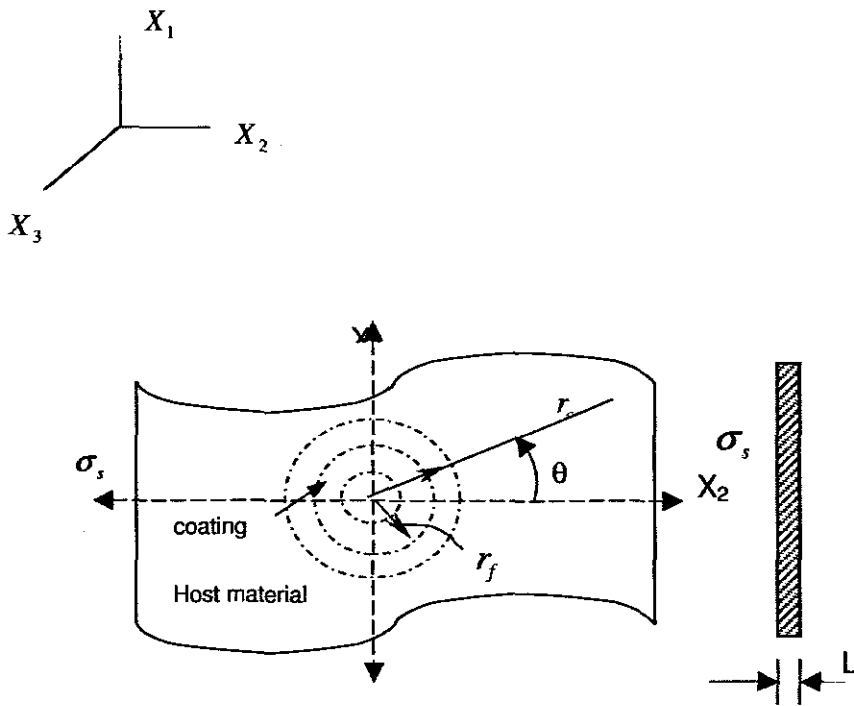


Figure 1.5: Schematic representation of coated optical fiber embedded in an infinitely large isotropic composite host.

The composite material is subjected to an axial traction σ_s , which can be considered in a cylindrical coordinate system along the radius r_c and on the cross section at its width L .

The interaction mechanism of the system can be expressed by the Navier Stokes equation in polar coordinates, which gives us a general solution for the interfacial continuity condition at any given loading [18].

Chapter 2

2.0 Crack Propagation Versus Optical Light Beam Theory Mechanisms

2.1. Introduction

Phenomena of crack propagation have been studied some decades ago. Within linear-elastic fracture mechanics theory, for example, Griffith [24] sought to explain why the observed strength of materials is considerably less than the theoretical strength based on forces between atoms. In his conclusion, he observed that real materials must contain small defects and cracks, which reduce their strength. The developed cracks cause stress concentrations but they cannot be allowed for by calculation of a linear-elastic stress concentration factor K_t . This is because an elliptical defect, which has its stress concentration factor, defined by equation 2.1

$$K_t = 1 + 2 \left(\frac{a}{b} \right) \quad (2.1)$$

Where $2a$ and $2b$ are width and height of the crack respectively.

In the above assumption, it follows that as $b \rightarrow 0$ the defect becomes a crack and subsequently $K_t \rightarrow \infty$, which suggests that a material with a crack would

not be able to withstand any applied forces.

However Griffith postulated other wise; that a crack can only become unstable if there is an incremental of crack growth due to the stored energy. More ever, the stored energy can be released to create the new crack surface.

The analytical approach to fracture has been refined by Irwin [25] who inter related other parameters such as stress distribution in the vicinity of a crack tip, nominal stress applied to the structure and the size, shape and orientation of the crack.

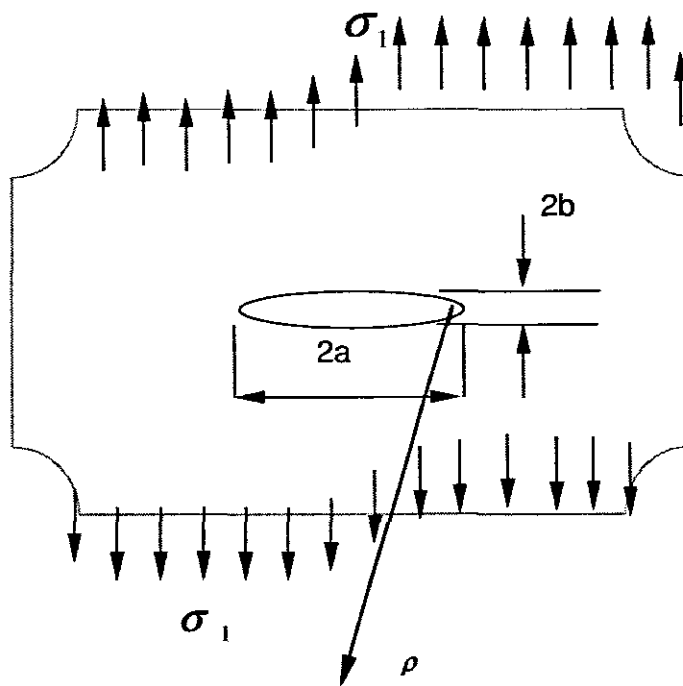


Figure 2.1: A crack length $2a$ in infinite plate subjected to a uniform stress σ_1 , radius ρ at near infinity

2.1.1 Modes of crack propagation

Crack as a separation of surfaces relative to the plane x-y-z may occur in three modes depending on the type of loading as well as the direction of the force action. The three independent kinematics movements of the upper and lower surfaces of these modes are considered as superposition that causes deformation. The following diagrams represent the three modes.

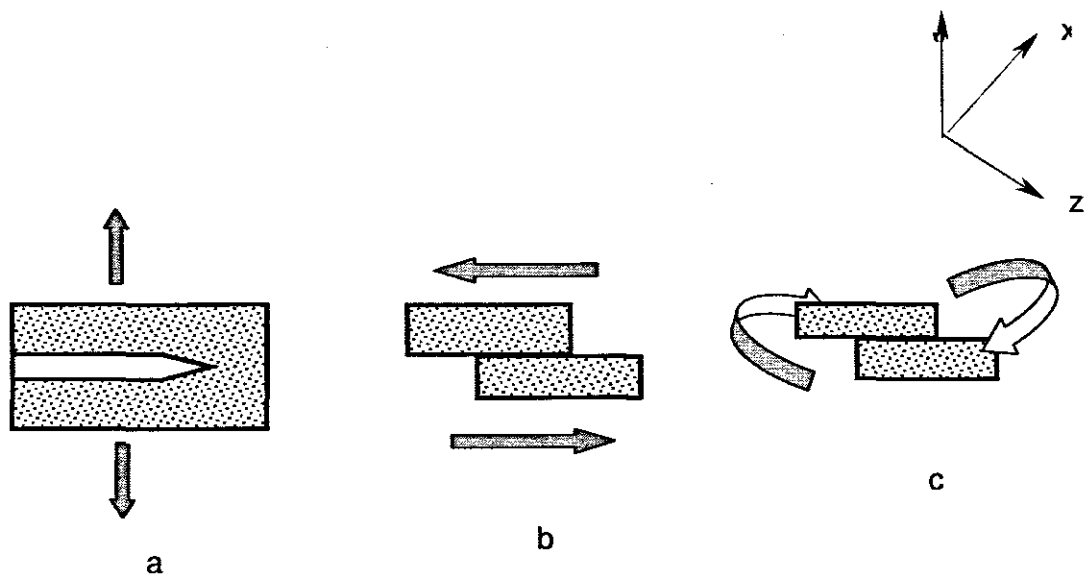


Figure 2.2: Three Modes of crack tip deformation

(a) Opening Mode I (b) Shearing Mode II (c) Tearing Mode III

Irwin developed the studies for the three modes of stresses in the vicinity of a sharp crack in a large plate, and further conceptualized the study of stress for brittle materials for the three modes of crack tip deformation.

The first mode, which is the opening mode, possesses the elastic stress distribution at the crack tip in the symmetry about the $(x-y)$ and $(y-z)$ planes as shown on figure 2.2 (a).

The second mode (shearing) on figure 2.2 (b) represents the type of crack surface sliding relative to each other in a symmetrical manner with respect to the plane $(x-y)$ and skew-symmetrically with respect to the plane $(x-z)$. The third tearing mode on figure 2.2 (c) has a crack surfaces slide relative to each other skew-symmetrically with respect to both planes $(x-y)$ and $(x-z)$. For the tearing mode of crack, the in-plane displacements u and v are zero, but it has a displacement of function w of the x and y coordinates.

2.1.2 Singular stress and displacement

Singular stress and displacement fields near the crack tip are very important components to study during the fracture process, due to their role in stress determining the crack properties. The stress component σ_{ij} and the rectangular components of the displacement U_i are presented in figure 2.3 below, while their corresponding equations are shown in (2.2); (2.5) and (2.7) respectively.

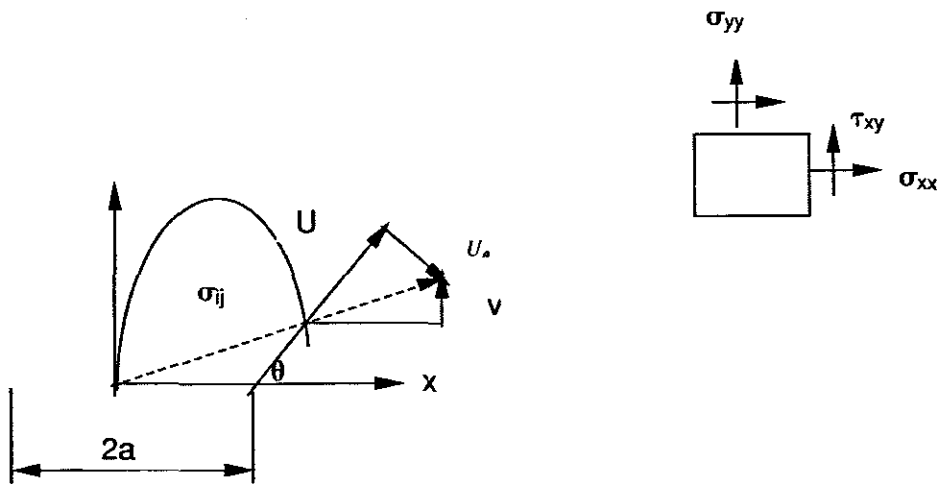


Figure 2.3: Stress component at crack tip in an elastic material for the mode I

The stress intensity factor Mode I is given by

$$\begin{aligned}\sigma_{xx} &= \frac{K_I}{(2\pi r)^{\frac{1}{2}}} \cos\left(\frac{\theta}{2}\right) \left[1 - \sin\left(\frac{\theta}{2}\right) \sin\left(\frac{3\theta}{2}\right) \right] \\ \sigma_{yy} &= \frac{K_I}{(2\pi r)^{\frac{1}{2}}} \cos\left(\frac{\theta}{2}\right) \left[1 + \sin\left(\frac{\theta}{2}\right) \sin\left(\frac{3\theta}{2}\right) \right] \\ \tau_{xy} &= \frac{K_I}{(2\pi r)^{\frac{1}{2}}} \sin\left(\frac{\theta}{2}\right) \cos\left(\frac{\theta}{2}\right) \cos\left(\frac{3\theta}{2}\right)\end{aligned}\quad (2.2)$$

In case of Plane strain

$$\sigma_z = \frac{2\nu K_I}{(2\pi r)^{\frac{1}{2}}} \cos\left(\frac{\theta}{2}\right) \quad (2.3)$$

For the principal singular stresses

$$\sigma_1 = \frac{K_I}{\sqrt{2\pi r}} \cos\frac{\theta}{2} \left(1 + \sin\frac{\theta}{2}\right) \quad (2.4)$$

$$\sigma_2 = \frac{K_I}{\sqrt{2\pi r}} \cos\frac{\theta}{2} \left(1 - \sin\frac{\theta}{2}\right) \quad (2.5)$$

The value of the vertical displacement is calculated using the formula

$$u_{\max} = \frac{k+1}{4\mu} \alpha_i \quad (2.6)$$

Where $k=3-4\nu$ for plane strain and $k=(3-\nu)/(1+\nu)$ for the generalized plane stress.

2.1.3 Crack Propagation Using an Open Mode I Type

Although it is assumed that crack propagation may be associated with combination of more than one mode, it is important in this work to identify the suitable type, which is more viable for our experimental expectations. The Mode I type was considered to be an ideal one, since it has supporting equipment to facilitate the testing, especially regarding fatigue tests. The fatigue-testing machine provides a perpendicular line of force action to the intended crack propagation path. It is also assumed that the number of cycles generated will tend to propagate the initiated crack along the x direction in Mode I type, at a given time function. In chapter three, we further investigate

the effect of the embedded optical fiber perpendicular to the intended crack propagation. The embedded optical fiber must at least acquire some properties the same as the host material in the cause of its deformation. This might be a very important condition that will lead to the practical use of the optical fibers to build sensors for detecting the crack initiation and propagation. The orientation of the optical fiber embedded into the host structure, (across the crack propagation path), possibly provides information for the mechanical deformation for both the optical fiber and host material. In that sense, the measure of any change along the crack-propagating path can be detected by the deformed optical fiber cable, which will provide a signal to the event, possibly due to the change of light intensity. The characteristics of the optical fiber are considered to have the mechanical properties, which permit it to withstand deformation under a certain reasonable extension. The optical fiber has been proved to have reasonably high enough elastic limit when subjected to a tensile force.

2.1.4 Plane Stress versus Plane Strain

Most of the classical solutions in fracture mechanics reduce the problem of Linear Elastic Mechanics Fracture (LEMF) to two dimensions. In this case, at least one of the principal stresses or strain is assumed to be zero.

Consider a cracked plate with thickness B subjected in a plane loading as shown on figure 2.4.

Without the crack, the material would be in a state of plane stress. However, material near the crack tip is loaded to higher stresses than the remaining surrounding area. Because of the large stress, normal to the crack plane, the crack tip material tries to contract in the x and z directions, but it is prevented from doing so by the surrounding material. This constrain causes a triaxial state of stress near the crack tip. For $r_0 \ll B$, plane strain condition exists in the interior of the plate. Material on the plate surface is in a state of plane stress, because there are no stresses normal to the free surface [28].

The through thickness variation of stress and strain in the z direction for $r_0 \ll B$, plain strain condition is shown in figure 2.4. It implies that, at the plate

surface, $\sigma_z = 0$ and ε_z is at its maximum (absolute value). At the mid plane ($z = 0$) as plane strain condition exist

For the condition that $\sigma_z = \nu(\sigma_x + \sigma_y)$ we are assume that $r_0 \gg r_y$. The region near the plate surface where the stress state is neither plane stress or plane strain lays at the elastic-plastic boundary and it depends on the plastic zone size relative to the plate thickness.

Plane strain conditions exists at the boundary if the plastic zone is small compared to the thickness, but the stress of the same order as the thickness Nakamura and Parks [29] in their work defined the boundary, which demarcates the plastic zone at mid thickness, computed from a three-dimensional elastic-plastic finite element analysis, of which the elastic boundary is defined at $\sigma_e = \sigma_{Y_s}$.

As the relations of $\left(\frac{K_I}{\sigma Y_s}\right)^2$ increase relative to thickness, the plastic zone grows as one might expect. We have therefore the plane stress and plane strain equations for Mode I defined below.

Plane stress

$$\sigma = \frac{K_I}{Y(\pi a)^2} \quad (2.7)$$

and

$$K_I = Y\sigma(\pi a)^2 \quad (2.8)$$

Plane strain

$$\sigma_z = \frac{2\nu K_I}{(2\pi r)^{\frac{1}{2}}} \cos\left(\frac{\theta}{2}\right) \quad (2.9)$$

For the plane stress, the $\sigma_z = 0$

Where σ is a characteristic stress

Plane stress and Plane Strain can also be determined by using the tensor method.

For the plane stress

$$\sigma = \begin{bmatrix} \sigma_{xx} & \sigma_{xy} & 0 \\ \sigma_{xy} & \sigma_{yy} & 0 \\ 0 & 0 & 0 \end{bmatrix} \quad \varepsilon = \begin{bmatrix} \varepsilon_{xx} & \varepsilon_{xy} & 0 \\ \varepsilon_{xy} & \varepsilon_{yy} & 0 \\ 0 & 0 & \varepsilon_{zz} \end{bmatrix} \quad (2.10)$$

Here $\varepsilon_{xx} \neq 0$

For the plane strain

$$\sigma_{xx} = \begin{bmatrix} \sigma_{xx} & \sigma_{xy} & 0 \\ \sigma_{xy} & \sigma_{yy} & 0 \\ 0 & 0 & \sigma_{zz} \end{bmatrix} \quad \varepsilon = \begin{bmatrix} \varepsilon_{xx} & \varepsilon_{xy} & 0 \\ \varepsilon_{xy} & \varepsilon_{yy} & 0 \\ 0 & 0 & 0 \end{bmatrix} \quad (2.11)$$

2.1.5 Plastic zone shape and size.

The singular stress fields represent the asymptotic fields as the distance from the crack tip to zero and their applicability is confined to a very small region around the tip. The estimated extent of the plastic zone attending the crack tip can be obtained by determining the locus of points where the elastic stress field satisfies the yield criterion. More over, the plastic zone can be determined from an elastic –plastic analysis of the stress field around the crack tip. By introducing the expression for the singular principal stress (2.4) into the Von Mises yield criterion, we obtain the following expression for the radius of the plastic zone for plane stress.

$$r_p(\theta) = \frac{1}{4\pi} \left(\frac{K_I}{\sigma_{YS}} \right)^2 \left[\frac{3}{2} \sin^2 \theta + 1 + \cos \theta \right] \quad (2.12)$$

for the plane strain

$$r_p(\theta) = \frac{1}{4\pi} \left(\frac{K_I}{\sigma_{YS}} \right)^2 \left[\frac{3}{2} \sin^2 \theta + (1 - 2\nu)^2 + (1 + \cos \theta) \right] \quad (2.13)$$

Where σ_Y is the yield stress

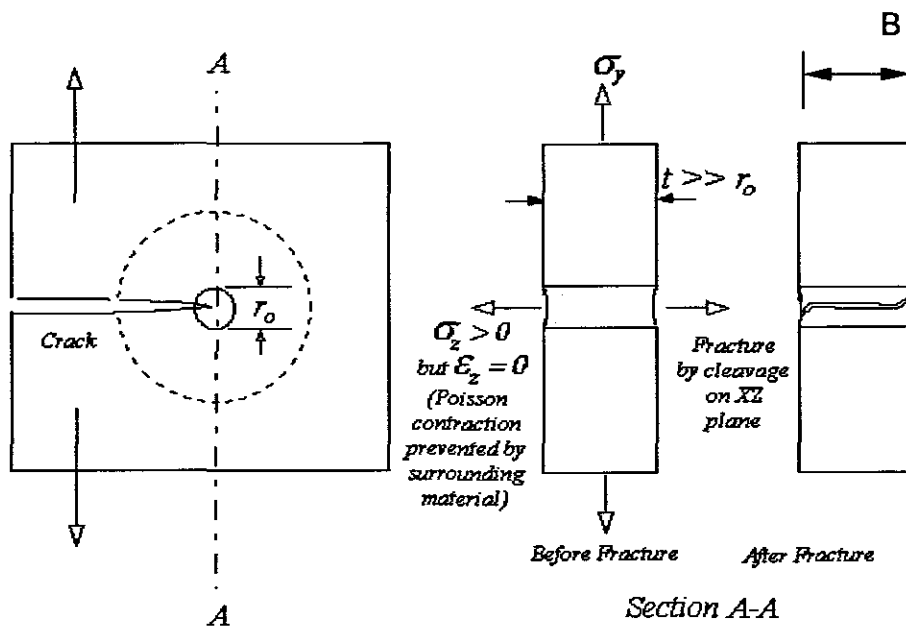


Figure 2.4: crack dimensional changes influenced by plane strain.

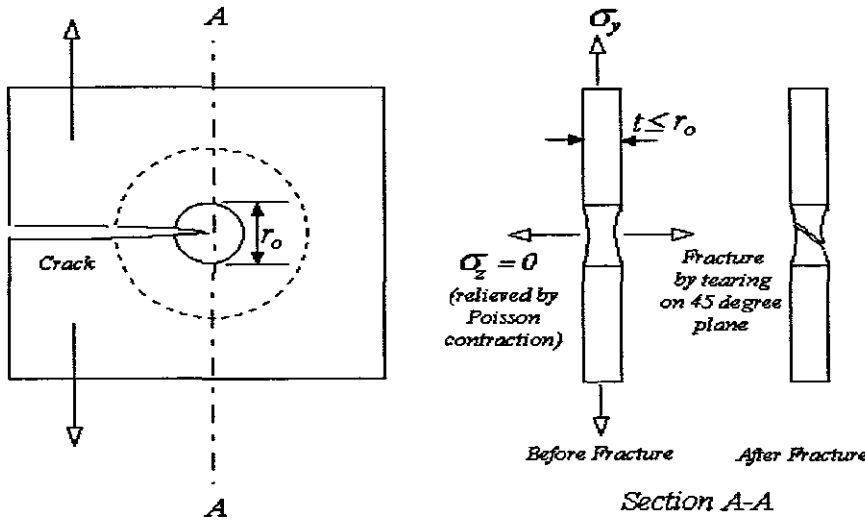


Figure 2.5: Stress influence on crack dimensional changes.

The extent of the plastic zone along the crack axis ($\theta=0$) for the plane stress is given by

$$r_p(0) = \frac{1}{2\pi} \left(\frac{K_I}{\sigma_Y} \right)^2 \tag{2.14}$$

and for the plane strain

$$r_p(0) = \frac{1}{18\pi} \left(\frac{K_I}{\sigma_Y} \right)^2 \tag{2.15}$$

2.1.6 Crack tip opening displacement (CTOD)

The crack tip opening displacement (CTOD) according to Wells [30], occurs when the crack faces have moved apart prior to fracture. Gradually, the degree of crack blunting increases in proportion to the toughness of the

material. This observation led Wells to propose the opening at the crack tip as a measure of fracture toughness known as crack tip opening displacement (CTOD). Thus, we can estimate CTOD by solving for the displacement at the physical crack tip assuming the effective crack tip length of $a+r_y$ is given by

$$u_y = \frac{k+1}{2\mu} K_I \sqrt{\frac{r_y}{2\pi}} \quad (2.16)$$

Using the Irwin model for plastic zone correction for plane stress

$$r_y = \frac{1}{2\pi} \left(\frac{K_I}{\sigma_{Ys}} \right)^2 \quad (2.17)$$

Substituting eq. (2.13) into eq. (2.12) the CTOD is given by

$$\delta = 2u_y = \frac{4}{\pi} \frac{K_I^2}{\sigma_{Ys} E} \quad (2.18)$$

The standard CTOD can be obtained from the geometrical configuration after the test by using the method below.

$$\delta = \delta_e + \delta_p$$

Where δ_e is CTOD due to elasticity and δ_p is CTOD due to plasticity

$$\delta_e = \frac{K_I^2 (1-\nu^2)}{2\sigma_Y E} \quad \text{and} \quad \delta_p = \frac{V_p r b}{r b + a + z} \quad (2.19)$$

Where V_p the plastic component is measured displacement, while r, b, a and z are the geometrical configuration of a crack. Further, the expression is

obtained from the reduced values of geometrical configuration of

$$\delta_p = \frac{V_p r b}{r b + a + z} \text{ to } \delta_p = \frac{0.4(W-a)V_p}{0.4W + 0.6a} \quad (2.20)$$

$$\text{Therefore } \delta = \frac{K_I^2 (1-\nu^2)}{2\sigma_y E} + \frac{0.4(W-a)V_p}{0.4W + 0.6a} \quad (2.21)$$

Equation (2.21) is called a standard equation for the crack opening displacement (CTOD)

Alternatively, the CTOD can be obtained by relating the energy release rate defined as

$$\delta = \frac{4}{\pi} \frac{G}{\sigma_{YS}} \quad (2.22)$$

2.1.7 Crack length value

The crack length value or crack size is a linear measure of principal planar dimension of a crack. The measure is commonly used in calculating the quantities descriptive of stress and displacement fields, and sometimes is termed as crack depth

For the single specimen test method, using an elastic compliance technique on compact specimen with crack opening displacements measured on the load line, the crack length is given as follows:

$$\frac{a}{W} = [1.000196 - 4.06319u + 11.242u^2 - 106.043u^3 + 464.335u^4 - 650.677u^5] \quad (2.23)$$

where:

$$u = \frac{1}{[B_e E C_{c(i)}]^2 + 1} \quad (2.24)$$

and $C_{c(i)}$ = Specimen load line crack opening elastic compliance $\left(\frac{\Delta v}{\Delta P}\right)$ on unloading / reloading sequence corrected for rotation as in expression (2.23) below

In order to account for crack opening displacement in Compact Tension (CT) specimen, the crack length estimation shall be corrected for rotation as indicated on figure 2.6

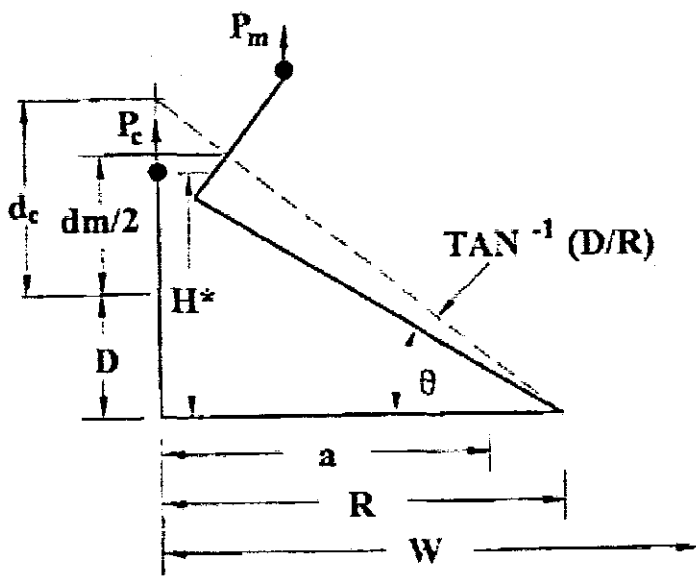


Figure 2.6: Compliance Correction for Specimen Rotation

$$C_{c(i)} = \frac{C_i}{\left[\frac{H^*}{R} \sin \theta_i\right] \left[\frac{D}{R} \sin \theta_i - \cos \theta_i\right]} \quad (2.25)$$

where

C_i = measured specimen elastic compliance (at load line)

H^* = initial half span of the load points (center of the pin holes)

R = radius of rotation of the crack centerline, $(W+a)/2$ where a is updated crack length

D = one half of the initial distance between the displacement measurement points

θ = angle of rotation of a rigid body element about the unbroken midsection line,

$$\theta = \sin^{-1} \left[\frac{\left(\frac{d_m}{2} + D \right)}{\left(D^2 + R^2 \right)^{\frac{1}{2}}} \right] - \tan^{-1} \left(\frac{D}{R} \right) \quad (2.26)$$

d_m = total measured load line displacement

2.1.8 Stress concentration

Stress concentration, according to Griffith [26], indicates that the discrepancy between the actual strength of the brittle materials and theoretical estimates is due to flaws in materials.

However, fracture cannot occur unless the stress at the atomic level exceeds the cohesive strength of the material. Thus, flaws must lower the global strength by magnifying the stress locally. A rough estimate for remote stress failure is given by

$$\sigma_f = \left(\frac{E\gamma_s}{4a} \right)^{\frac{1}{2}} \quad (2.27)$$

and for local stress concentration at the tip of a sharp crack is given by

$$\sigma_A = 2\sigma \sqrt{\frac{a}{x_0}} \quad (2.28)$$

an approximation of stress concentration due to notch which is not elliptical except at the tip is given by

$$\sigma_A = 2\sigma \sqrt{\frac{a}{\rho}} \quad (2.29)$$

Further, Griffith's equation was modified by Irwin and Orowan to form equation

$$\sigma_f = \left(\frac{2E(\gamma_s + \gamma_p)}{\pi a} \right)^{\frac{1}{2}} \quad (2.30)$$

Where γ_p is the plastic work per unit area of surface created, and is typically much larger than γ_s ; and γ_s is the total energy of material.

2.1.9 Energy release rate

In 1956, Irwin [27] proposed an energy approach for fracture that is essentially equivalent to Griffith's mode. Energy release rate G is a measure of energy available for an increment of crack extension.

$$G = \frac{\partial \Pi}{\partial A} \quad (2.29)$$

For a through crack with length $2a$ in an infinite body of a unit thickness (fig 2.1) the surface energy U_s , stored in material due to the formation of crack is given by

$$U_s = (2a)2\gamma \quad (2.30)$$

$$\gamma = \frac{1}{2}G$$

Where γ = surface energy per unit area, G is energy absorbed per unit area of crack, which will be half the new surface area, resulting in

$$U_s = 2aG \quad (2.31)$$

The elastic energy U_e , released by the formation of crack is given by

$$U_e = \frac{1}{2} \int_a^{\Delta} \sigma(x) \Delta(x, a) dx \quad (2.32)$$

Where $\sigma(x)$ is the stress distribution in the vicinity of the crack, and $\Delta(x, a)$

is the vertical opening of the crack, while for the same crack length $2a$ in the infinite

plate the elastic energy is given by

$$U_e = \frac{\pi \sigma^2 a^2}{E} k \quad (2.33)$$

Where $k = (1 - \nu^2)$ for plane strain and ν is Poisson's ratio.

We can observe from the above that the surface energy that is developed in the material is increasingly proportional to crack length, where as the energy released by the formation of the crack increases with crack length.

Therefore the total energy that is released is the summation of the surface energy U_s and the elastic energy U_e .

However, from Griffith's proposal, the threshold between a stable crack and unstable crack occurs when an increment of crack growth causes more energy to be released than that which can be absorbed in the material. Thus the critical condition is when $\frac{\partial u}{\partial a} = 0$, and since the critical crack length a_c is defined from equations (2.31) and (2.33), we obtain

$$\frac{d}{da} (2aG_c - \frac{\pi^2 a^2}{E} k) = 0 \quad (2.34)$$

from above

$$2G_c = \frac{2\pi\sigma^2}{E} k \quad (2.35)$$

Which reduces to

$$\left(\frac{EG_c}{1 - \nu^2} \right)^{\frac{1}{2}} = \sigma (\pi a)^{\frac{1}{2}} \quad (2.36)$$

and

$$(EG_c)^{\frac{1}{2}} = \sigma(\pi a)^{\frac{1}{2}} = K \quad (2.37)$$

Where G_c is Griffith surface energy and K is the stress intensity factor.

2.2 Optical Fiber mechanical deformation response under extension loading

2.2.1 Introduction

Consider a single optical fiber that is embedded across the propagated crack. Due to the reason that the optical fiber is supported at two fixed end points as shown in figure 2.6, then the opening of the crack on the host material influences the embedded optical fiber to extend towards the direction of the crack opening. The optical fiber is stripped from its cladding material to allow the inner diameter (core) to be bonded together with the host materials. The assumption here is that the effect of the bending of the fiber in this action is negligible while the effect of extension is assumed dominant.

By considering and relating the same characteristics of a single fiber in a composite material, then the prediction of mechanical properties such as applied loads, related stresses, and elastic constants can be applied similarly to the optical fiber.

Consider figure 2.6, we have a single fiber, which can represent a number of fibers that can be laid parallel across the direction of crack propagation, while the load P is assumed to act normal to them. Knowing the mechanical response of the single fiber, it is then possible to predict the sequence response of other fibers as question of a function of time.

Similarly, we assume that the load acts axially to the single fiber, to cause strain. Using the above assumption we conduct the tensile test for the individual fiber in order to relate the result obtained when it is embedded with a host material.

The fiber component in this case undergoes the longitudinal elongation Δl . Thus the strain is given by

$$\varepsilon_f = \frac{\Delta l}{l} \quad (2.38)$$

where ε_f is the strain in the fiber in the longitudinal direction.

However in the situation of embedment, the equation becomes

$$\varepsilon_f = \varepsilon_h = \frac{\Delta l}{l} \quad (2.39)$$

Where ε_h is the strain of the host material or the crack opening δ at the point in question.

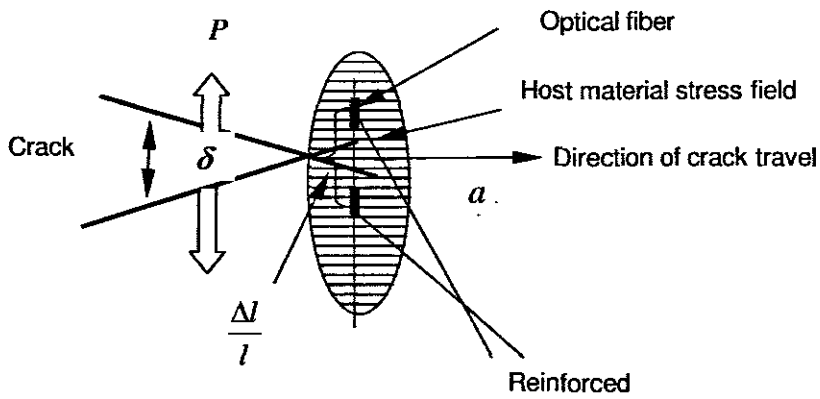


Figure 2.7: Features of the participation of the optical fiber strain on crack propagation

According to W.Voigt [28] both the host and the optical fiber are elastic and related to the stress σ in the two components of the strain ε_i by Young Modulus E , thus

$$\sigma_f = E_f \varepsilon_{cl} \quad \text{and} \quad \sigma_m = E_m \varepsilon_{cl} \quad (2.40)$$

Now, again by considering the single optical fiber, we have

$P_c = P_f$, where P_f is the load acting along the fiber direction.

Let the cross section area of the fiber A_f , we have

$$P_f = \sigma_f \cdot A_f \quad (2.41)$$

and from the equations (2.37) and (2.28), we have

$$\sigma_f \cdot A_f = (E_f \cdot A_f) \epsilon_{cl} \quad (2.42)$$

2.2.2 Variability of individual optical fiber strength

Most of the optical fibers are considered brittle. The single mode optical fiber is primarily made of silica (SiO_2) and it has properties as summarize on table 2.1 below.

The concern on the mechanical properties of the optical fiber such as tensile strength, impact resistance, flexing and bending becomes a part of the tradeoffs during the embedment with a host material, as well as its important role of minimizing attenuation. This is because; the amount of stress surrounding the embedded optical fiber will determine how effective the optical fiber is, in its role of detecting the changes around the surface. More ever, in this study, we consider the fiber to take part of carrying the distributed stress and manifesting it as a change of intensity of the light beam that it carries.

Properties	Manufacture values
Tensile strength at yield (MP_a)	56
Tensile elongation at yield (%)	3
Tensile strength at break (%)	>50
Tensile modulus (MP_a)	2470
Flex strength at 3.5 % strain (MP_a)	72
Notched Izod impact strength kJ/m^2	5.5
Transition or melting point $^{\circ}C$	1175
Thermal conductivity $^{\circ}C$	1.38
Thermal expansion coefficient $10^{-6} \text{ }^{\circ}C^{-1}$	0.55
Young Modulus (GP_a)	70-100

Density (g/cm^3)	2.20
----------------------	------

Table 2.1: Selected mechanical properties of the S_iO_2 fiber.

2.3 Mechanical deformation of the embedded Optical Fiber within a host material under tension loading.

2.3.1 Introduction

Aveston et al. (1971) and Budiansky et al. (1986) stated that in the linear elastic fracture mechanics (LEFM) of the crack propagation for the composite materials, the crack involves a steady matrix cracking normal to the fiber. In the wake of the crack, the Aveston model assumes that the bridging fibers can slip against the matrix in friction. The extent of fiber slippage depends on the frictional shear strength of the fiber-matrix interface. On the other hand, the Budiansky model allows for conditions of no slipping, frictional slipping and debonding. For both models, a balance of energy is written across the steadily moving crack front, for the prediction of the critical stress, which is independent of the initial crack length.

Consider a fiber of length l embedded in a matrix subjected to a strain as indicated in figure 2.8. Assuming that: (a) there exists a perfect bonding between the fiber and matrix (i.e. that there is no sliding between them) and (b) that the poisson ratios of the fiber and matrix are equal, which implies an absence of the transverse stresses when the load is applied along the fiber direction.

Let the displacement of a point at a distance x from one extremity of a fiber be u in the presence of a fiber and v in the absence of a fiber. Then we can write the transfer of load from matrix to the fiber

$$\frac{dP_f}{dx} = B(u - v) \quad (2.43)$$

Where P_f is the load on the fiber and B is a constant that depends on the

geometric arrangements of fibers, matrix type, moduli of the fiber and matrix. Differentiating equation (2.43) we get

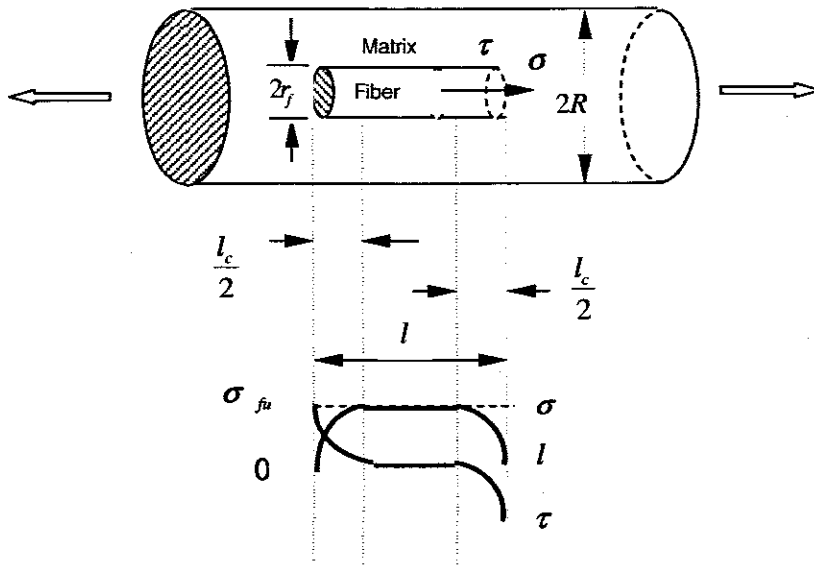


Figure 2.8: Load transfer in a fiber /matrix composite material and variation of tensile stress (σ_f) in the fiber and interfacial shear stress (τ) with distance along the interface.

$$\frac{d^2 P_f}{dx^2} = B \left(\frac{du}{dx} - \frac{dv}{dx} \right) \quad (2.44)$$

We have

$$\frac{du}{dx} = \text{Strain in fiber} = \frac{P_f}{E_f A_f}$$

$\frac{dv}{dx}$ = strain in the matrix away from the fiber, which is equal to the imposed

strain, e .

Equation (2.43) can be rewritten

$$\frac{d^2 P_f}{dx^2} = B \left(\frac{P_f}{A_f E_f} - e \right) \quad (2.45)$$

Which has the solution of

$$P_f = E_f A_f e + S \sinh \beta x + T \cosh \beta x \quad (2.46)$$

Where

$$\beta = \left(\frac{B}{A_f E_f} \right)^{\frac{1}{2}}$$

Using the following boundary condition to evaluate the constants S and T :

$$P_f = 0 \text{ at } x=0 \text{ and } x=l$$

we obtain the following result

$$P_f = E_f A_f e \left[1 - \frac{\cosh \beta(l/2 - x)}{\cosh(\beta l/2)} \right] \text{ For } 0 < x < l/2 \quad (2.48)$$

or

$$\sigma_f = \frac{P_f}{A_f} = E_f e \left[1 - \frac{\cosh \beta(l/2 - x)}{\cosh(\beta l/2)} \right] \text{ for } 0 < x < l/2 \quad (2.49)$$

The maximum possible values of strain in the optic fiber are the imposed strain e , and thus the maximum stress is $(eE)_f$. Therefore, if we have a long enough fiber, the stress in the optical fiber will increase from the two ends to maximum value, $\sigma_{fu} = (Ee)_f$

2.4 Mechanism of interaction between optic fibers with host material.

In the introductory chapter, we discussed the use of a composite material as a best candidate to host the optical fiber. Due to the fact that a large amount of

research work has been done specifically on composite materials, we find it appropriate to extend the findings also to simple materials such as steel and wood.

2.4.1 Mechanisms of optical fiber attenuation due to micro and macro bending

Small amount of a fiber bend causes a small amount of light loss through the wall of the fiber. The amount of bend of the optical fiber must have a limit, beyond, which further bending, may cause the fiber to break. The bend of the fiber may be caused by its presence in various conditions of application, as well as its environmental surroundings.

Figures 2.9 (a, b, c) show different geometrical configurations with respect to the numerical aperture (NA) of the transmission path of the light beam within the section of the core fiber bound by the cladding.

The efficiency of a single mode fiber optic in transmitting and reflecting a light beam is depends on numerous influencing factors. The experiment on the possible parameters affecting the performance of the fiber optics was conducted in depth. For example, we have seen that the voltage output domain versus displacement has a direct dependence to reflectivity and sensitivity of the sensor probe. It is through this experiment that we are able to relate other external factors such as thickness of the transparent materials as well as the angle of the reflectivity. The above may virtually affect the measurement of proximity and their allied parameters. However, such effects may be considered as external factors, as they depend less on the geometrical size and construction of the optical fiber.

2.5 Change of optical light intensity influenced by physical deformation on the optical fiber.

2.5.1 Introduction

An optical fiber is a structure that is designed to carry and guide light over a

distance, or path, that is not necessarily straight. Optical fibers accomplish light confinement by the total internal reflection of the light source that is coupled into the end of the fiber. Figure 2.8 shows a typical optical fiber as a solid cylinder, an adequate model to illustrate the light propagation within it.

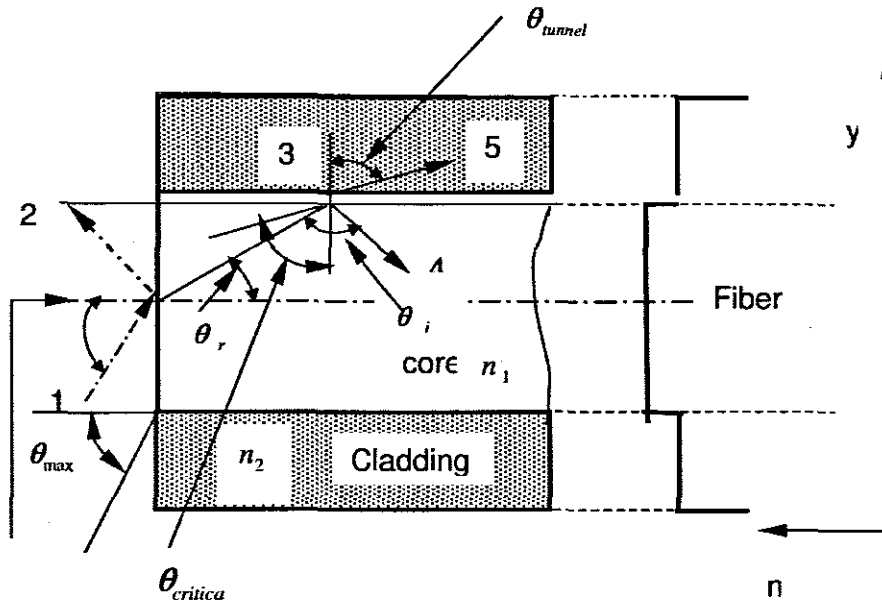


Figure 2.9: (a) Ray path transmission in a step-index fiber (b) Step index profile.

A possible meridional path in a step-index fiber, is one in which the core region has a refractive index n_1 and the cladding region refractive index n_2 lower than n_1 . The incoming ray strikes the core-air boundary at angle θ_0 to the fiber axis. The air has a refractive index n_0 , less than that of either the core or cladding. This ray is, in part, reflected from the core interface with the same angle of θ_0 and, in part, transmitted into the core. The transmitted part of the original ray is refracted at the core surface and continues at an angle θ_r relative to the centerline of the fiber. The ray continues on to strike the core-cladding interface at point 3 and will be totally reflected to point 4, if θ_i is greater than a critical angle $\theta_{critical}$. At the θ_{max} , which is the entering ray, the

total internal reflection at the core cladding occurs. If an entering ray strikes the core –cladding interface at an angle smaller than $\theta_{critical}$, it will be only partially reflected at the cladding, giving rise to a refracted ray in the cladding at point 5. The refracted ray initially propagates at an angle θ_{tunnel} within the cladding. This ray is only loosely bound within the fiber structure and eventually escapes from the fiber.

The ray angles in figure 2.8 are related through the laws of reflection and refraction.

The transmission theory is governed by the mathematical expression, known as Snell's Law of

$$n_o \sin \theta_o = n_i \sin \theta_i \quad (2.50)$$

where n_o is the index of refraction of the medium in which a beam light ray is initially traveling

n_i is the index refraction of the second medium

θ_o is the angle between the incident ray and normal to the interface

θ_i is the angle between the refracted ray and the normal to the interface.

The sine of the critical angle is determined by

$$\sin \theta_{critical} = \frac{n_2}{n_1} \quad (2.51)$$

From this relation ship, the numerical aperture (NA) value is defined by

$$NA = \sin \theta_{max} \quad (2.52)$$

Where

$$\sin \theta_{max} = (n_1^2 - n_2^2)^{1/2} \quad (2.53)$$

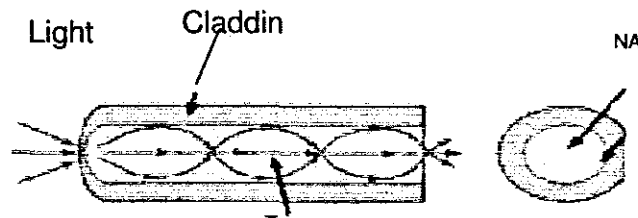


Figure 2.10: (a): Effect of the light configuration on a multimode graded index and their path as measured by the NA

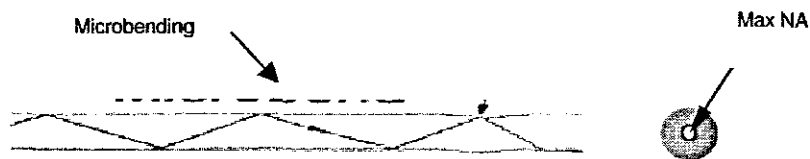


Figure 2.10 (b): Micro-bend effects of the light beam cause little diffraction

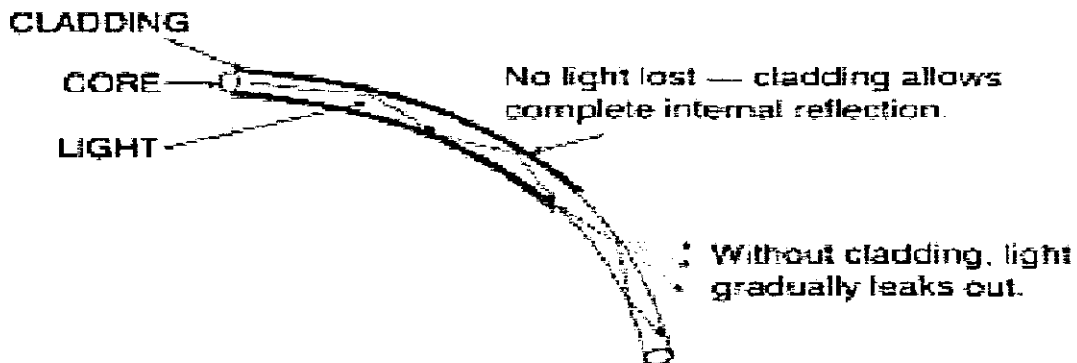


Figure 2.10 (c): Macrobend effects of the light beam causes large amount of diffraction

Other factors affecting the NA value include the fiber core material by transition metals such as copper, chromium, iron, and hydroxyl irons. For example, typical fiber loss for a telecommunication grade fiber due to the presence of iron and copper has shown a reduction of optimized transmission. Figure 2.11 shows the relationship of the factors such as absorption and

scattering against the wavelength

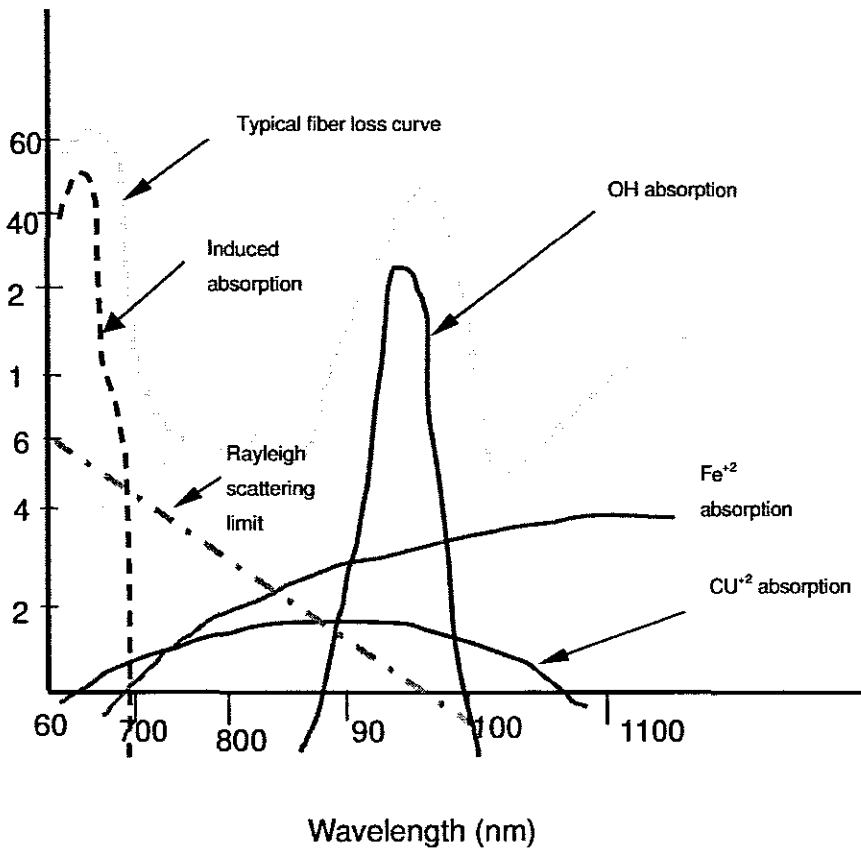


Figure 2.11: Absorption and scattering as function of wavelength.(reprinted from AMP Inc.)

It is accepted that the attenuation or loss of power within a length of a fiber is given by

$$A = -10 \log \frac{P_i}{P_o} \quad (2.54)$$

Where: P_i and P_o are input and output power.

The losses caused by factors such as absorption, scattering, micro bend/macro bending and end losses due to reflection, can also be obtained by following:

Reflection losses by Frensel is given by

$$R = \left[\frac{n_o - 1}{n_o + 1} \right]^2 \quad (2.55)$$

Where n_o is the index refraction of the core material. Using the classical definition of absorption:

$$P_o = P_i e^{-\alpha L} \quad (2.56)$$

Where α is the attenuation coefficient (unit /length), and L is the fiber length.

The loss due to the transmission can also be calculated in percentage, and it is given by:

$$T = (1 - R)^2 e^{-\alpha L} \quad (2.57)$$

Where the term $(1 - R)^2$ is the reflection loss for the entrance and exit ends of the fiber. The effect of the reflections is multiplicative and therefore accounts for the square term since there are two surfaces (exit and entrance).

The properties of the common optical fibers are shown on table 2.2 below.

Type	Loss (dB/km)	NA	Core size(O.D) (μ)	Core to core ratio	Bandwidth (MHz-km)
Multimode Step Index Glass-clad (Bundle)	400-600	0.4-0.6	50-70	0.9-0.95	20
Plastic-clad silica	3-10	0.3-0.4	200-600	0.7	20
Glass-clad glass (Low loss)	2-6	0.2-0.3	50-200	0.4-0.8	20
Single Mode	<1	0.15	5-8	0.04	1000

Table 2.2 : Typical properties of various Fiber Types

2.6 Mechanisms of optical fiber attenuation due to micro-extension

The effect of an extension on a OF has been taken with less consideration when it is applied into structures. More facts have been developed regarding the micro and macro bending than it has been reported for its tensile participation. Parallel to extension in the OF, the study of the corresponding light intensity change has been investigated. As the applied load on the optical fiber diameter tends to pull (extend), and consequently, its size (diameter) tends to reduce while elongation takes place. This phenomenal is compared to a common tensile test on a thin rod, or a wire. However, the added distinct is when we consider both the physical change of the fiber and the light which is passing through it. Consider a typical diagram below, where we have both fiber deformation and light passing through it.

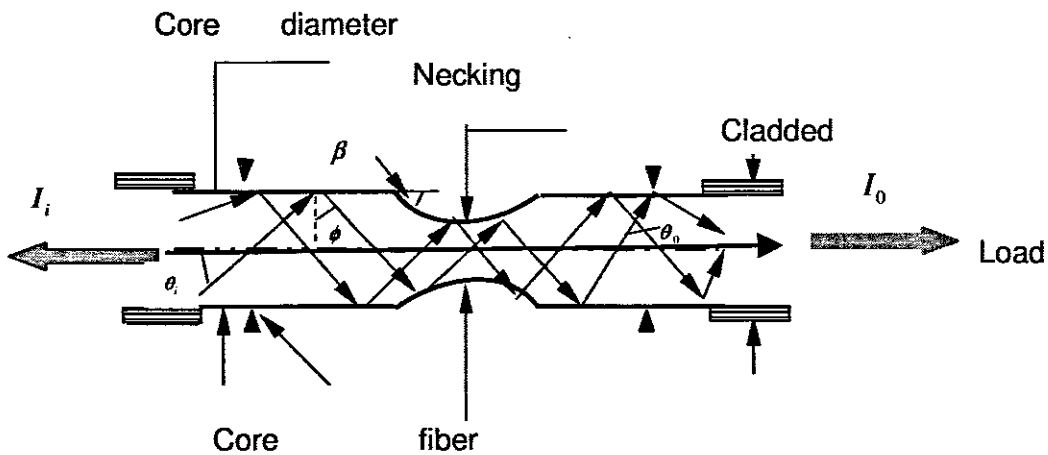


Figure 2.12: Propagation modes of optical light beam on a fiber at deformation due to tension.

The optical power I_i is launched at the input side of the fiber, propagates, distributing itself among the guided modes that are compatible with the guiding structure. When the fiber is stretched, the propagated beam meets the necked section of the fiber, whereby the effect of the reduced numerical aperture occurs. Therefore some of the higher order modes are no longer guided by the core and diffuse into the cladding with a spatial distribution that,

in the fused common region is nearly uniform. After this region the optical power in the cladding is split by the bifurcation of which finds the reversed taper at the output side.

A beam propagating along the necked (characterized by a taper angle β) will undergo an increase in its propagation angle (i.e, the angle formed with the fiber axis). Starting at an initial value θ_i , the propagation angle will increase by 2β at each reflection at the core-cladding interface. As long as the incidence angle ϕ is larger than the critical angle (for total internal reflection), the beam is still guided and emerges from the taper region, forming an angle θ_0 with the fiber axis. If the taper of the necking is smooth and number of reflections is high, θ_0 is given by

$$\sin \theta_0 = \frac{\frac{D_1}{2}}{\frac{D_2}{2}} \sin \theta_i \quad (2.60)$$

$$\frac{D_1}{2} = R_1 \quad \text{and} \quad \frac{D_2}{2} = R_2$$

and R_1 and R_2 are the core radii before and after elongation .respectively.

Therefore, the propagation angle of the optical beam at the output of the necked depends on the tapering ratio $\frac{R_1}{R_2}$. When the incidence angle ϕ becomes smaller than its critical value, the optical beam is no longer guided by the core, yet it can still be confined within the cladding, provided that

$$\sin \theta_0 \leq \sin \theta_{0M} = \frac{(n_1^2 - n_0^2)^{1/2}}{n_1} \quad (2.61)$$

Where n_0 and n_1 are the refractive indices of the outer medium and of the core, respectively, θ_{0M} is the maximum propagation angle within which the optical beams are still confined. At the output side, the maximum launching angle θ_{iM} is limited by the numerical aperture of the fiber, according to

$$n_1 \sin \theta_{iM} = NA = (n_1^2 - n_2^2)^{1/2} \quad (2.62)$$

To avoid radiation outside the cladding, by any accepted optical beam, θ_0 (θ_{iM}) must be limited:

$$\theta_0(\theta_{iM}) \leq \theta_{0M} \quad (2.63)$$

Therefore, from equations (2.57) and (2.59),

$$\frac{R_1}{R_2} \leq \left(\frac{n_1^2 - n_0^2}{n_1^2 - n_2^2} \right)^{1/2} \quad (2.64)$$

For the input -output optical power transmission ratio with respect to the change in optical fiber diameter we have equation

$$\frac{P_{(r)}}{P_{(o)}} = \left[1 - \left(\frac{\Delta d}{d} \right)^\alpha \right] \quad (2.65)$$

Where $P_{(r)}$ and $P_{(o)}$ are the input and output optical power through the fiber, and Δd and d are the optical change and original in diameters of the optical fiber.

Using the above concept, the use of fiber optic as strain measurement gained popularity. Hale et al. [43] in 1980 firstly reported the use of FOS in sensing the crack propagation in metals, whereby the embedded silica glass optical fibers elongation due to the opening crack has shown a very large failure strain (~5%). There has also been evidence that as the optical fiber stretches, there is a loss of transmission at the output of the optical fiber or from the light bleeding at the point of failure.

Chapter 3

3.0 Designs and Manufacture of Effective Terminals for the Transmission of the Optical Beam

3.1 Introduction

General overview of the fiber optical sensors with some of their applications has been briefly discussed in section 1.4, while the specific problem of the crack detection is discussed on section 1.4.3. This chapter has been divided into two parts. Part (a) explains the preparatory work for manufacturing the effective connectors, which are the primary linking components between points within the FOS system.

Part (b) discusses the interrelations between components necessary to form a complete system able to detect crack occurrence using fiber optic technology. Discussion on techniques and steps used for the preparation and manufacture of the optical transmission system capable to link between the light sources and receivers has been addressed.

3.2 Preparation and manufacturing the fiber optic connections.

In order that the designed type of sensor meet the functional requirements, it is necessary to provide proper and reliable connections. Due to the reason that standard connectors are not always available to facilitate the transmission of the optical network, the demand to design and manufacture compatible connectors to suit the specific application is inevitable.

The process of connecting the optical fiber with terminal connector is an art which requires high degree of keenness and attention.

In this section, there will be a discussion on the fabrication of the optical fiber connectors, splicing process, as well as fiber terminating techniques.

Quality assurance, the inspection of the joints and end terminals is also discussed.

3.2.1 Equipments and tools for termination

In the process of splicing and terminating the optical fiber, the specialized tools and equipment designated for the purpose. Proper use of the tools is among the contributing factor towards the final predetermined condition for the quality of fiber end surface. The cutting, edging, stripping, splicing and terminating is basic operations in making effective connections.

Cutting: Normally, the optical fiber cables are available in a reel of which sometimes only a certain amount of its length is needed. Unlike the other type of cables such as electrical wires the ends of the optical fiber edges fiber must remain perpendicular to its axis after termination.

Edging: The edging is a cut that is 90° to fiber axis. Good edging determines the extent of accuracy of mating between the two surfaces during the splicing process.

Stripping: The action of separating the cladding surface from the core

diameter of the fiber is termed stripping. The stripped length gives a clear and clean surface of the fiber during the fusion of inner-to-inner core of an optical fiber.

Splicing: The splicing process enables the joining of two ends of the fiber surfaces together by using a fusion process. The compact fusion set provides all necessary directions, through the manipulation of the longitudinal axes, that brings together the two ends of the fiber and align them before discharging an arc for their fusion. The compact fusion set is shown on figure 3.3(a)

Inspection: For the inspection of the fiber end, a X100 magnification microscope is used. The result shown on the magnified regions the appearance of clear region describes perfection of surface condition, which determines the amount of light that can be transmitted and reflected at these ends. Figure 3.2(a) shows some images as a result of magnification

Ferrule connectors: Ferrules are commercially available depending on their applications. Connectors are normally supplied with ceramic ferrules as a complete assembly (ferrule with a pig tailed fiber). However the components are also available individually in a variety of designs, whereby the procedure of assemble them is indicated on section 3.3(a)

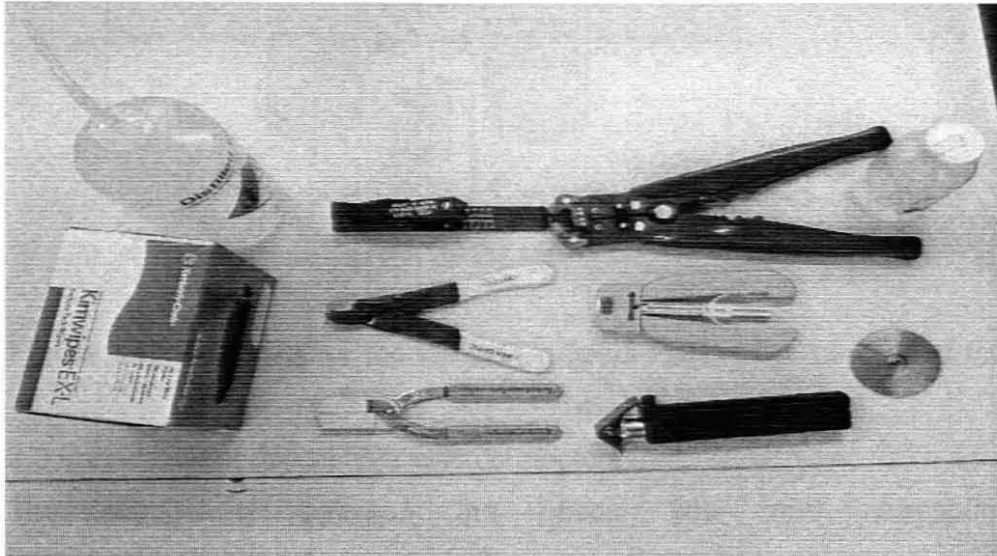
Epoxy: The epoxy material is applied to reinforce and bond together the surfaces (circumferential) between the fiber and the ferrule. The epoxy TRA from the BIPAX product is suitable

Polishing paper: These are graded surface texture of a special paper meant for providing the polishing of the fiber end. Numbers grade the paper, starting from 5 which is a coarse and ascending to 0 for the fine finishing.

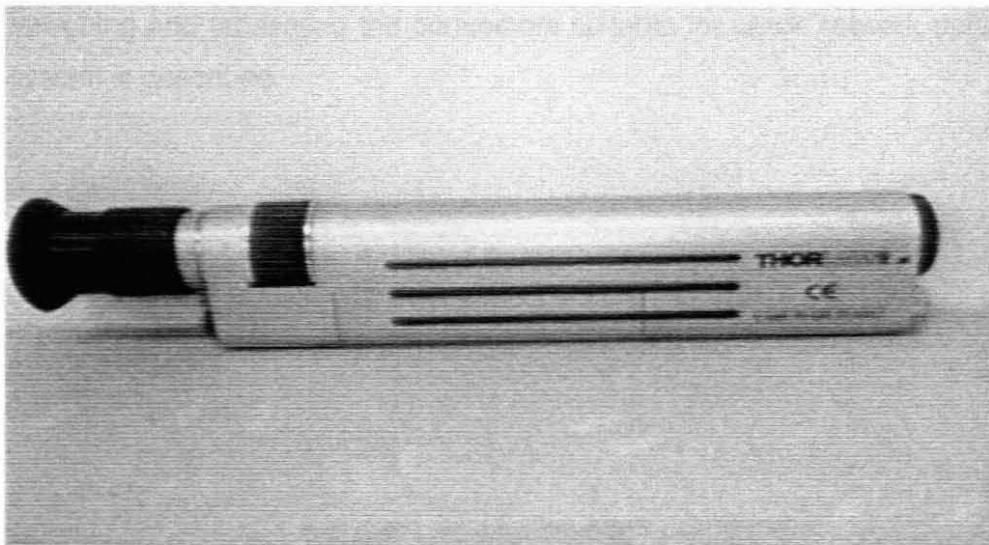
Isopropyl alcohol: The alcohol-based fluid is used as a surface-cleaning agent at various stages of the fabrication process. It enables to clear any contamination that may hinder good result of transmission during the polishing

process.

Distilled water: Is applied at various stages of the polishing procedure to assist in acquiring a sound surface finish of the fiber end.



a



b

Figure 3.1(a): Tools and accessories for splicing and terminating process
Figure 3.1(b): X100 magnification microscope for the ferrule ends observation

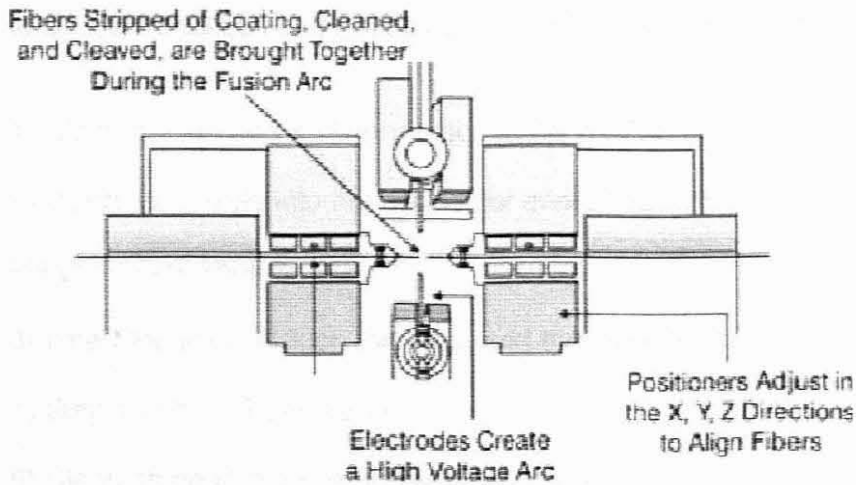


Figure 3.2: Schematic of the OF on Compact Fusion Device aligned for the fusion process.

3.3 Fabrication of optical fiber with connectors

The connectivity between the optical fiber and corresponding instruments/equipment requires high degree of accuracy, to ensure reliability of transmitting signals at input /output ends. In this work, the procedure of designing and fabricating the connectors suitable for crack network detection system is described.

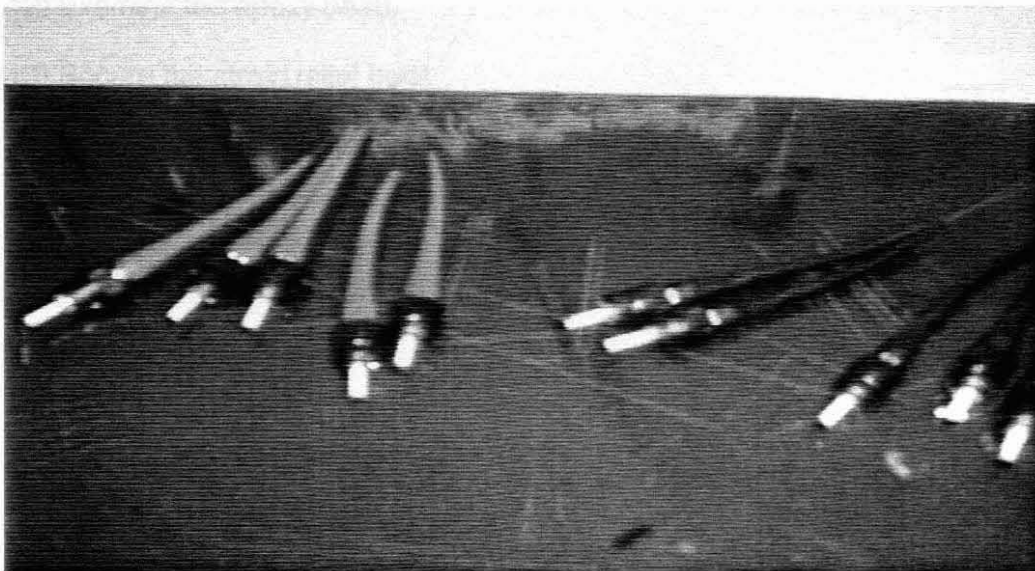


Figure 3.3: Optical fiber cable end product before polishing

To best achieve a good connectivity of the fiber ends, one must strictly follow the procedure for splicing, fabrication and polishing, as indicated in the "Guide

to Connectorization and Polishing Optical Fiber [44] manual.

- 1) Clean the ferrules and connector shells with reagent-grade alcohol
- 2) Insert the ferrule into the connector shell. The ferrule has a transitional fit to the connector shell
- 3) Insert the fiber through the tube, and trim fiber to length
- 4) Strip and trim fiber to length
- 5) Clean stripped area using reagent-grade alcohol
- 6) Test fit fiber and connector
- 7) Prepare epoxy-filled syringe
- 8) Add epoxy to connector
- 9) Insert the fiber into connector filled by epoxy
- 10) Full seat connector
- 11) Secure crimp sleeve
- 12) Examine the epoxy bead
- 13) Secure the strain relief boot
- 14) Allow the epoxy to cure
- 15) Score the fiber
- (15) Follow the polishing procedure (starting from the course to fine surface finish)

3.3.1 Inspection and observation of optical fiber end surfaces through macroscopic magnifications.

After the final polishing stage has been achieved, the connector ferrule is cleaned using the isopropyl alcohol. Using the X100 microscope ensure that there is no heavy scratches through the core of the fiber. The fiber should be free from all visible scratches or defects. The region around the core of a

single mode fiber should have no visible scratches. Typically, there are random scratches across the connector ends as shown in figure 3.3 below.

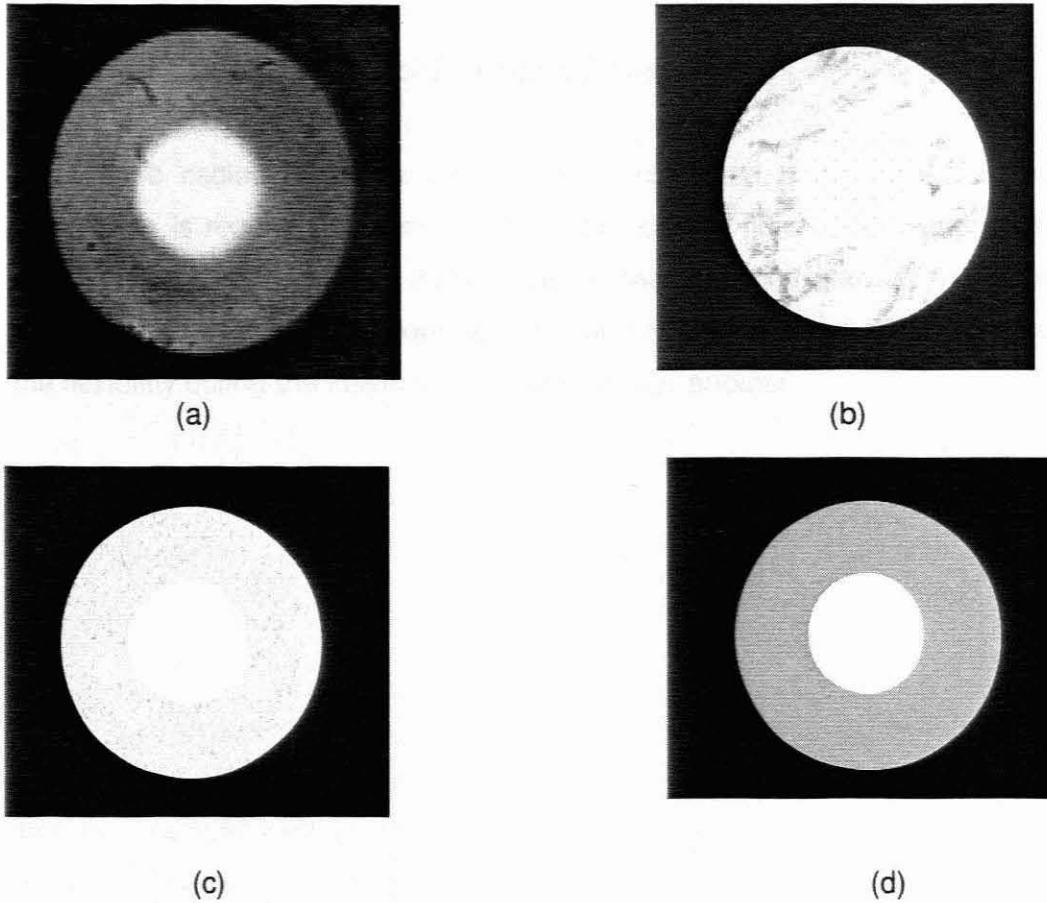


Figure 3.4: Samples of the 100X magnification of the end ferrule.

- a) End finish without clear inner core protrusion (b) End surface affected by scratches during polishing (c) Clear inner core protrusion with slight bourses (d) Clear end surface for maximum transmission efficiency

The end surface of the fiber condition is considered acceptable only if there are only light random scratches or there are no chips at the edges of the fiber that extend into the core of the fiber; or there are no more than two chips in the edge of the fiber, such that the length plus the width of the chip doesn't exceed 20% of the circumference of the optical fiber.

The quality of finishing plays a very big role in ensuring the best of the light beam transmission. However this work has not gone as far as analysing the

contributing factor for the surface condition. but the experience showed that proper polishing procedure contributes to large extent in obtaining a sounding surface finish.

3.3.2 Terminating and splicing of optical fibers

Fiber optic cables as any other type of cable need to be joined where connection is required. The only distinct with optical fiber cable compare to other conventional cables is its peculiar properties. Silica glass is the main material for the fiber optical core section which characterizes the fiber to obey the flexibility during the fusion process of one fiber another.

Chapter 4

4.0 Fiber Optic Sensor for Crack Propagation and Detection

4.1 Introduction

In the previous chapters, we have discussed the sequence operations for preparing good sound transmission and receiving ends of the fiber optic cable that will be employed in making a sensor for crack detection. One of the important aspects to observe in making the sensor is the quality of terminals, which have the task of receiving and transmitting the beam light between the illumination source, and the detection points through the signal acquisition devices.

This part of the chapter deals with the details of each component in a cascade arrangement and their designated role. We will also discuss the design issues pertaining some of the components in the system.

Earlier, it was shown in figure 1.7 the sensor components that have been employed in this work. The laser source being the component emitting the light beam, which was selected after an acceptable wavelength range and rated power were considered. The type of optical fiber cables and their characteristics will also be discussed. This involves all the interaction conditions of the fiber optic with the host material, especially on the localized

or affected area of the deformed material. The interaction condition is a very critical aspect as it is a guideline to ensure the optimum service of the optical fiber before, during and at the stages of total deformation of host material.

On the signal-receiving end, the photo-detector has to be sensitive enough to detect the differential changes of the original intensity of the light beam being transmitted in the fiber optic as soon as deformation of the material begins. It is reasonable to assume that as the sensor is attached to the component the fiber optic will accompany the material deformation and in turn will change shape affecting the intensity of the light being transmitted within it. The detection of the deformation can be made by using a single point (single fiber) laid across the intended crack path, which is expected to propagate perpendicularly to the applied load. Alternatively the sensor can comprise of a single strand, or it can be laid in a multiple fiber bundle which should be affected by the line of forces across their paths, and hence be able to detect deformation at different levels of the crack propagation. Along the test line, it is possible to develop an algorithmic programme to provide information at any desired point. Such a task can be the subject of a future investigation. The optical signal carried by the fiber is converted to an electrical signal and displayed as an out-put DC voltage. The effects of various events during the deformation of the structure can be easily interpreted from graphical and other data analysis. The setup of the integrated system for crack detection is illustrated on the schematic diagram figure 4.1 below.

4.2 Sensor system component specification and design aspects

4.2.1 Photo diode laser source.

As discussed earlier in section 1.4.2.2 photo diodes are available in a wide range, for a variety of applications. Considering our application i.e. the sensing of mechanically deformed structures, LED transmitters (0P17 692) have been employed to fabricate an instrument able to transmit through the electronic circuit board the laser light beam of 850nm wave length, which is received on the side of the silicon PIN photo detectors. The designed component has been equipped with the feature that facilitates balancing the

signal out put.

Characteristics of the Fiber Optic LED are shown in table 4.1

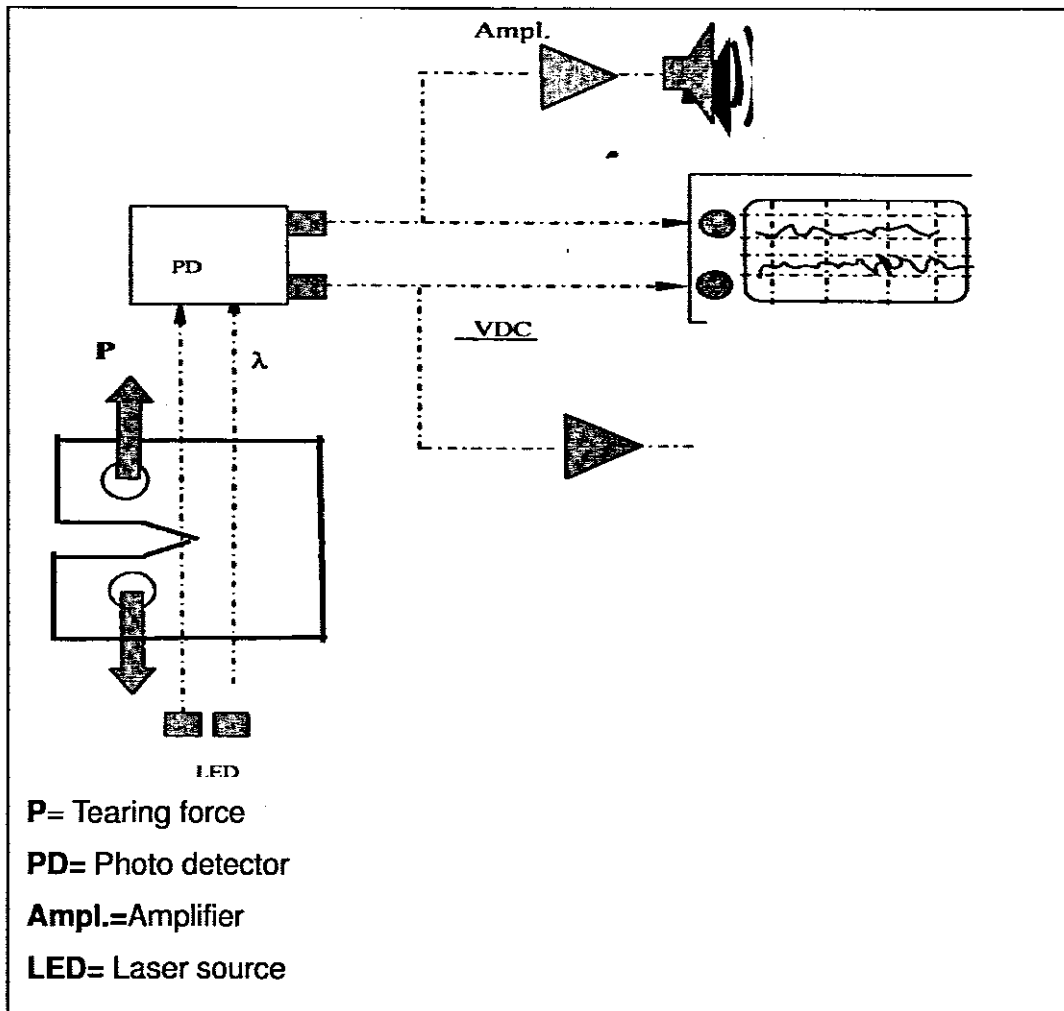


Figure 4.1: Schematic layout of the test specimen with a two fiber sensor, for example, and respective light beam emitting and receiving components

Another option as a laser source was using an available unit from "ThorLabs Inc", The Thorlabs item SIFC635 is a fiber coupled optic laser source with a maximum power of 2.89mW and a wavelength of 635 nm with a variable range of out-puts. The fiber coupled optical laser accommodates a single line to be coupled to the high-speed photo detector (SUV7).

4.2.2 Photo detectors

The OPF 792 photo detectors are selected being compatible with the OPF 692 LED in transmitting and receiving the light beam. Using our designed electronic circuit facilitated the connection of the two. The function of our designed electronic circuit mentioned above was to convert the received light beam into an electric signal. The characteristics of the type of photo-diode chosen is given below in table 4.2

Symbol	Parameter	Min	Type	Max	Units	Test conditions
P_{T50}	Coupled out put power	-20		-15	dBm	$I_F = 100\text{mA D. C}$
P_{T50}	Coupled out put power	-17		-12	dBm	$I_F = 100\text{mA D.C}$
V_F	Forward voltage	1.48		2.09	V	$I_F = 100\text{mA D. C}$
V_{BR}	Reverse input voltage	1.8				$I_R = 100\text{-}\mu\text{A}$
t_r, t_f	Rise time, fall time		4.0	6.5	ns	$I_F = 100\text{mA}$
λ_p	Peak output wavelength	830	840	870	nm	$I_F = 50\text{mA}$

Table 4.1: Characteristics of the fiber optic LED model OPF 692

Symbol	Parameter	Min	Typ	Max	Unit	Test condition
R_p	Responsivity	0.4-5			A/W	$V_R = 5.0\text{ V}$
I_p	Dark current		0.5	5	nA	$V_R = 5.0\text{ V}$
t_r	Output rise time		2.0		ns	$V_R = 5.0\text{ V}$
BW	Bandwidth		115		MHz	$V_R = 5.0\text{ V}$

Table 4.2: Characteristics of the PIN Photo diode model OPF 792

The laser source was able to supply the maximum power of 2.89 mW, in the 635nm wavelength. The emission of a visible light beam from the supply can

be of great use especially in testing and verifying the reliability of beam transmission. It means that it is easy to detect the light continuity from the supply to any point in the system, visually. The high-speed photo detector SUV7 whose characteristics are shown in table 4.3 below was chosen as the receiver of the laser light beam from the Thorlab unit,

Parameter	Data
Wave length range	350-850 nm
Detector material	GaAs
Detector area (interdigitated)	0.2 x 0.2mm
Bandwidth (-3 dB point)	-7 GHz
Raise and fall time	< 50ps
After pulse ringing	< 20% of max
Dark current	5nA @20V
Junction capacitance	<0.4pF @20V
NEP	4 x 10E-15W/sqrt (Hz)
Dynamic range	Calculate from NEP and 2V maximum output into 50 Ω
Fiber input receptacle	FC
Out Impedence	50 Ω
Typical peak optical input power for a 2V output	500mW
Maximum safe output voltage	2V
Battery power supply	20V
Battery shelf line	190mAh of stored charge lifetime depends on signal rep-rate, etc.
Dimensions	25x25x38 mm

Table 4.3: Characteristics of the high-speed photo detector model SUV7-F
4.2.2

4.2.3 Design of the crack propagation detection instrument

The crack propagation detection instrument (CPDI-01) was designed and manufactured at the CRATECH Research Unit at Cape Peninsula University of Technology and it was designated as CPDI-01. It

is a physical component as it is illustrated in figure (A.4 no 4) appendix (B) and its characteristics are tabulated in table (4.4) below.

The CPDI-01 unit was designed for the purpose of detecting the deformation of a structure due to an external load. Crack formation and propagation is one of the mechanical deformations that can result, due to an external load on a critical component, and it can be detected using this unit. The CPDI -01 is a 3-channel device consists of a 3-channel optical fiber input and output (ST-type connectors), as well as 3-channel oscilloscope interface through BNC connectors. The unit is reasonably lightweight featuring an ABS protective housing.

The CPDI-01 has the ability of simultaneously detect the state of 3 optical fibers aligned through the deformed zone.

Output Characteristic	ON	OFF
Channel 1	4.2V \pm 0.5	100mv \pm 1 00mV
Channel 2	4.2V \pm 0.5	100 mv \pm 1 00mV
Channel 3	4.2V \pm 0.5	100mv \pm 1 00mV

Table 4.4: General characteristics of the CPDI-01

4.2.4 Fiber optical cables

The single mode optical fiber was considered and selected as most suitable for the embedment in structures. The 50/125-size fiber cable is compatible to the ST type connector. The light beam intensity change during bending or stretching of the fibers affords us less complexity when employing the single mode fiber rather than multi-mode or other modes of fibers. The 630-HP fiber cable characteristics are shown in table 3.5

Parameter	Manufacture specification	EOP Data	BPO Data
Second mode cut off	570±30nm	544.0	549.0
MFD@630nm(near field)	4.0±0.5μm	4.2	4.3
Core-clad concentricity	<0.5μm	0.1	0.1
Attenuation @630 nm	< 12dB/km	9.3	9.3
Fiber diameter	125±1.5 μm	124.9	124.9
Coating diameter	245±15μm	247	248
Proof Test	≥200 kpsi(1.4GN/m ²)	200	200
Design Information			
Parameter	Nominal value		
Operating wave length	610-770 nm		
Numerical aperture	0.13		
Core composite	SiO ₂ /GeO ₂		
Coating type	UV curable, Dual Acrylate		

Table 4.5: Fiber optic characteristics and design profiles

4.2.5 Signal output, amplification and displays

It is important for the transmitted and received signals to be captured and displayed in a real time. The signals from the photo-detector are commonly of the order of micro-volts and must be amplified before reaching the display devices. The amplified out put voltage is able to drive a triggered device such as buzzer, an LED or actuators, all of which require reasonable amperes. The voltage domain can be displayed on the multi-meter or oscilloscope in waveform. In future work, it is suggested that the algorithmic work be carried out for the interface with a computer.

In this work, CPDI-02 unit has been designed and constructed to facilitate the signal amplification in driving a relay switch, a buzzer and a LED light.

The CPDI-02 consists of three input and out put channels, in the front panel marked TX1 and RX1 respectively. The built in circuitry accommodates the LEDs detectors and the amplification of the signal. The signal is then

channelled to the 3 Mode out-put as shown in table 4.6 below. The provision of the connectors at the rear panel enables connection to auxiliary components that might operate on a timer related to an interval of actuation.

4.3 Component requirements in setting-up the integrated crack detection system

The assembled detection system's functionality depends much on the quality of the individual components before bringing them together. Due to the reason that fiber breakage can occur at the critical crack opening, as well as in the connections to the rest of the system the light beam supply or receiving/sensing side, several splicing and terminations are required to make effect new connections during or after each test. This involves the standby positioning of the splicing machine directly at the testing machine table. The process is carried very carefully without disturbing the already positioned structure embedded with fiber optical cable(s) into the machine's jaws.

The sequential steps in setting-up the crack detection system (CDS) begins by ensuring the initial preparations to separate ends of fiber connectors with a reasonable protrusion of the fiber length. Alternatively, the two connector ends may be joined with a length of up to 15 mm. On the test specimen, grooves of 0.5mm depth are made to accommodate the optical fiber. At the selected position along the optical fiber line, the embedment of the fiber is done and with an aid of adhesives, the optical fiber is bonded on both ends to resist tension along the line of force action as shown in figure 1.3. After the embedment of the fiber into the host material, the inspection of light continuity can be effected by connecting one end of the fiber terminal into the fiber optic LED unit, which emits sufficient light for visual observation.

Subsequent to ensuring the continuity of the light beam, one end of the ST type terminal is connected into the fiber optic LED channel on the CPDI -01 unit. The fiber cable from the 1st LED channel is then bonded on the test specimen, which is mounted on the tensile testing machine ready for mechanical tests. The fiber is bonded almost at the point where the beginning of the crack is expected to occur. Leaving the test specimen, the fiber terminal

is connected to the receiver side (on the side of the photo detector). On the same channel on the CPDI-01 unit, the BNC port is available to accommodate the converted optical power into electric signal. The procedure is repeated in the same manner for the other two channels with the distance between the parallel fiber embedded into the test specimen selected according to the desired interval or length of crack propagation to be detected.

It is obviously imperative that the linkage of the light source from the CDPI-01 LED to the test specimen and from it to the CDPI-01 photo receiver is continuous.

At this stage adjusting the voltage each channel is set to an initial datum acting as reference. The final check-up for continuity is done before starting the mechanical deformation on the test piece by adjusting the regulating knobs to ensure the presence of signal variations.

Figure 4.2 below depicts the experimental set-up with the test specimen positioned in the tensile testing machine, as well as the light emitting, sensing and monitoring equipment in position.



Figure 4.2: CPDS set up during the mechanical deformation test.

4.3.1 Performance analysis and assessment of the crack detection warning system

The objectives of this work as stated in the section 1.3 (c) enables us to further utilize the above-integrated components into one useful unit for analyzing the tendency of the propagated crack. Several parameters are considered to be influencing factors for analyzing the tendency of crack occurrence and growth. Considering the aspects of the mechanical deformation test, the applied load on the specimen during fatigue or tensile test is proportional to the crack opening, displacement and formation of the stresses around the fore tip of the crack propagation. In the case of the fatigue test, the propagated crack is considered to be of Mode 1, which possesses the elastic stress distribution at the crack tip in the symmetry about the $(x-y)$ and the $(y-z)$ planes as previously illustrated on figure 2.3.

During the continual applied load on the specimen, the initiated crack tends to open at the rate proportionally $\gg (N \ll W/10)$. This phenomenon allows the first embedded fiber to experience greater tension with the second and consequently third fibers experiencing lesser tension. Thus it is possible to capture and analyze the phenomenon or process of crack growth in real time. The recorded load-displacement data from the tensile testing machine can be utilized in the prediction or analysis of the crack growth. The results of the analysis are the key factor in building up the logic arguments pertaining to the process of our sensory system.

Chapter 5

5.0 Experimental Results of Crack Propagation due to Mechanical Deformation

Introduction

The chief aim of conducting the experiment on mechanical deformation of a compact specimen is to obtain the necessary information regarding conditions around and along the path of the crack propagation. The results from this chapter shall be linked to those obtained from chapter 6 which discusses the test of an individual OF, and the results obtained with it as it was placed across the expected crack path.

This test has a significant role to play due to the fact that the standard test piece, which is subjected to the fatigue test, develops a stress concentration field around the tip, as well as energy release during the crack extension. The optical fibers are hosted across the path of the crack propagation, assumed to experience the same or similar conditions during the process of deformation of the host test piece.

The interaction point or area between the optical fiber and the crack

propagation path will be analyzed using the concepts of Linear Elastic Fracture Mechanics (LEFM). In order to obtain the integrated output characteristics of the optical fiber sensor, the study of separate entities before and during the investigation is vital. For example, individual tests for each entity, e.g. host material and optical fibers are done separately. In this chapter, we will be discussing the experiment and results of the LEFM fatigue test, as well as the response of a standard compact specimen subjected to a tensile test, as per E-Series of ASTM –399.

5.1.1 Assumption

As the intension of this work has been signified, i.e. to construct a sensor element that is able to detect and signal the propagation of a crack, several parameters and conditions were considered. For example the size (thickness) of the specimen, mode of testing, and the optical fiber response upon loading etc.. It is assumed that the sensor would give an initial warning at the onset and continue through out the crack propagation stages, till total failure.

5.2 Test requirements

5.2.1 Compact Specimen Configuration

The standard specimen used for the fatigue test experiment is specified according to the ASTM series E-399-81 [37], [38]. The standard specimen, $C(T)$, is a single edge-notched fatigue plate loaded in tension. It has generally been used only for testing the plane-strain fracture toughness (K_{Ic}); and it has no provision for load-line displacement measurement. Normally, this specimen is not used for ductile fracture toughness measurement.

5.2.2 Specimen Selection and manufacturing

The compact specimen was identified and selected because due to its

initiated notch it gives a convenient almost assured path for the crack to propagate after initiation. In order to correctly manufacture the specimen, the following steps must be followed. Determine the critical dimensions of the specimen (a, B, W) according to ASTM-E399. Prepare the drawing, e.g. specifying a chevron notch crack starter refer figure 5.1 then manufacture the specimen according to table 5.1.

Ratio (mm)	6-7	0.5W	1.25W	2E	0.55W/2	0.5W	0.25W	Defined
BS	B	H	W1	F	E	a	D	W
7448	6.35	30	62.5	27	13.3	17.5	12.5	50

Table 5.1: Specimen Dimensions

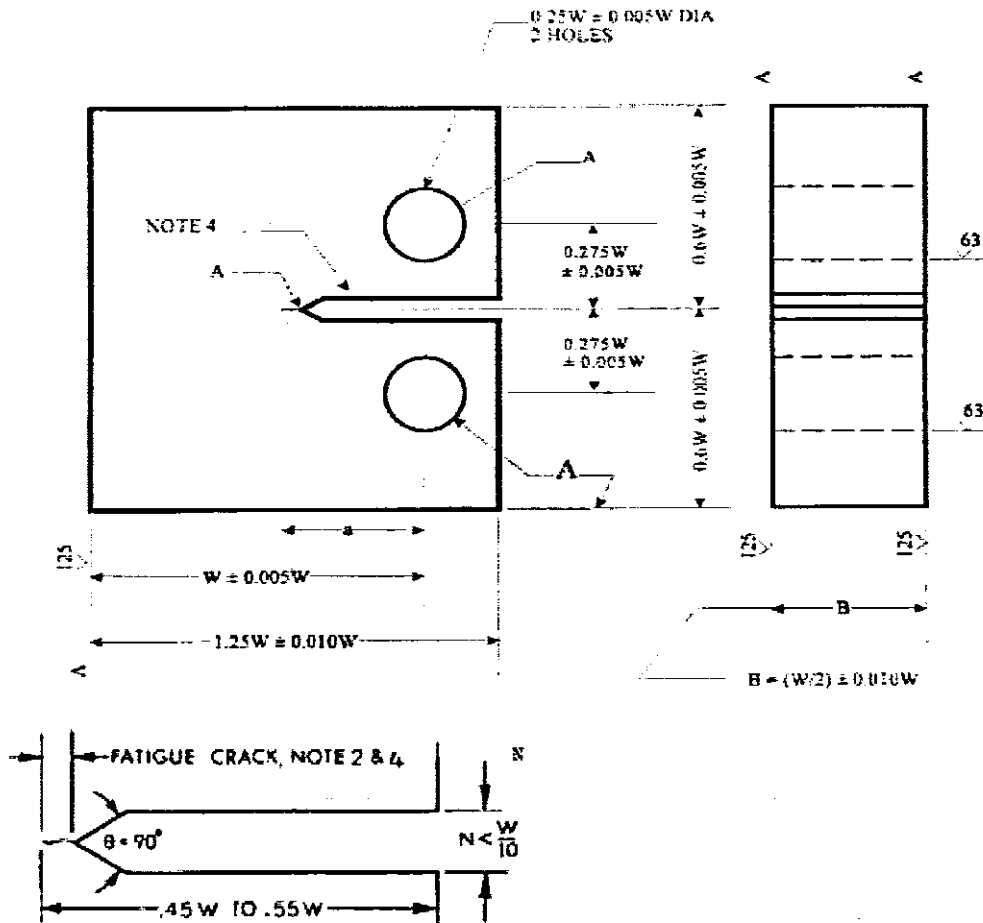


Figure 5.1: Specimen Geometry according to ASTM International Standards E 399-81, E-1820 and BS 7448

Fatigue crack extension on each surface of the specimen containing a

straight-through notch shall be at least $0.025 W$ (1.3 mm), whichever is larger, cutter tip angle 90° max. The intersection of the crack starter notch tips with the two specimen surfaces shall be equally distant from the top and bottom edges of the specimen within $0.005 W$.

5.3 Experimental Procedure

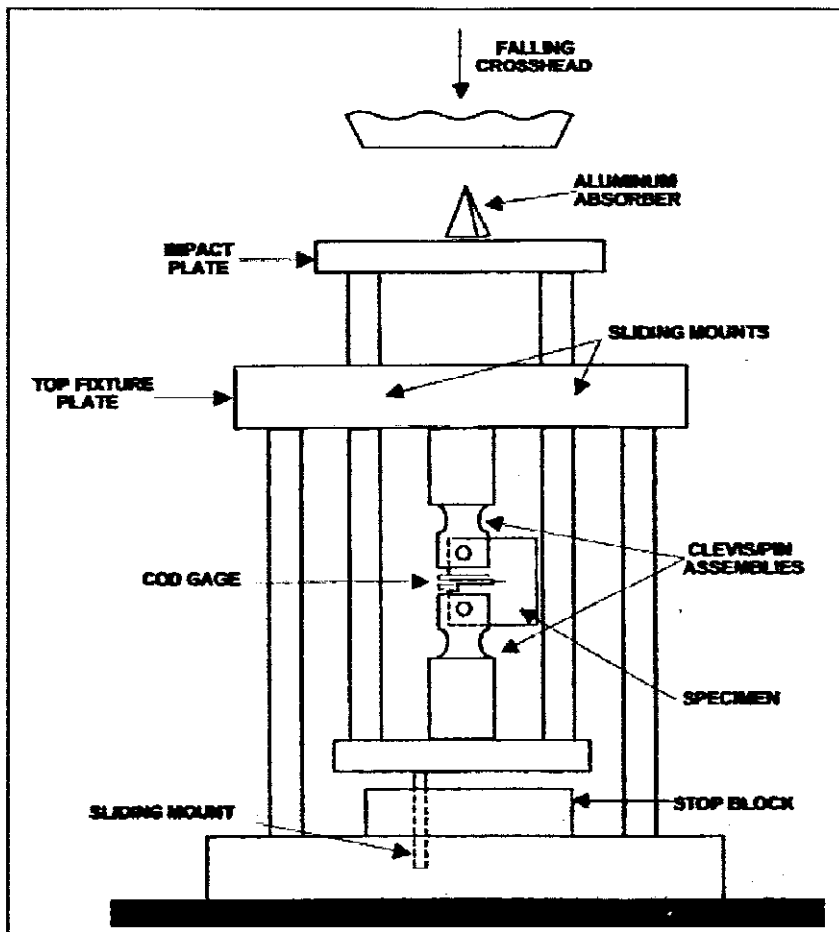
The experimental procedure when testing the individual compact specimen, for determining the fracture toughness is outlined below:

Test specimens (two from each) of the materials i.e. mild steel, composite fiber material and wood

- i) Load the specimen in tension to determine the P vs. δ
- ii) Determine the load at fracture P_Q
- iii) Determine the Stress intensity factor K_Q using equation (5.3)
- iv) Continue test till P_{max}
- (vi) Verify the condition of $\frac{P_{max}}{P_Q} \leq 1.1$
- v) Final check for validity (K_{Ic}) (whether the fracture toughness is in the plane strain) and fulfils the condition on equation (5.1)
- vi) Determine whether the fracture is in plane stress, plane strain or a mixed mode figure 5.4.
- vii) Form a table of results (table 5.3)

5.3.1 Apparatus

The Equipment for fatigue testing and crack initiation with uniform stress distribution through the specimen thickness is important. This will enable the crack to grow uniformly. Stress distribution should also be symmetrical about the plane of the prospective crack. This will prevent the crack to deviate unduly from the plane and hence facilitate the results. Applicable specifications concerning the loading clevis and displacement gage are shown in figure 5.2



Figure

5.2:

Schematic diagram of Specimen mounted on the Universal Fatigue Test Machine.

5.3.2 Analytical Procedure

The K_{Ic} value is determined (from the test record) while the value of PQ from the curves in figure 5.3 for the value of $\frac{P_{max}}{P_Q}$; this ratio should not exceed the recommended value of 1.10, [35]

$$B \geq 2.5 \left(\frac{K_{Ic}}{\sigma_y} \right)^2$$

$$a \geq 2.5 \left(\frac{K_{Ic}}{\sigma_y} \right)^2 \quad (5.1)$$

$$W \geq 2.5 \left(\frac{K_{Ic}}{\sigma_y} \right)^2$$

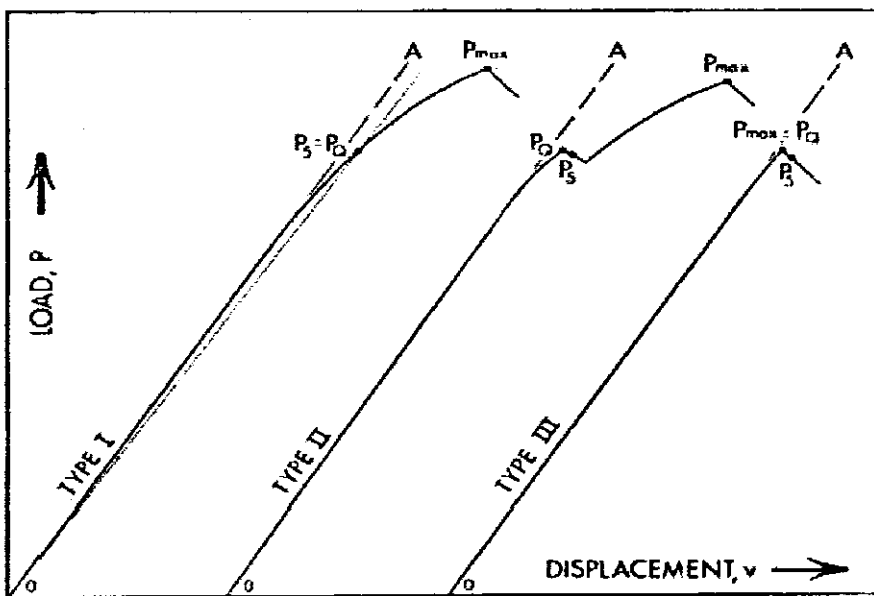


Figure 5.3: Load-displacement record for K_{Ic} determination

Governing expressions for the determination of K_{Ic} , based upon the load P

as follows

$$P = \frac{0.5 B b_0^2 \sigma_y}{(2W + a_0)} \quad (5.2)$$

Where σ_y is the yield stress or 0.2% off set yield strength at a given temperature of interest,

b_0 is the original remaining ligament, which is given by $b_0 = W - a_0$, and

a_0 which is the original crack size

For the specimen opening, due to tension, - mode intensity factor K_I , [40]

$$K_I = \frac{P}{BW^{\frac{1}{2}}} \frac{\left(2 + \frac{a}{W}\right) \left[0.886 + 4.64 \frac{a}{W} - 13.32 \left(\frac{a}{W}\right)^2 + 14.72 \left(\frac{a}{W}\right)^3 - 5.6 \left(\frac{a}{W}\right)^4\right]}{\left(1 - \frac{a}{W}\right)^{\frac{3}{2}}} \quad (5.3)$$

The accuracy of determining the intensity factor is within 0.5% under the

condition that $0.2 < \frac{a}{W} < 1$

By using the Empirical relationship between the specimen thickness and critical stress intensity factor (K_C)

$$(EG_c)^{\frac{1}{2}} = \sigma (\pi a)^{\frac{1}{2}} = K_c \quad (5.4)$$

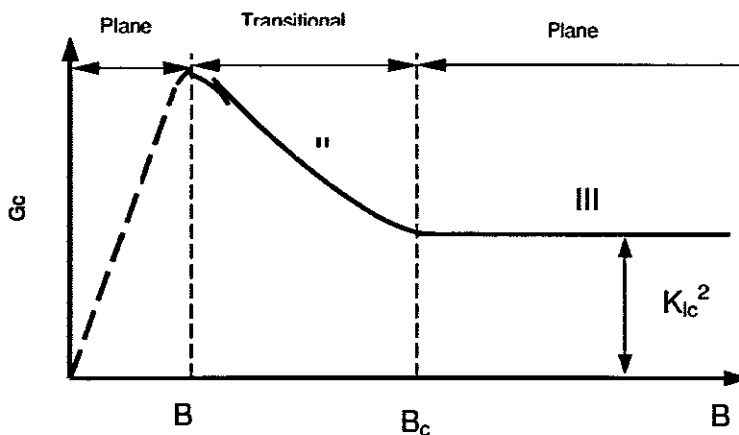


Figure 5.4 Critical fracture toughness G_c (or K_{Ic}^2) versus plate thickness B

From equation (4.3) the expression for the value of $\frac{a}{W}$ is obtained from the ASTM values shown in table 4.3 below,

$$K_c = K_{Ic} \sqrt{1 + \frac{1.4}{B^2} \left(\frac{K_{Ic}}{\sigma_y} \right)^4} \quad (5.5)$$

Where σ_y is the yield stress

a/W	f(a/W)	a/W	f(a/W)
0.450	8.34	0.500	9.66
0.455	8.46	0.505	9.81
0.460	8.58	0.510	9.96
0.465	8.70	0.515	10.12
0.470	8.83	0.520	10.29
0.475	8.96	0.525	10.45
0.480	9.09	0.530	10.63
0.485	9.23	0.535	10.80
0.490	9.37	0.540	10.98
0.495	9.51	0.545	11.17
-	-	0.550	11.36

Table 5.2: Tabulated values for the ratio $\frac{a}{W}$

5.4 Test results and discussion

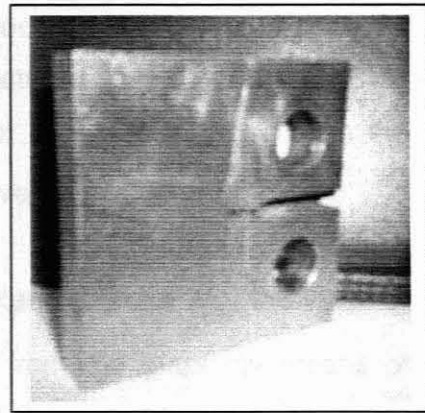
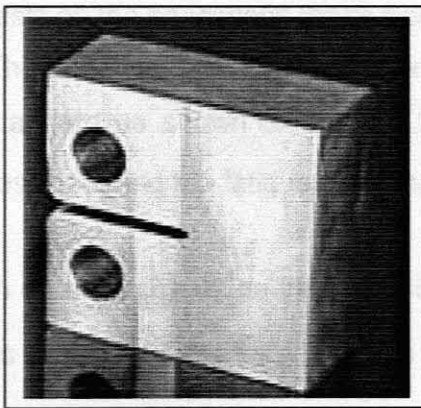
5.4.1 Fatigue Test

The tensile test on the mild steel compact specimen has been pursued. For the fatigue tests on the specimen, measurements of the load versus displacement depend on the dimension of the specimen, which has been a key influencing parameter in determining the stress intensity factor, as well as

the stress around the crack propagation path. As discussed earlier in this chapter, the suitable mode for the crack deformation was opted to be mode no I. The fatigue pre-cracking range was selected between 10^4 to 10^6 cycles and the loading range of 0.55 to $2.75 MP_a m^{\frac{1}{2}} / sec$. Fatigue crack length was calculated by using $(0.45-0.55) W$ in order to determine the value of K_{IC} . By selecting the load-displacement option, the test begins recording values of the load against displacement. The data were captured and translated using the logger soft ware, which is interfaced with the Universal Testing Machine (Si-Plan fatigue- testing machine) as shown in figure 5.2

The value of P_Q was determined from the graphs in figure 5.3 for the condition of $\frac{P_{max}}{P_Q} < 1.10$. The P_Q value can be used to determine the value of K_Q in equation (5.2).

Table 5 gives us standard values of σ_Y and K_{IC} for various materials. Experimental results are summarized in table 5.4.



a) Compact specimen before fracture

b) Compact specimen after fracture

Figure 5.5: Mode I fracture of a standard compact specimen before and post fatigue induced fracture.

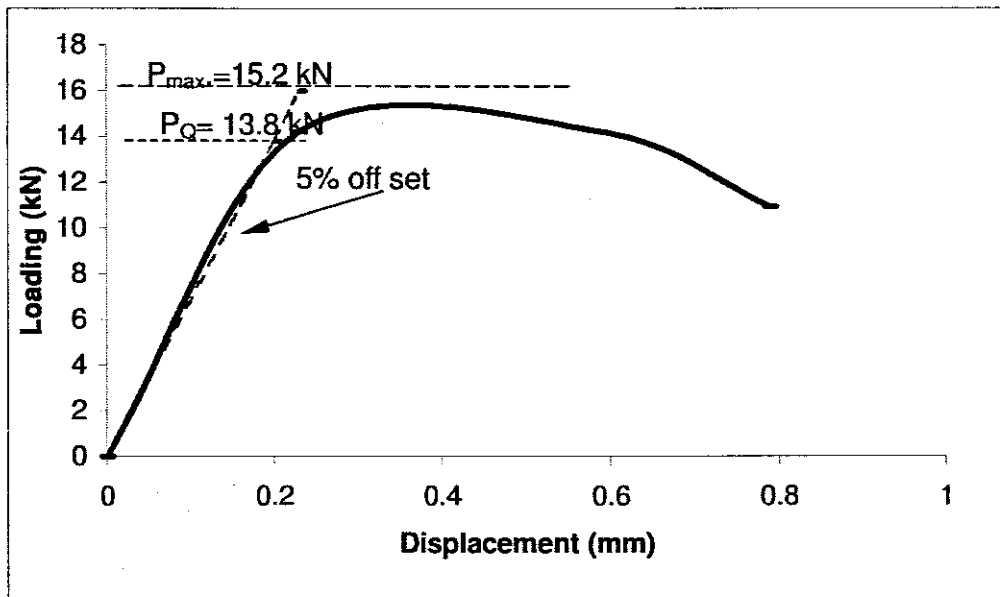


Figure 5.6: Typical Load –Displacement curve as obtained from the fatigue tests.

The fracture toughness K_{IC} value is arrived at after conducting several fatigue tests on the specimens made from mild steel, wood and composite materials. The dimensions of the specimen were manufactured according to the ASTM standard as shown on table 5.1. The value of P_{max} was obtained from the results during the fatigue tests that yielded an average value of 15.2 kN.

In order to determine the value of the stress intensity factor K_Q , the value of its corresponding load P_Q was first obtained from the graph by means of geometry. The secant line of 5% off- set to the initial linear portion of the $P-v$ curve is constructed to intersect the curve at a point which defines the P_Q at 13.8 kN. By using the pre- determined value of P_Q the K_Q is obtained to justify the condition of the K_{IC} from equation (5.3). Using the equivalent table

4.3 the ratio $\frac{a}{w}$ gives $f\left(\frac{a}{w}\right)=9.66$. The condition $\frac{P_{max}}{P_Q} \leq 1.10$. is satisfied since

$$\frac{P_{\max}}{P_Q} = \frac{15.2}{13.8} = 1.10 \text{ Therefore, it agreed upon the value of the stress intensity}$$

factor of 59.62 Mpa \sqrt{m} .

In order to determine whether the test specimen was subjected to plane strain or plane stress conditions we look at results from equation (5.1). Since the value of B seems too small, the dominant stress is Plane Stress.

Calculation to determine the value of the plastic zone size r_0 , is done using equations [5.6] and [5.7] respectively. The crack opening δ is determined by equations [2.16] [2.17] and [2.18]. The value of the crack length a_0 is determined depending on parameters such load the stress around the crack tip as well duration of test.

Data	Specimen
(a) Material properties, initial sample dimensions	
Specimen Materials	Plain Carbon Steel
Yield Strength (Mpa)	340
Specimen half height h (mm)	30
Specimen width measured to hole centers w (mm)	50
Specimen thickness B (mm)	10
Crack length (measured after fracture from hole centers a_i)	17
(b) Load at fracture	
Initial slope of elastic deformation line m_t	2.05
$m_s = 95 \% m_t$	1.94
Maximum Load P_{\max}	15.2
P_Q ($MP_a\sqrt{m}$) from figure 2.7.	13.8

(c) Stress intensity at fracture	
Non- dimensional crack length (mm) $\alpha = \frac{a_i}{w}$	0.34
Stress intensity at fracture K_Q ($MP_a\sqrt{m}$)	59.62
$2.5\left(\frac{K_Q}{\sigma_o}\right)^2 \leq B, a$ (mm)	B = 10 < 76.8 a = 17 < 76.8
$\frac{P_{max}}{P_Q} \leq 1.1$	1.1 ≤ 1.101
(d) Plastic zone size and final results	
For plane strain	
Plastic zone size $r_0 = \frac{1}{18\pi}\left(\frac{K_Q}{\sigma_o}\right)^2$ (mm)	5.42
Plane strain fracture toughness $K_{Ic} = K_Q$	
For plane stress	
Plastic zone $r_0 = \frac{1}{2\pi}\left(\frac{K_Q}{\sigma_o}\right)^2$ (mm)	4.89

Table 5.3. Summary of experimental results from the standard fatigue test.

5.4.2. Determining the values of crack tip size $r_p(\theta)$ under the plane stress conditions

The crack tips size r_p ahead of the plastic zone is determined by using Irwin

and Dugdale Modes [] equations (5.6 and (4.7) The r_p value has a significant role in estimating the magnitude of plasticity at a given angle. For our test the variation angle up to 45° was used and the results are summarized in table 5.5.

$$r_p(\theta) = \frac{1}{4\pi} \left(\frac{K_I}{\sigma_Y} \right)^2 (1 - 2\nu^2)^2 (1 + \cos \theta + \sin^2 \theta) \quad (5.6)$$

Polar coordinate at $\theta = 0.5^\circ$

$$\frac{1}{4\pi} \cdot \left(\frac{K}{\sigma} \right)^2 \cdot (1 - 2\nu^2)^2 \cdot \left(1 + 0.99996 + \frac{3 \cdot 0.000076}{2} \right) = 3.292 \cdot 10^{-3}$$

5.4.3 Determining the value of crack tip size $r_p(\theta)$ under plane strain conditions

$$r_y(\theta) = \frac{1}{4\pi} \left(\frac{K_I}{\sigma_Y} \right)^2 \left[1 + \cos \theta + \frac{3}{2} \sin^2 \theta \right] (m) \quad (5.7)$$

Polar coordinate at $\theta = 0^\circ$

$$\frac{1}{4\pi} \cdot \left(\frac{K}{\sigma} \right)^2 \cdot \left(1 + 1 + \frac{3}{2} \cdot 0 \right) = 4.896 \cdot 10^{-3} \quad \blacksquare$$

The magnitude of the stress surrounding the affected area is proportional to the size and shape of the plastic zone. In order for the localized stress to grow along the direction of x , we assume values for the variation angle θ . The results indicate that the singular and yield stresses are almost constant till at certain point where they begin to fall sharply due to loss in internal resistance around the crack zone. Figure 5.7 and 5.8 show typical results obtained from the test.

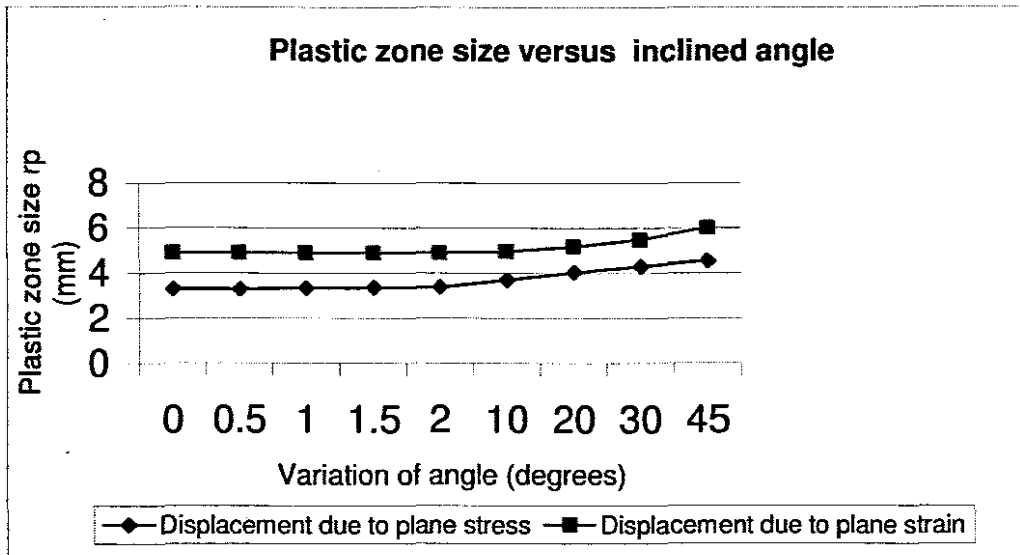


Figure 5.7:Effect of incline θ angle caused by the compliance Load to the plastic zone size r_p

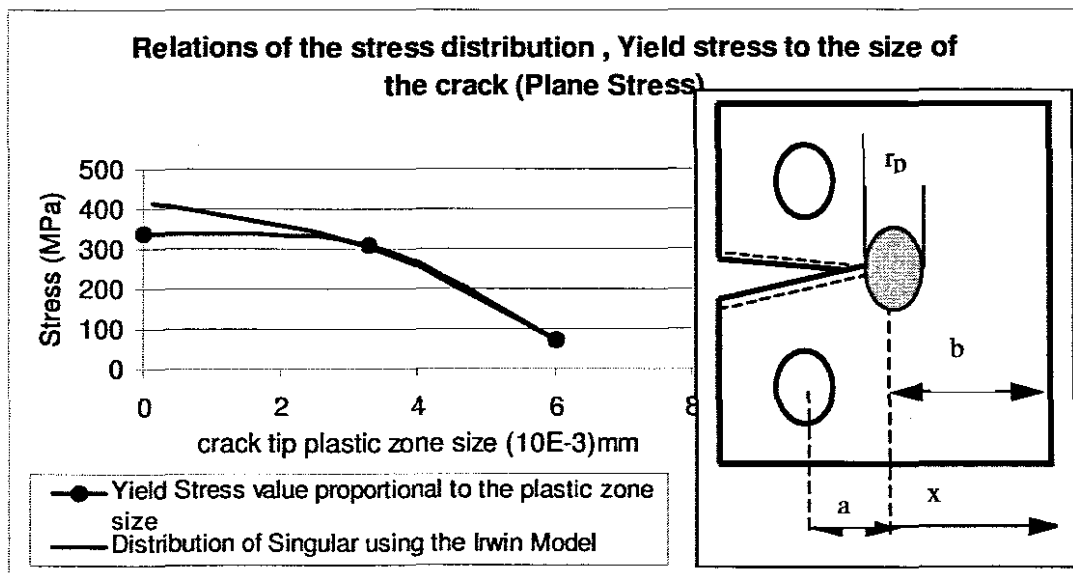


Figure 5.8: Stress distribution related to the crack tip size under plane stress conditions

5.4.4 Determining the value of crack opening displacement (δ)

The COD values were obtained from the experiments and analytically. Using equation (2.16), the value of critical COD is 0.0665mm while the standard COD is calculated using expression (2.14). It is also possible to determine the COD, using the parameters available from the measured crack configuration, where $V_p = 0.05\text{mm}$, the value which is obtained by drawing a line parallel to the line of plastic zone joining with the maximum load; $z=0$; $r = 0.15\text{mm}$; $\nu=0.3$; $b=(W-a)=50-17.5=32.5\text{mm}$. Utilizing the above parameters in equation (2.17), we have the standard $\delta = 0.011\text{mm}$.

The value of δ shows that it is far too small to be accurately measured under experimental conditions. Perhaps the use of a strain gauge might be the means to measure the extent of the crack opening displacement. The value of δ has an important role to play in the formulation of the sensor equation presented in chapter 6.

Inclination (θ)	Stress Intensity factor $K_{IC}(MPa\sqrt{m})$	Poisson ratio (ν)	Material Yield Stress σ_Y (MPa)	Plastic Zone Size (r_p)m (Plane Stress)	Plastic Zone Size (r_p)m (Plane Strain)
0°	59.62	0.3	340	$3.292 \cdot 10^{-3}$	$4.896 \cdot 10^{-3}$
0.5°	59.62	0.3	340	$3.292 \cdot 10^{-3}$	$4.896 \cdot 10^{-3}$
1°	59.62	0.3	340	$3.335 \cdot 10^{-3}$	$4.897 \cdot 10^{-3}$
1.5°	59.62	0.3	340	$3.356 \cdot 10^{-3}$	$4.898 \cdot 10^{-3}$
2°	59.62	0.3	340	$3.377 \cdot 10^{-3}$	$4.899 \cdot 10^{-3}$
10°	59.62	0.3	340	$3.696 \cdot 10^{-3}$	$4.97 \cdot 10^{-3}$
20°	59.62	0.3	340	$4.037 \cdot 10^{-3}$	$5.178 \cdot 10^{-3}$
30°	59.62	0.3	340	$4.306 \cdot 10^{-3}$	$5.486 \cdot 10^{-3}$
45°	59.62	0.3	340	$4.556 \cdot 10^{-3}$	$6.015 \cdot 10^{-3}$

Table 5.4: Summary table representing the experimental values pertaining to the crack plastic zone, size, stress and strain.

5.4.5 Determining the crack length value (a_i)

The value of crack length can be determined from the results of the fatigue test,

The values of crack length obtained from the experiment are shown in the figures below, in relation to other parameters such as applied load, potential energy (U), no of cycles, (N) and the stress intensity factor (K_{IC}).

The results from the experiments indicate that the value of the applied load during the pre-crack initiation stage is expected high. However, the picture changes as the crack is initiated. Further propagation causes the load to reduce sharply. This is due to the fact that as the crack travels, the lesser the fracture resistance is built-up. At a given point, the value of the reduced load tends to remain constant for the rest of the crack travel.

Parameters such as the amount of the energy U and applied load rate contribute in the initiation of the crack and its propagation. Figures 5.10 and 5.11 show the relationship.

The crack length propagation is also a function of the "lifetime", which is determined by the number of cycles N of loading that the specimen is subjected. During the fatigue test, the hysteretic loop is formed defining the limit of the maximum load, as well as the range of the cycling distance in (mm). Typical cyclic loading of the specimen is indicated on figure 5.12.

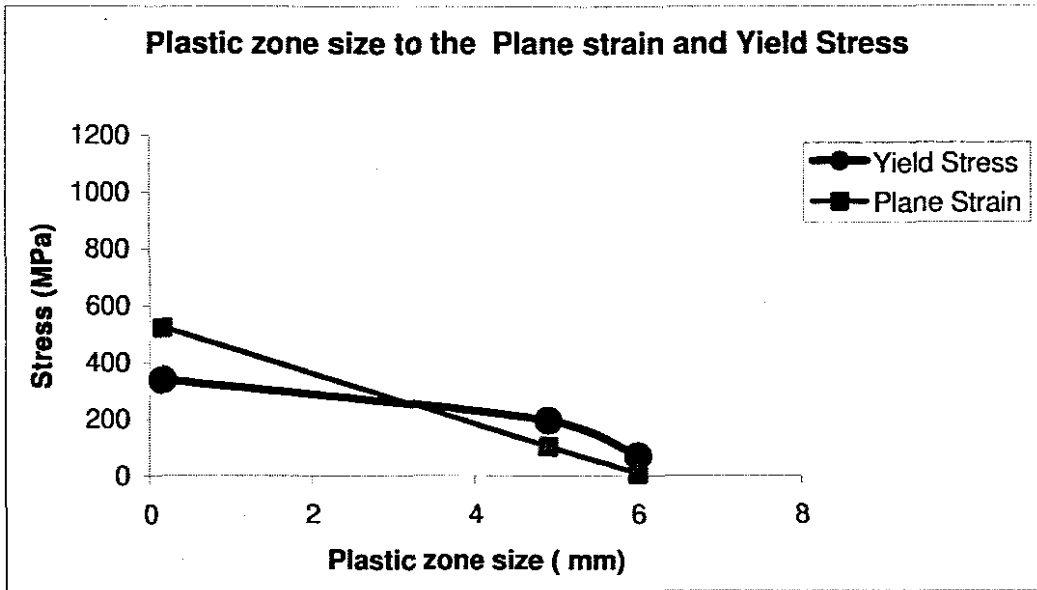


Figure 5.9: Yield stress and plane strain as they affect the value of plastic zone size

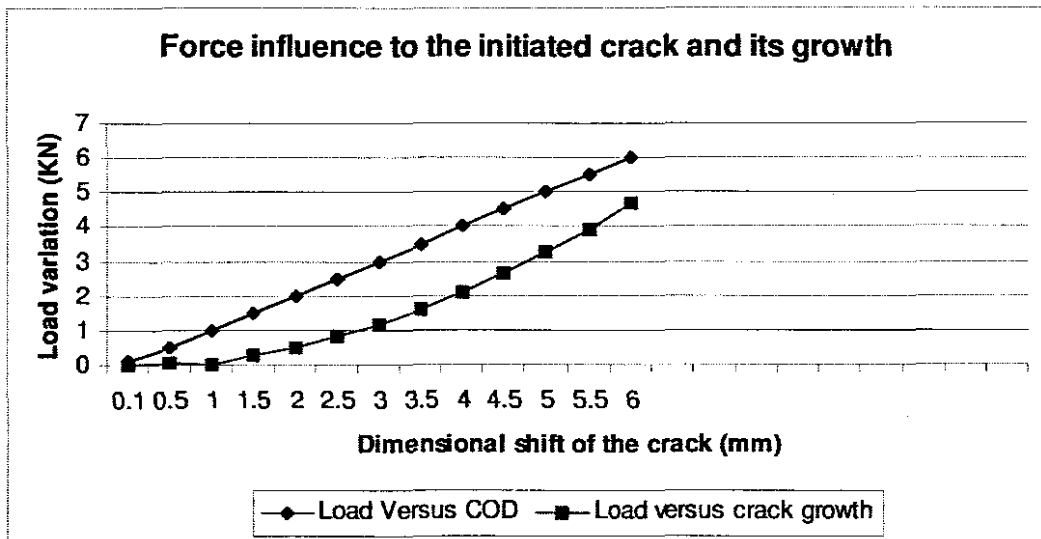


Figure 5.10: Influence of load on the COD and the crack length.

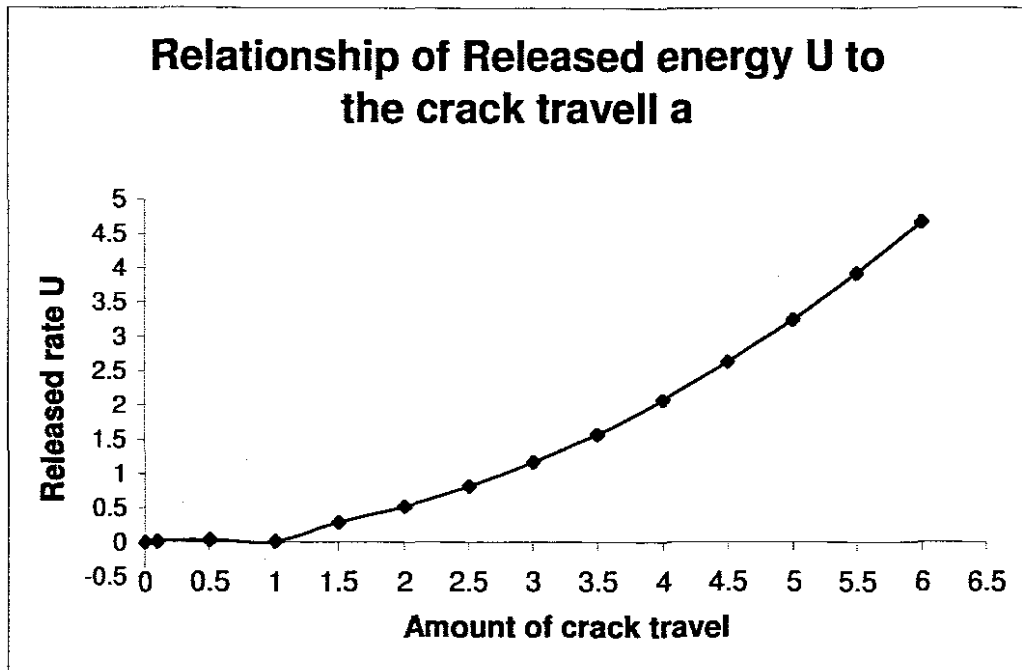


Figure 5.11: The effect of released energy rate to the crack growth

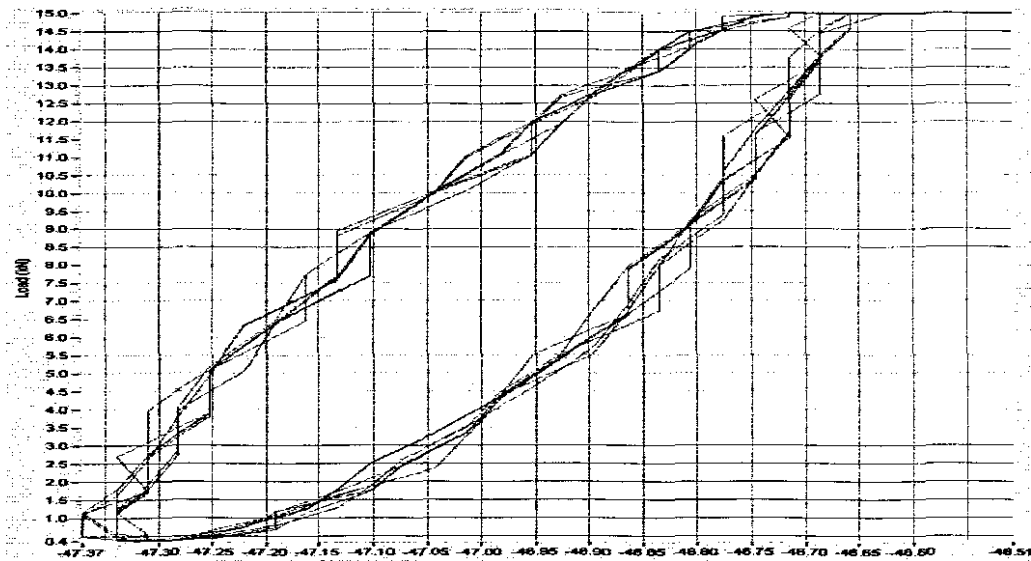


Figure 5.12: Typical Stable hysteresis loop obtained experimentally

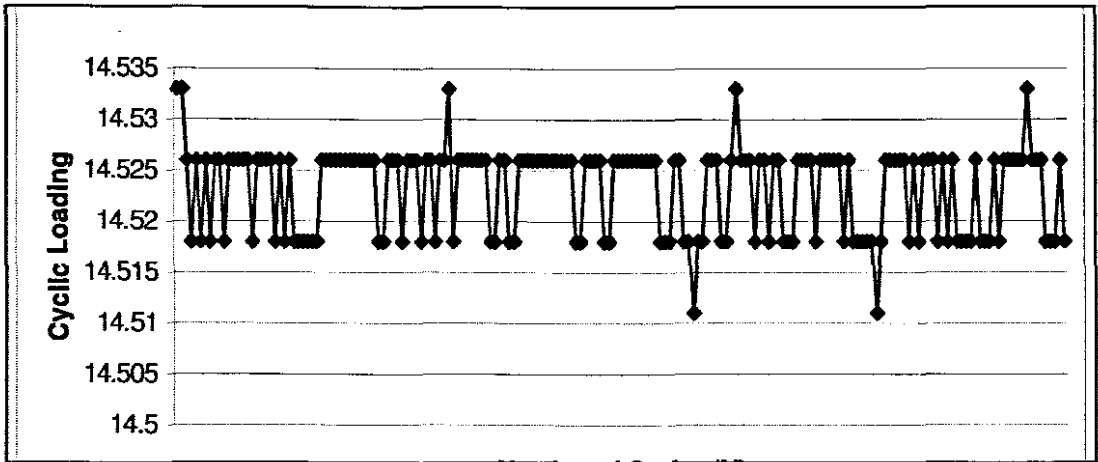


Figure 5.12: Values of Compressive and tensile loading for a number of cycles (N).

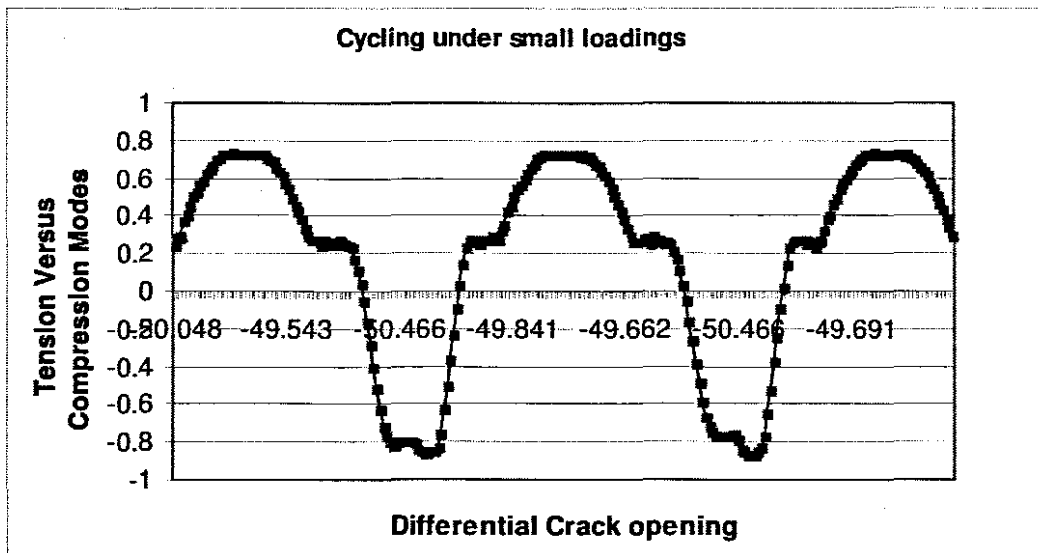


Figure 5.13: Tension/compression under fatigue loading

Chapter 6

6.0 The Effect of Optical Fiber Elongation to its Performance as a Light Conduit

6.1 Introduction

Background information on optical fiber properties was presented in chapter 2, sections 2.2; 2.4; and 2.5, while in chapter 3 we discussed the concept of networking optical fibers with engineering components to produce a failure warning sensor.

Results obtained during experiments when stressing the optical fiber sensor, have shown up influencing factors such as the fiber gripping mechanism, finish quality of the end of the fiber, direction of the force action etc. There exists a relationship between the mechanical deformation and the amount of the light or light intensity that is transmitted through the optical fiber.

6.1.1 Influencing factors on the optical fiber output

The set-up for manufacturing an optical fiber sensor is fairly complex. Depending on the methods used in fabricating the test piece, i.e by bonding and joining the various materials, or the type of holding and gripping devices; or the direction of the applied load, the amount of the light throughput varies accordingly. The optical fiber presents a challenge when embedded in the host specimen due to the fact that its inner diameter has cladding with plastic material. This presents problems in the case when the axial load is applied through the test piece on the optical fiber thus attempting to stretch it.

The outer plastic material (or fiber cladding) is meant to serve as the containment for the light to travel without attenuation through it; as well as protecting the inner material i.e the optical fiber from damage due to micro-bending, impact forces etc.

However, the cladding has the disadvantage, that under a pulling load, it tends to slip off from the core material. This is a drawback in that it gives false information about the actual deformation of the optical fiber.

This fact was observed during our experiments; therefore it is imperative that the gripping mechanism holds rigidity both end points of the OF during the pulling process.

It is also important that the alignment of the axes, i.e. fiber axis and that of the testing machine, be inline. Misalignment may cause micro-bending on the optical fiber, which might be a contributing factor towards light output efficiency.

Figure 6.1 shows the design of the optimum gripping mechanism that has been adopted.

6.1.2 Experimental Procedures

The following steps were taken as we attempted to observe the behaviour of the optical fiber in a “stand alone” situation when subjected to a tensile load. (see figure 6.1)

- Strip the fiber as described in section 3.2.1.
- Prepare fiber ends with ferrules (fiber cemented into ferrules)
- Fix the the ferrules between the gripping jaws.
- Select the suitable load range for the tensile testing machine
- Start the tensile test, monitor the extension of the optical fiber
- Monitor and record the fiber elongation till fracture occurs.

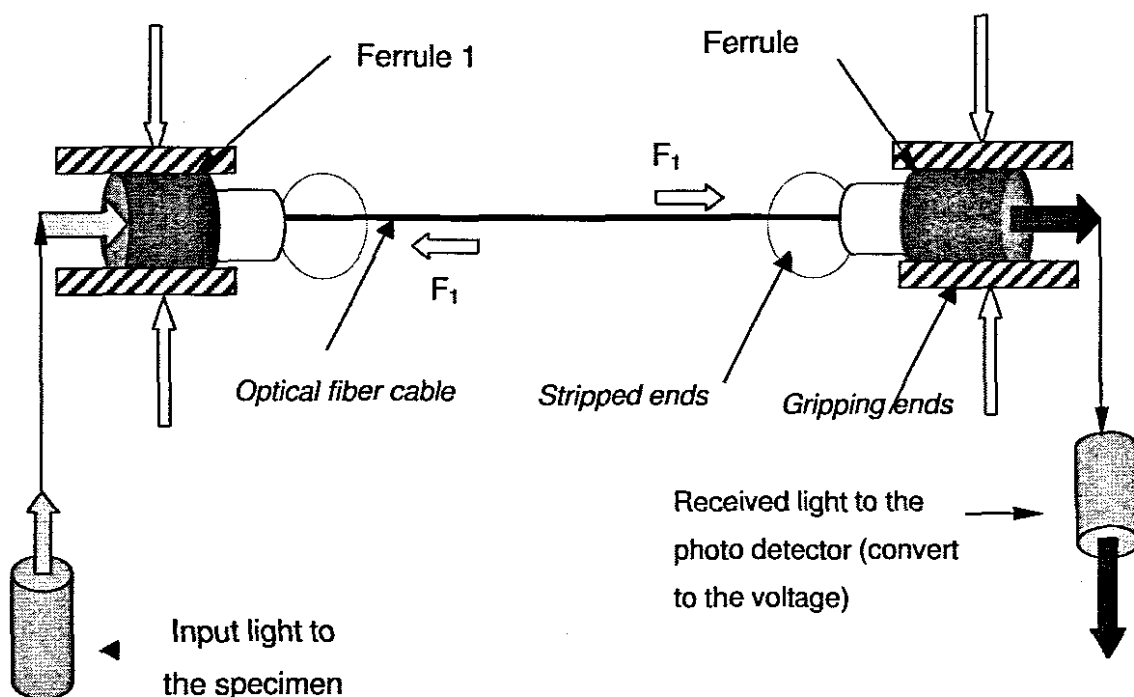


Figure 6.1: Schematic diagram of the gripping of optical fiber during the elongation test.

In order to ensure proper gripping of the fiber ends, the ends of the fiber are stripped from their cladding. They are inserted through sleeves or ferrules and cemented in position by applying an adhesive. This action ensures strong bonding which resists the fiber cable from slipping in the machine jaws during the application of the tensile force. From both ends of the fiber beyond the ferrules, a reasonable amount of stripped length of fiber was provided. The protruding lengths (about 10mm) were spliced with optical fibers from the light

source and the photo detector respectively. The optical fiber carried the light from the source (emitter), through ferrules 1 and 2 and reached the photo detector, which converted the light intensity into a voltage read out. The optical fiber between the two ferrules 1 and 2 was stretched under a tensile load, observing its elongation and recording the voltage read out as a function of light intensity through the optical fiber.

6.2 Preparing a failure warning sensor

The test for the optical fiber deformation when embedded into a host specimen was carried out on a fatigue-testing machine as indicated earlier in section 5.3.1.

Three optical fibers were placed transversely to the crack's intended direction of propagation at an interval of 2mm apart, one at a point behind the notch tip (fiber no 1); one at the tip of the notch (fiber no 2) and another at a distance of 2mm in front of the notch tip (fiber no 3).

The fiber specimens were laid into 1mm depth grooves, and cemented in place leaving a span or "gauge length" of 4mm between the fixed ends. The schematic of the test specimen as a failure-warning sensor is shown in figure 6.2.

The optical fibers extending from both sides of the specimen were terminated with ferrules that connected, to the light source and to the photo detector, respectively.

During the fatigue testing the crack initiates and propagates along the x -direction while at the same time the crack widens and the embedded fibers extend along the y -direction. Therefore, we observe that the amount of the crack widening or opening has the same value as the extension of the particular optical fiber.

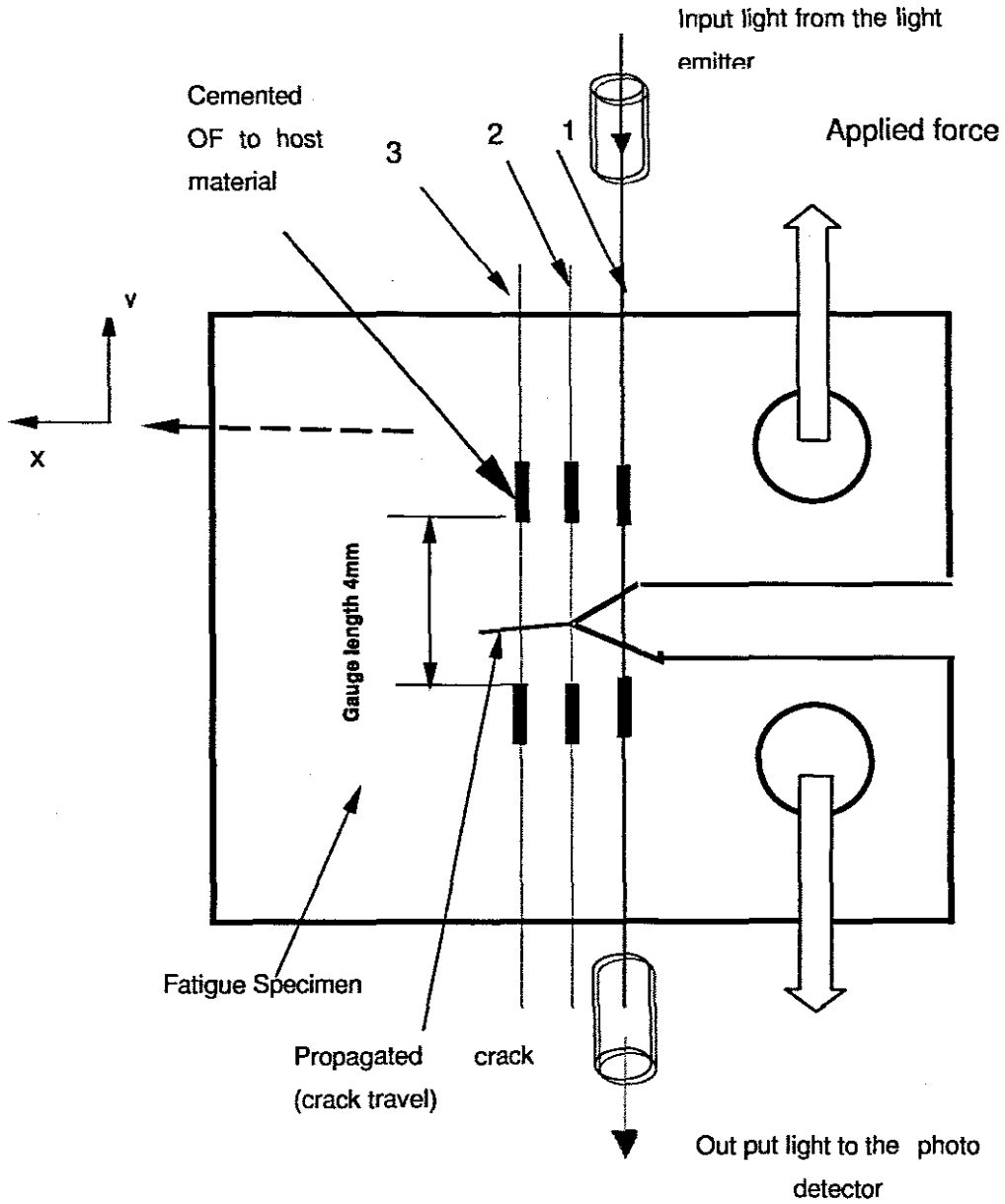


Figure 6.2: Schematic diagram of optical fibers embedded within the test specimen.

6.3 Discussion

6.3.1 Optical fiber extension due to loading

This section discusses the outcomes from the tensile test on an individual optical fiber (stand alone) as well as during the time that fibers were embedded in the host specimen.

Figure 6.3 shows the plasticity behaviour of the OF, where the constant increase of the tensile load on it, is proportional to its strain. The graph shows that at the start of the tensile test there is a sudden rise of the load with a negligible increase of fiber elongation. This was the cause of the pre-load of about 1KN on the fiber before the actual test had begun. At the conclusion of the test, the optical fiber had undergone a total elongation of 1.73mm, just before the instant that failure occurred.

6.3.2 Voltage output (light intensity) versus optical fiber elongation

Under the conditions of stretching the OF while light was being transmitted through it, the following was observed. In figure 6.4 we note that the light intensity (as measured voltage) begins to decline proportionally, while the OF elongation increased up to approximately 1.3mm. Further loading caused a non-linear voltage reduction against a non-linear increase in elongation, until finally the voltage dropped sharply to zero as the optical fiber elongated to 1.7mm just prior to failure.

6.3.3 Voltage output of the OF due to tensile loading

The stretching of the optical fiber affects the optical fiber geometry by increasing its length, while its diameter decreases. In figure 6.5, the graph characterises the trend of light intensity through the fibers voltage output from the light detector against tensile loading of an individual optical fiber.

The test begins by increasing the load gradually, to stretch the specimen. We note that, as we apply load, the value of the voltage out put decreases, which is in accordance with previous work by Takeda Nobuo; et el [45].

6.3.4 Interdependence of the applied tensile load, light intensity output and elongation of the OF

Figure 6.6 is presented for the purpose of demonstrating the interdependence of the variables measured when we subjected the OF as a stand alone specimen to a tensile load until failure occurred. The results are as expected, in that with an increase in loading the specimen elongates, which in turn affects the amount of light that is allowed through it, until when maximum load for failure is reached the fiber breaks and no light is transmitted.

6.3.5 Determination of the light intensity output value relative to the crack opening

Figure 6.7 presents the relationship of the crack opening with respect to the light through put (as a voltage). As the crack propagates and grows, it opens further, and the elongation of the fiber that is positioned at a given spot monitors this crack opening.

Therefore the elongation of each fiber, which is indicated by the light intensity through it, can be associated with the measured crack growth.

The significance of using the optical fibers embedded in the test specimen is to have real time information on the crack occurrence at the tip of the notch of the sensor specimen.

In order to detect the crack a fiber must be positioned before the notch tip. It is felt that in this manner the crack will be detected as it has grown to a certain size commensurate with sufficient crack opening and hence fiber elongation which will be signalled by a decrease of light intensity through the fiber.

6.4 Experimental results

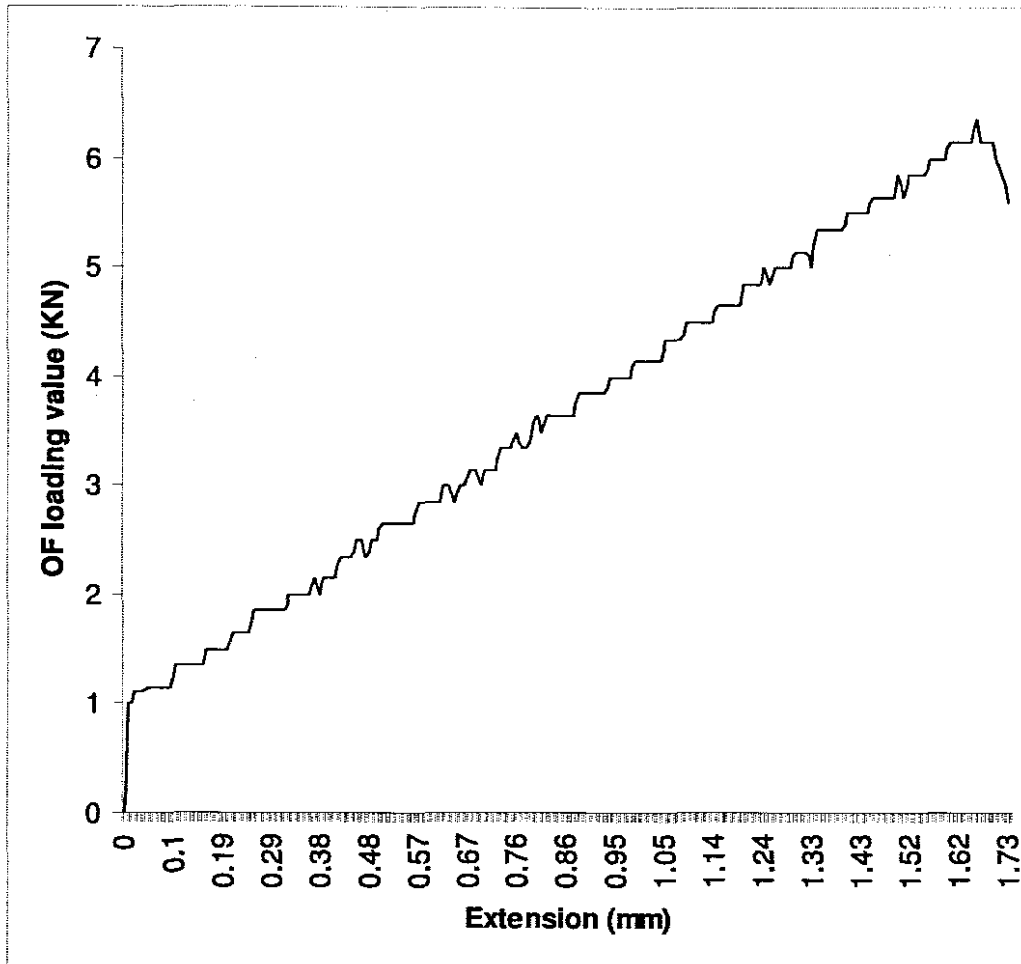


Figure 6.3: Typical results from individual optical fiber elongation under tension

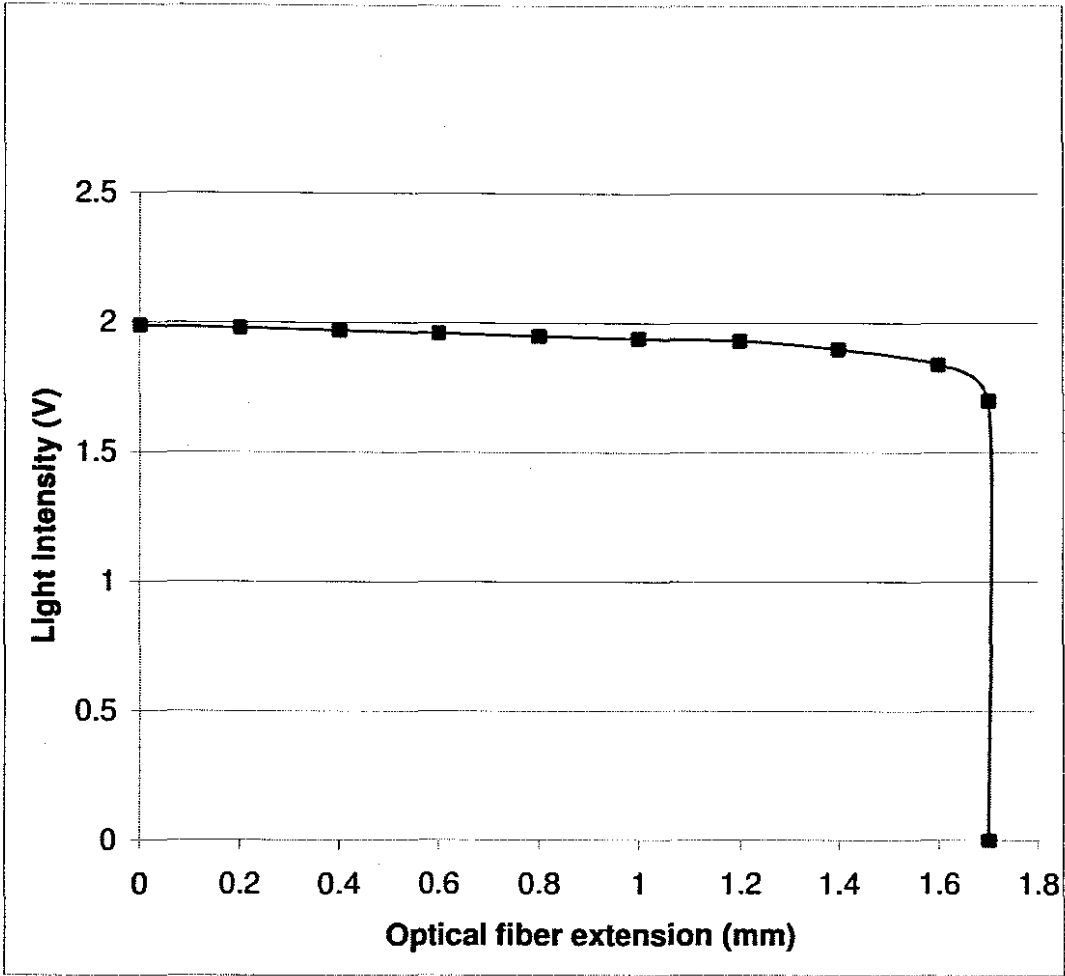


Figure 6.4: Decrease of light intensity through the optical fiber versus fiber elongation

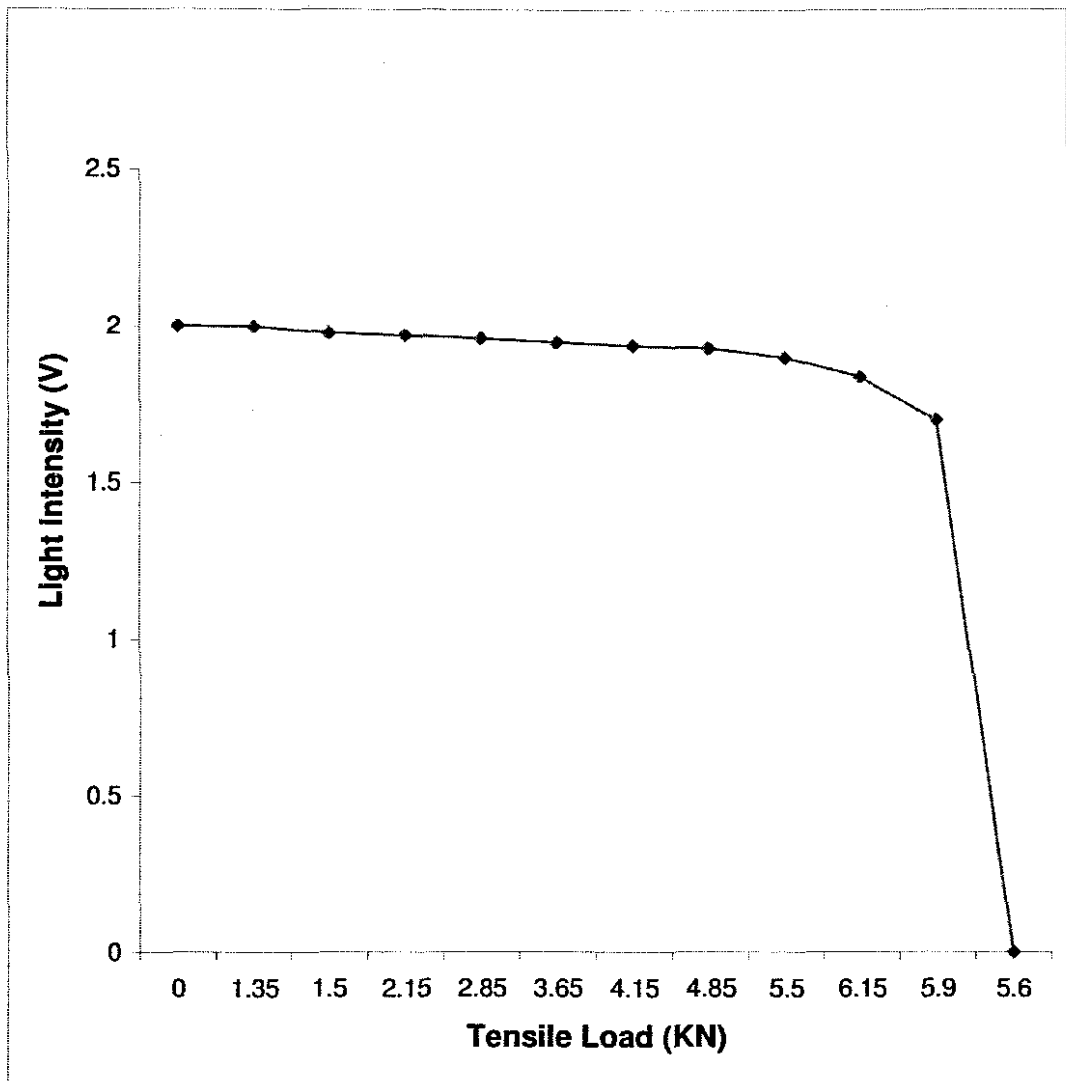


Figure 6.5: Voltage drop manifesting light intensity through the OF versus applied load in stretching the OF.

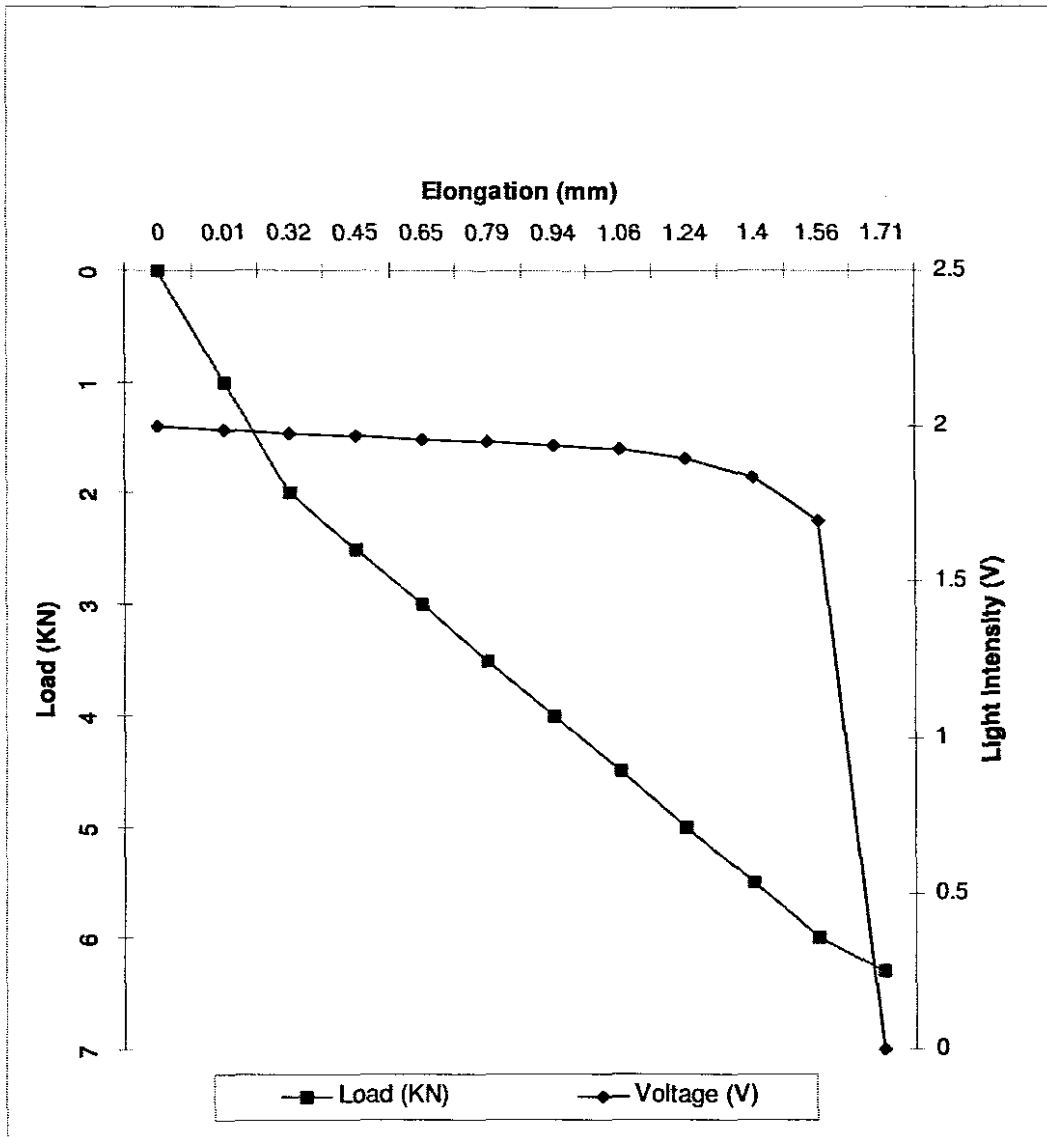


Figure 6.6: Light intensity through the OF as a function of tensile load and fiber elongation

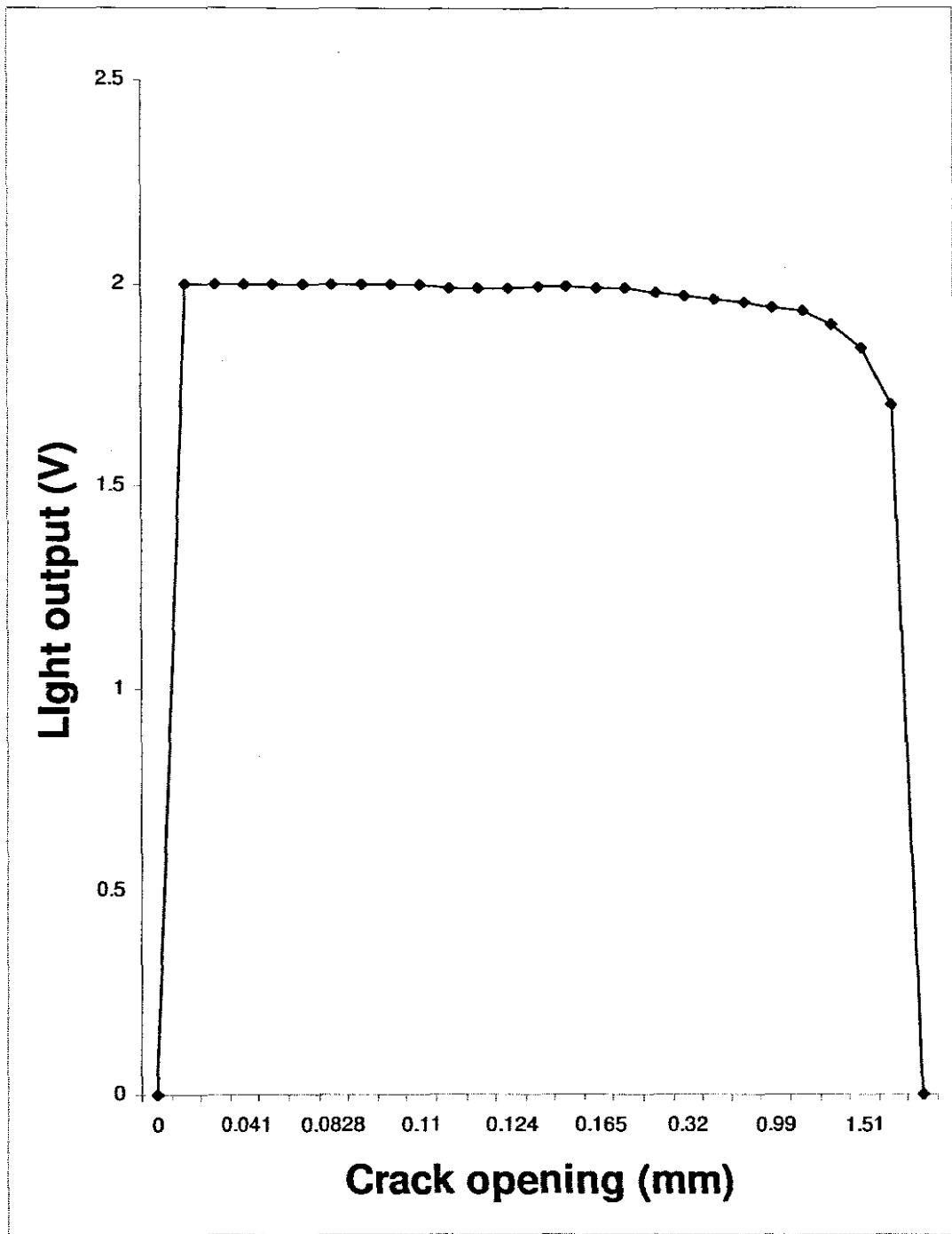


Figure 6.7: Fiber light intensity output versus crack opening

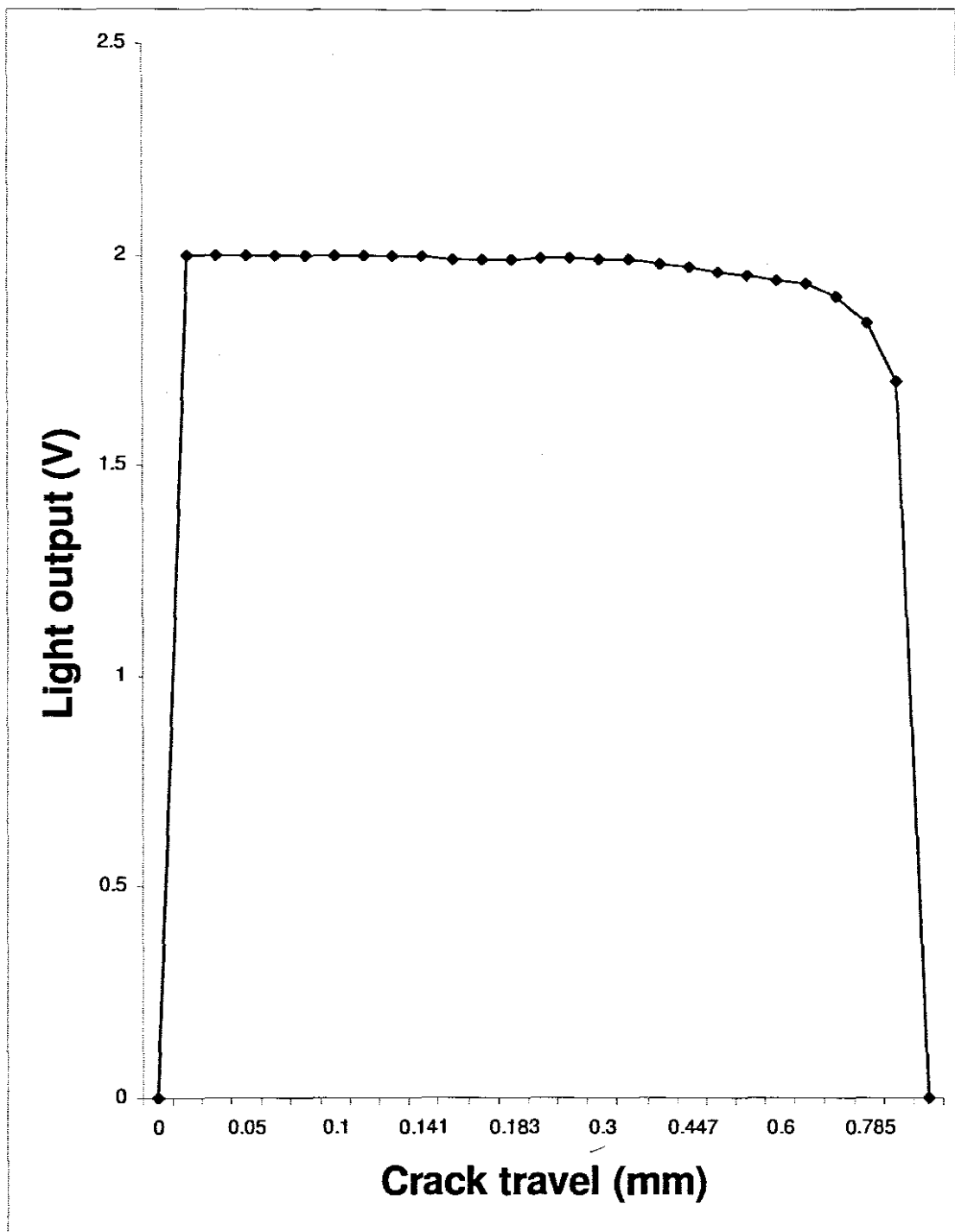


Figure 6.8: Fiber light intensity output versus crack travel

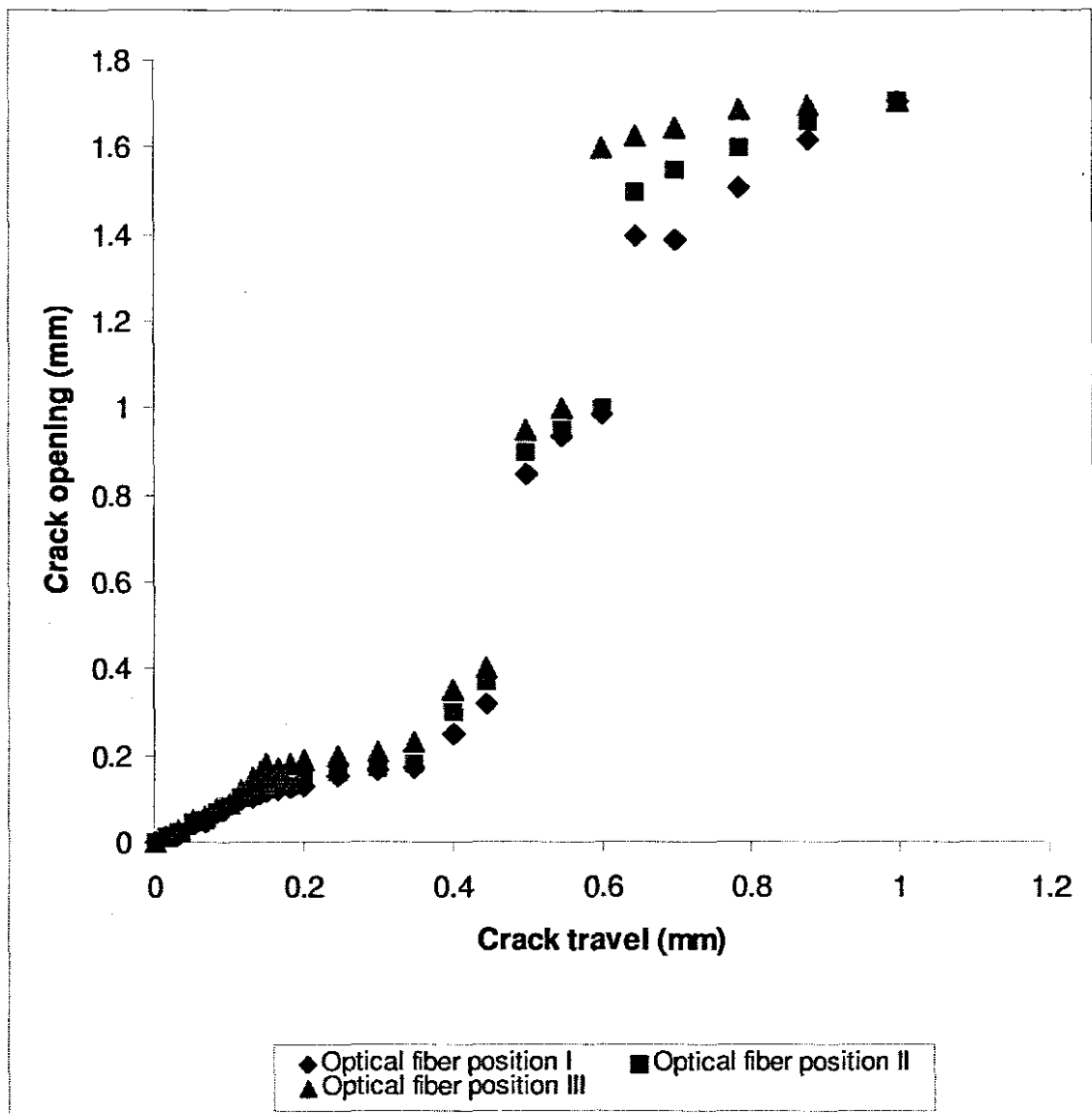


Figure 6.9: Relationship between the crack travel and opening for the positions I, II; and III of the optical fibers.

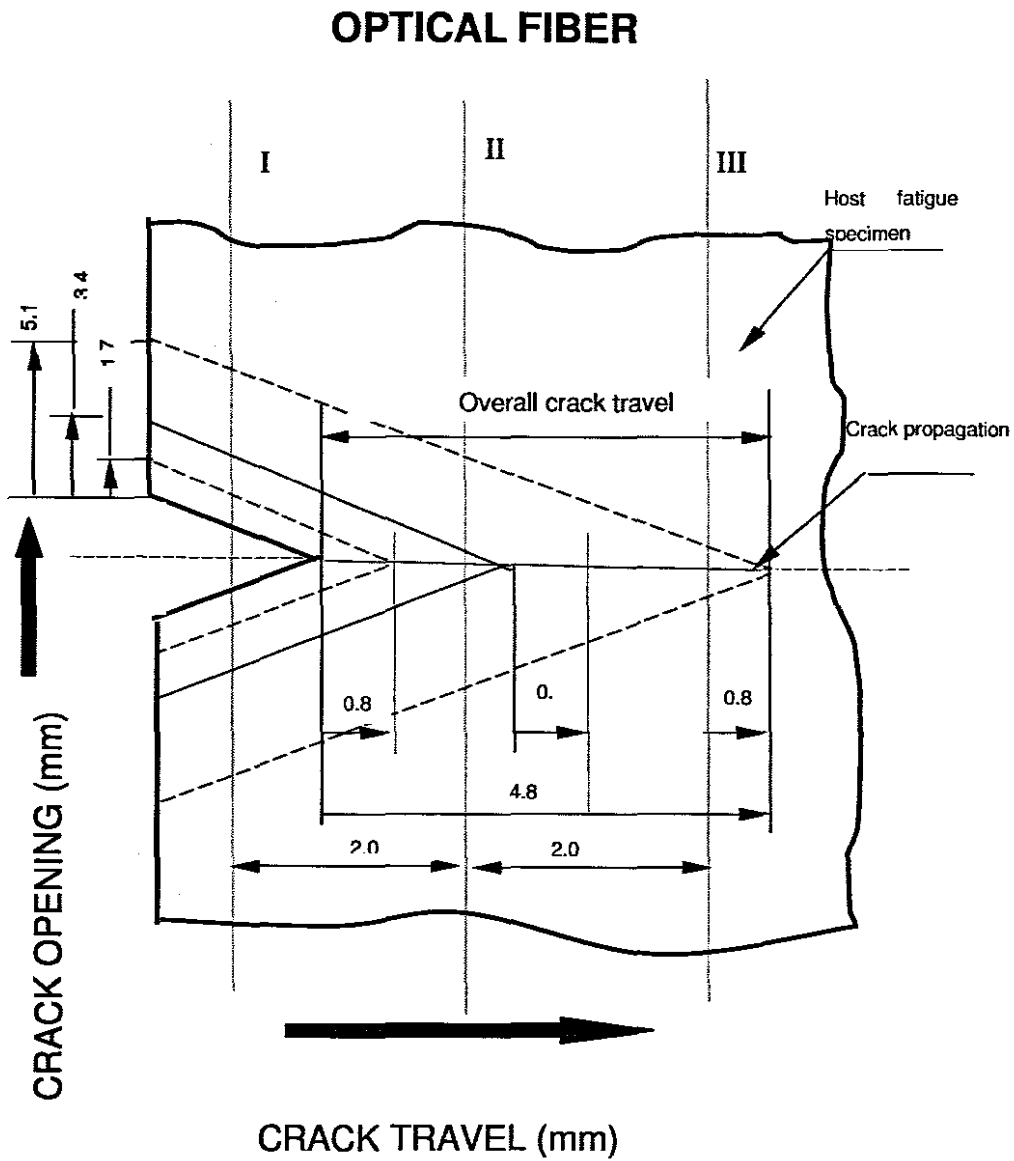


Figure 6.10: Schematic diagram indicating the crack travel trend versus crack opening for the three positioned optical fiber. (All dimensions in mm)

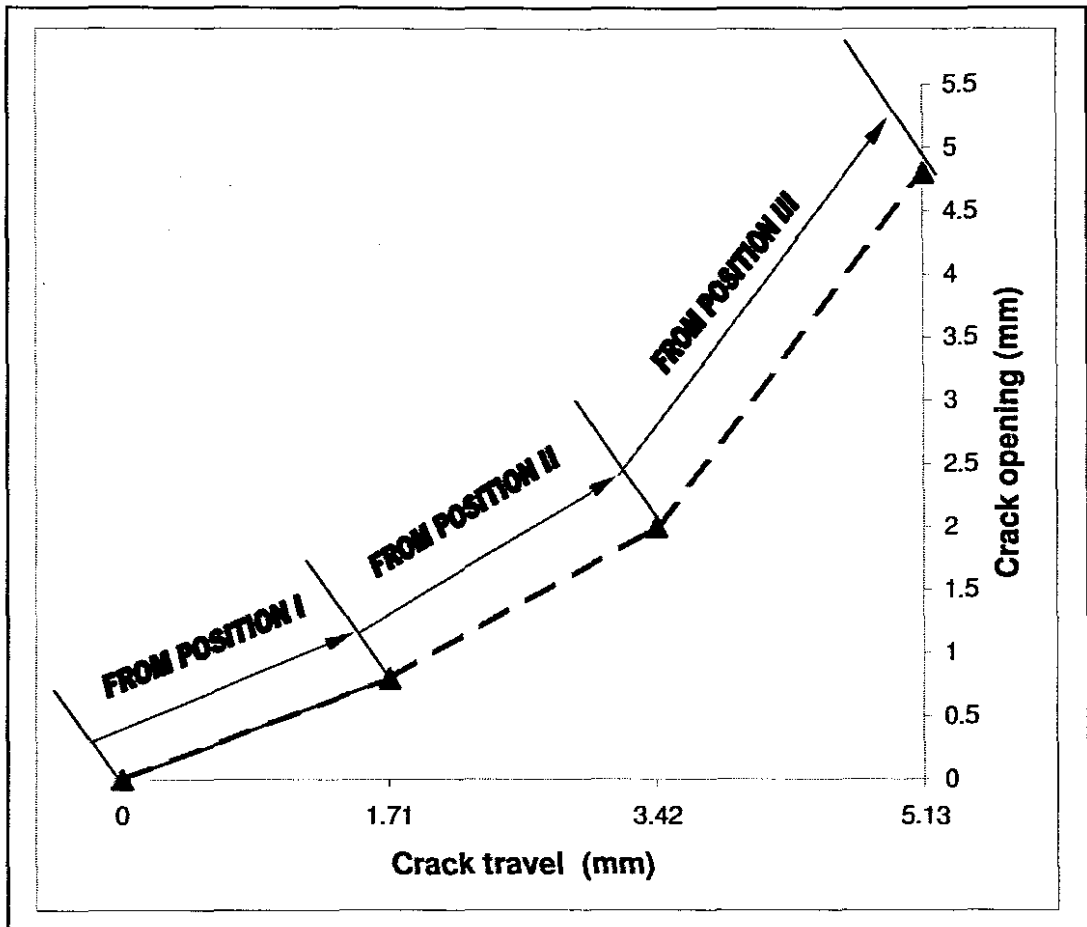


Figure 6.11: Overall-crack travel versus crack opening as viewed from position I

Chapter 7

7.0 Influencing Parameters in Formulating the Sensor Equation

7.1 Introduction

This chapter attempts to coordinate knowledge from the areas of fracture mechanics and optics and apply it to a single system that is able to function as a crack detection sensor. Each of the above mentioned knowledge areas are described by parameters, some of which could be integrated, in formulating the sensor equation.

The, sensor equation could perhaps comprise variables from fracture mechanics such as crack length a , Crack opening δ , plastic zone size r_0 and stress intensity factor K_{IC} . These parameters are normally obtained from the fatigue test on standard specimens.

The variables for the optical fiber mechanical properties such as tensile stress (σ_f), shear stress (τ), imposed strain (e), are obtained from tensile tests on the optical fibers.

The optical response of the fiber optic would involve variables such as optical

beam wavelength (λ) and light intensity (v) as voltage output

All the above-mentioned parameters are considered to be influencing factors that should characterize the system's response to mechanical deformation.

7.2 The area common around the deformation of the work piece and the embedded fiber (Mechanical).

The active area of sensing, is the common area of the crack propagation path and points of intersection of the fibers embedded in the specimen perpendicular to the probable crack propagation path. This area is common to mechanical deformation of the two materials, which incidentally have different mechanical properties.

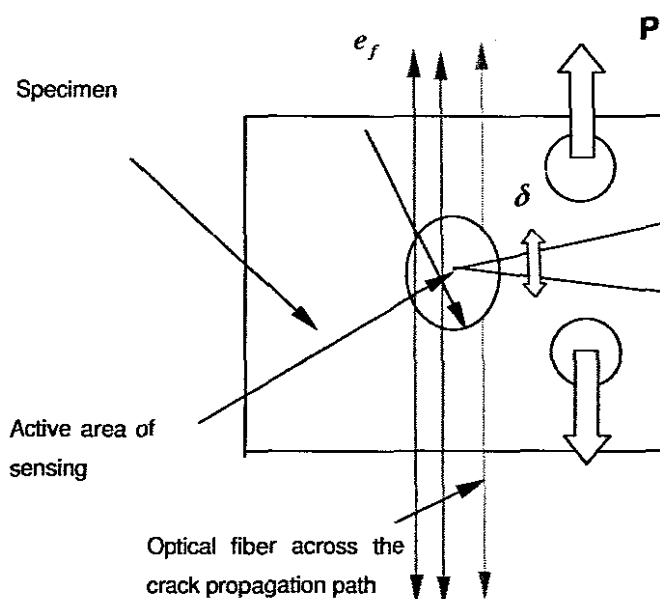


Figure 7.1: Area of sensing

During the process of the crack growth, it is assumed that not all the energy is consumed to form a new microscopic surface. At the point of intersection of the propagated crack and the optical fiber, there is dissipation of energy,

which takes place at a microscopic level in the form of yielding continuum mechanics.

The optical fiber is subjected to extension due to the opening of the crack. Therefore the opening of the crack, it can be said, is proportional or better equal to the extension of the optical fiber, where it is situated.

7.3 Mechano-opto relations

Both deformation of the fiber and the work piece are mechanical actions. Since the embedded fiber is assumed to elongate relative to the extent of the crack opening, a change in fiber geometry takes place. As the fiber extends it tends to reduce its diameter. This phenomenon has direct influence on the amount of light passing through it. Later in this chapter we discuss the development of the sensor equation, which brings together the crack propagation and fiber extension phenomena.

7.4 Development of the sensor equation

7.4.1 Formulation of the sensor equation.

Our sensor equation is developed in order to afford the quantification of a suitable system in the detection of crack initiation and propagation.

The model showing the relationship of the opto-mechanical; and opto-electrical parameters for the developed sensing system is shown on figure 7.2

7.4.1.1 Deformation of the optical fiber.

The stress developed on the optical fiber as a result of its extension is

$$\sigma_f = \frac{P_f}{A_f} = E_f \varepsilon_f \left[1 - \frac{\cosh \beta(l/2 - x)}{\cosh \beta(l/2)} \right] \text{ (Equation 2.49 repeated)}$$

We are able to solve for the strain on the fiber during elongation under the

tensile load

$$\epsilon_f = \frac{F_f}{A_f E_f} \left[\frac{\cosh \beta \left(\frac{l}{2} \right)}{\cosh \beta \left(\frac{l}{2} \right) - \cosh \beta (l-2)} \right] \quad (7.1)$$

But the term $\left[\frac{\cosh \beta \left(\frac{l}{2} \right)}{\cosh \beta \left(\frac{l}{2} \right) - \cosh \beta (l-2)} \right]$ in the above equation is

equal to unity; (for short length fibers). The value of strain (ϵ_f) of the optical fiber is obtained by the elongation divided by its original length (gauge length) (l_f)

Therefore

$$\epsilon_f = \frac{\Delta l_f}{l_f}$$

and since

$$E_f = \frac{\sigma_f}{\epsilon_f}$$

Substituting the value of ϵ_f into the expression above we obtain

$$E_f = \frac{\sigma_f l_f}{\Delta l} \quad (7.2)$$

Hence the fiber elongation is expressed by

$$\Delta l = \frac{F_f l_f}{A_f E_f} \quad (7.3)$$

Equation (7.3) describes the elongation of the optical fiber

7.4.1.2 Relationship between the host specimen deformation and the optical fiber elongation.

The physics of the problem dictate, that the crack opening is identical to the fiber elongation at the given position where the fiber is embedded.

Recalling the elongation equation on the optical fiber equation (7.3) and the crack opening of the host specimen equation (2.49), we have

$$\Delta l_i = \delta_{(i)} \quad (7.4)$$

Therefore

$$\Delta_{(i)} = \frac{F_f l_f}{A_f E_f} \quad \text{and} \quad \delta_{(i)} = \frac{K_{(i)}^2 (1 - \nu^2)}{2\sigma_{ys} E} + \frac{0.4(W - a)v_p}{0.4W + 0.6a} \quad (7.5)$$

From the equation above, we are able to determine the optical fiber diameter in relationship to the applied load.

$$d_{f(i)} = \sqrt{\frac{4}{\pi F_f l_f E_f} \left[\frac{K_I^2}{2\sigma E} + \frac{0.4(W - a)v_p}{0.4W + 0.6a} \right]} \quad (7.6)$$

The changes in optical fiber diameter is obtained by differentiating equation (2.6) above is written as

$$d_f = \sqrt{C \left[\frac{1}{F_f} \right]} \text{ and}$$

$$\frac{\Delta d_f}{\Delta F_f} = -\frac{1}{2} \sqrt{C F_f^{-3}} \quad (2.7)$$

$$C = \sqrt{\frac{4}{\pi d_f E_f} \left[\frac{K_f^2}{2\sigma E} + \frac{0.4(W-a)\nu_p}{0.4W + 0.6a} \right]}$$

Where C are the optical constants of the optical fiber and the host specimen

7.4.1.3 Relationship between optical fiber diameter change and the optical output power .

The change of the diameter of the optical fiber due to its elongation can be related to a change of transmitted power. Recalling equation (2.65) we have the ratio of input to the out power given by

$$\frac{P_r}{P_o} = \left[1 - \left(\frac{\Delta d}{d} \right)^2 \right] \text{ Equation (2.65) repeated}$$

Solving for the change in OF diameter Δd , we have

$$\Delta d = - \left(\frac{P_{(r)}}{P_{(o)}} - 1 \right)^{\frac{1}{\alpha}} d_f \quad (7.8)$$

By substituting equation (7.7) into (7.8) we have

$$\Delta d = - \left(\frac{P_{(r)}}{P_{(o)}} - 1 \right)^{\frac{1}{\alpha}} d_f = - \frac{\sqrt{C}}{2} \sqrt{\frac{1}{F^3}} \quad (7.9)$$

$$P_{(o)} = \frac{(P_{(r)} - 1)d_f}{\left[\frac{\sqrt{C}}{2} \sqrt{\frac{1}{F^3}} \right]^{\alpha}} \quad (7.10)$$

Equation (7.10) characterizes the optical power in the fiber due to deformation, where $P_{(r)}$ and $P_{(o)}$ are the optical rated power and transmitted power respectively, and d_f is the optical fiber diameter.

In summary, equation (7.10) is interpreted as the sensor equation for the crack detection system in terms of optical power transmission during the deformation of the optical fiber as the result of the host specimen experiencing a crack motion.

7.4.2 Output power transmitted in the optical fiber versus its deformation

It was been previously discussed in chapter 2.6 that the elongation of the optical fiber affects the performance of the light passing through it.

From the sensor equation (7.10) we are able to relate the deformation occurrence that was caused by the applied tensile loading, or by the crack opening of the host specimen. This deformation consequently changes the diameter of the optical fiber, hence the amount of the light passing through it.

Holding the physical parameters constant in equation (7.10), varying the value of the applied load and using the corresponding measured elongation, the fibers' changing diameter can be calculated thus we are able to predict the output power transmitted through the fiber.

The result of the input-output optical power ratio relative to the varying diameter ratio is shown in figure 7.3. As the fiber elongates its diameter (d_o) reduces, approaching zero dimension at rupture conditions. Reduction of light intensity (P_r) is observed during this process.

7.4.3 Development of the OF crack detection sensor model

The model of the sensor is shown here as a schematic diagram incorporating the main parameters that were used in formulating the system for the detection crack initiation and subsequent propagation Figure 7.2 comprises of elements of optical and mechanical inputs as well as light output response in form of voltage read out.

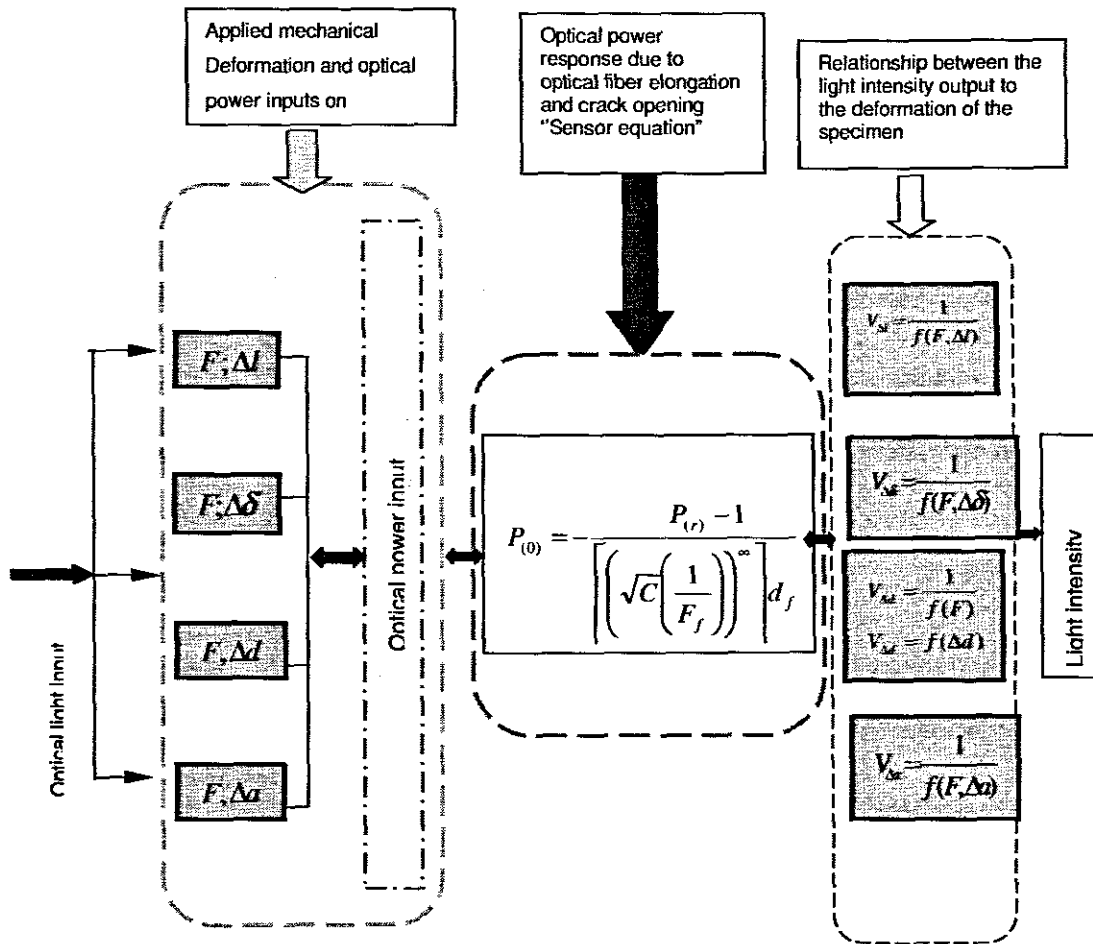


Figure 7.2: Optical fiber crack detection sensor model (CDSM)

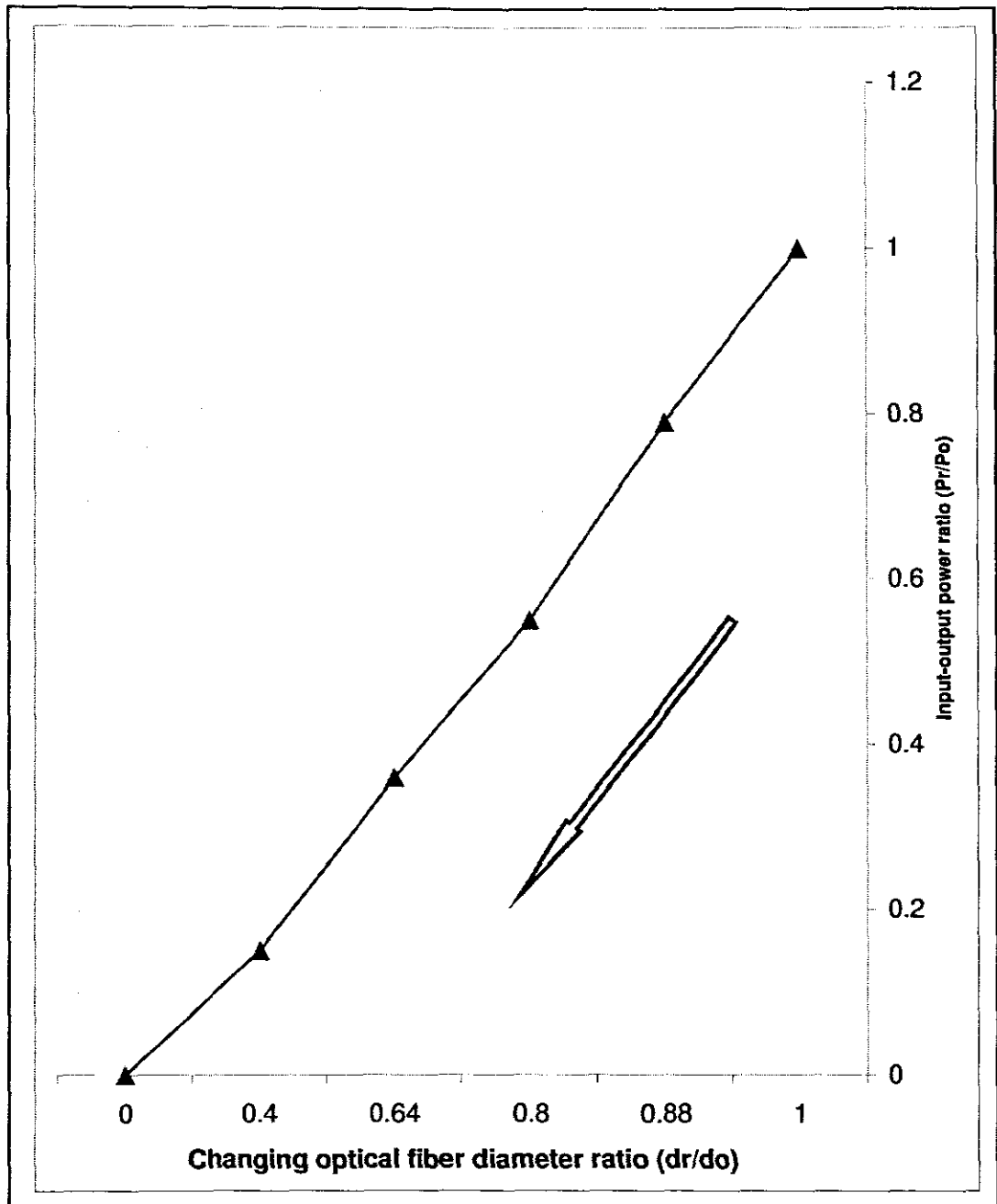


Figure 7 3: Relationship between the input-output power ratio and the change of optical diameter ratio

7.5. Discussion on theoretical –experimental comparison results

7.5.1 Comparison of Theoretical- Experimental results for the individual OF

The results of fiber elongation versus applied load are shown on figure 7.4. They indicate the relationship between the results obtained experimentally, and the theoretical predictions approaches using basic equation (7.3) Both results indicate reasonable agreement in trend.

7.5.2 Comparison of Theoretical- Experimental results for the fatigue loading versus CTOD.

We noted as previously stated that the value of the opening is assumed to be equal to the amount of the fiber elongation. However, in this case it is noted (fatigue specimen) that, with increasing opening of the crack, the lesser load is needed to propagate it. The load decreases at a stepped form to indicate the sudden separation of the material across some areas during fatigue deformation. The CTOD theoretical results were obtained from expression (2.49) and the comparison between the theoretical and experimental results for crack opening due to loading is shown in figure 7.5.

7.5.3 Comparison results of the theoretical- experimental between the optical fiber elongation and crack opening of the host specimen

Figure 7.6 represents the predicted (theoretically) and experimental results for the optical fiber elongation and the crack opening on the host specimen. The predicted result on the OF elongation and hence the crack opening was approximately 1.8mm which slightly exceeds the experimentally determined value of 1.71mm. However, in general the trend of both results is in good agreement.

7.5.4 Comparison of Experimental- Theoretical relationship of light intensity through the fiber against elongation

The comparison of the experimental and that of the predicted light intensity through the fiber while it elongates is shown in figure 7.7.

Reasonable agreement is observed.

7.5.5 Theoretical determination of fiber optical diameter change due to elongation

The phenomenon of the change of the optical fiber's diameter under tension has been previously discusses.

The relationship between the changes in diameter with the respect to its elongation is indicated in figure 7.8 where the increase in optical fiber length due to tensile loading is in proportion to its diameter decrease.

7.6 Validation of Experimental- Theoretical results

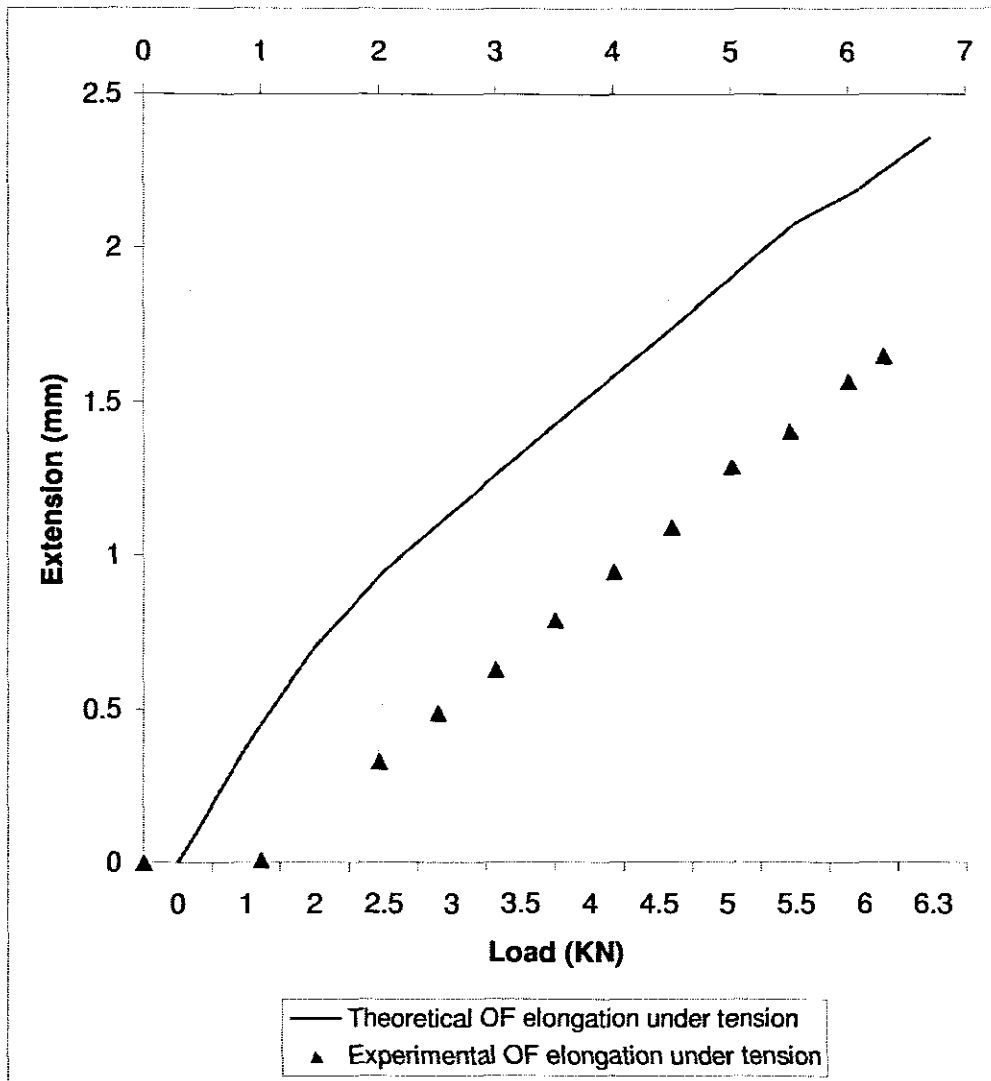


Figure 7.4: Theoretical-experimental comparison of applied tensile load versus elongation of the OF

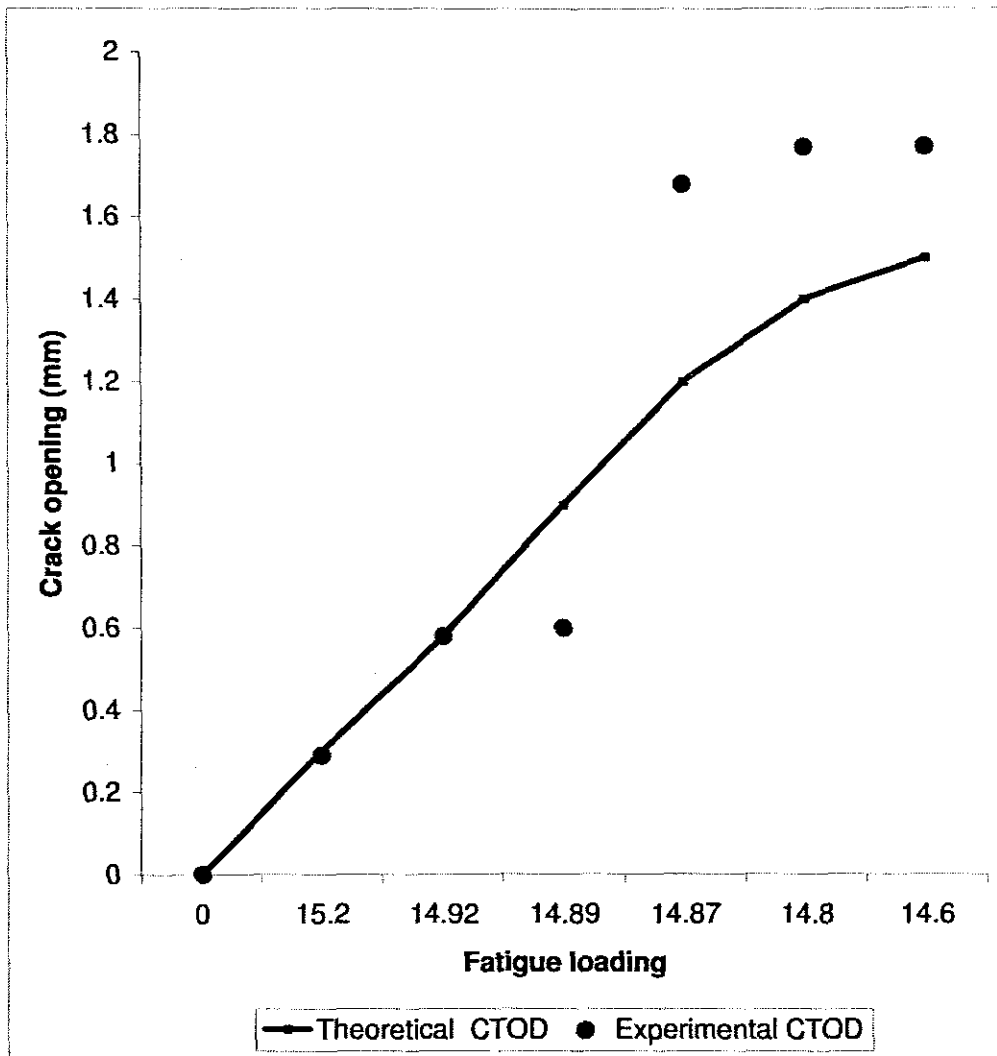


Figure 7.5: Theoretical-experimental comparison for the fatigue load versus crack opening

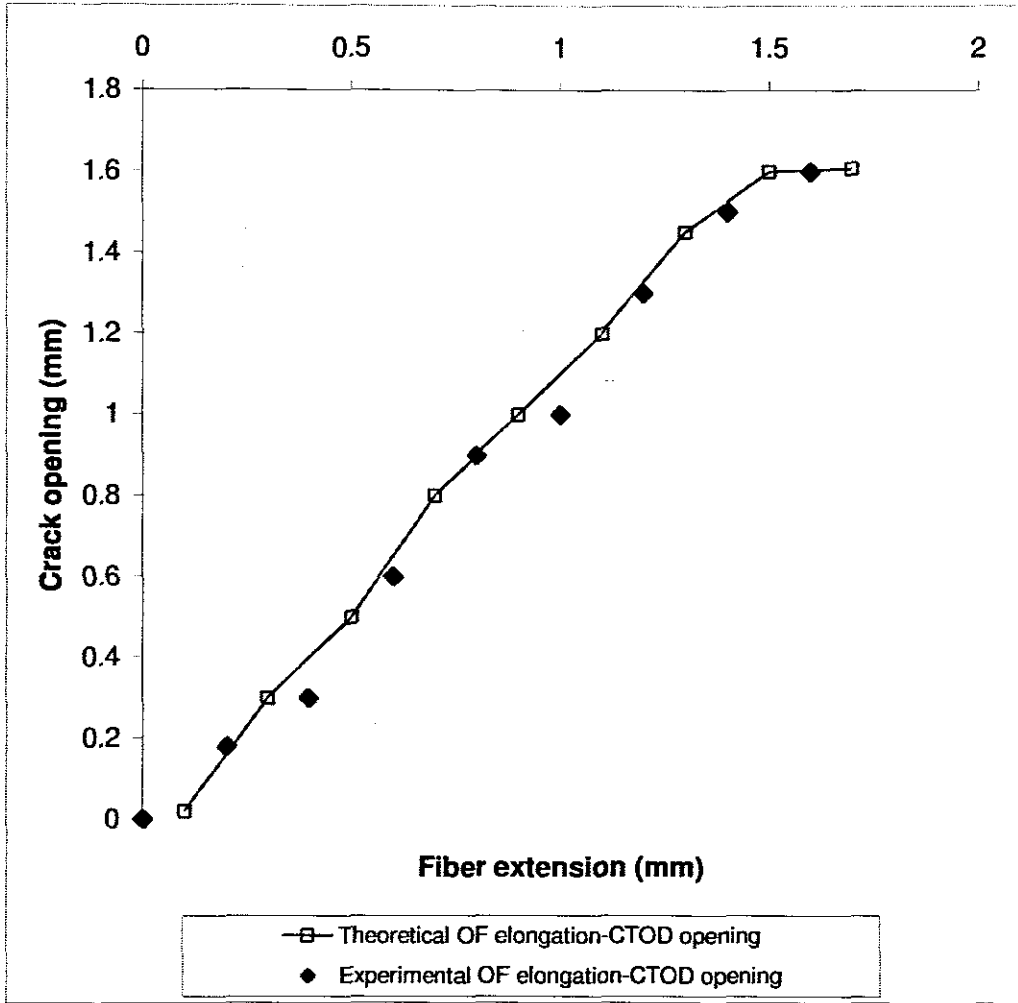


Figure 7.6: Theoretical-experimental comparison of OF elongation versus CTOD

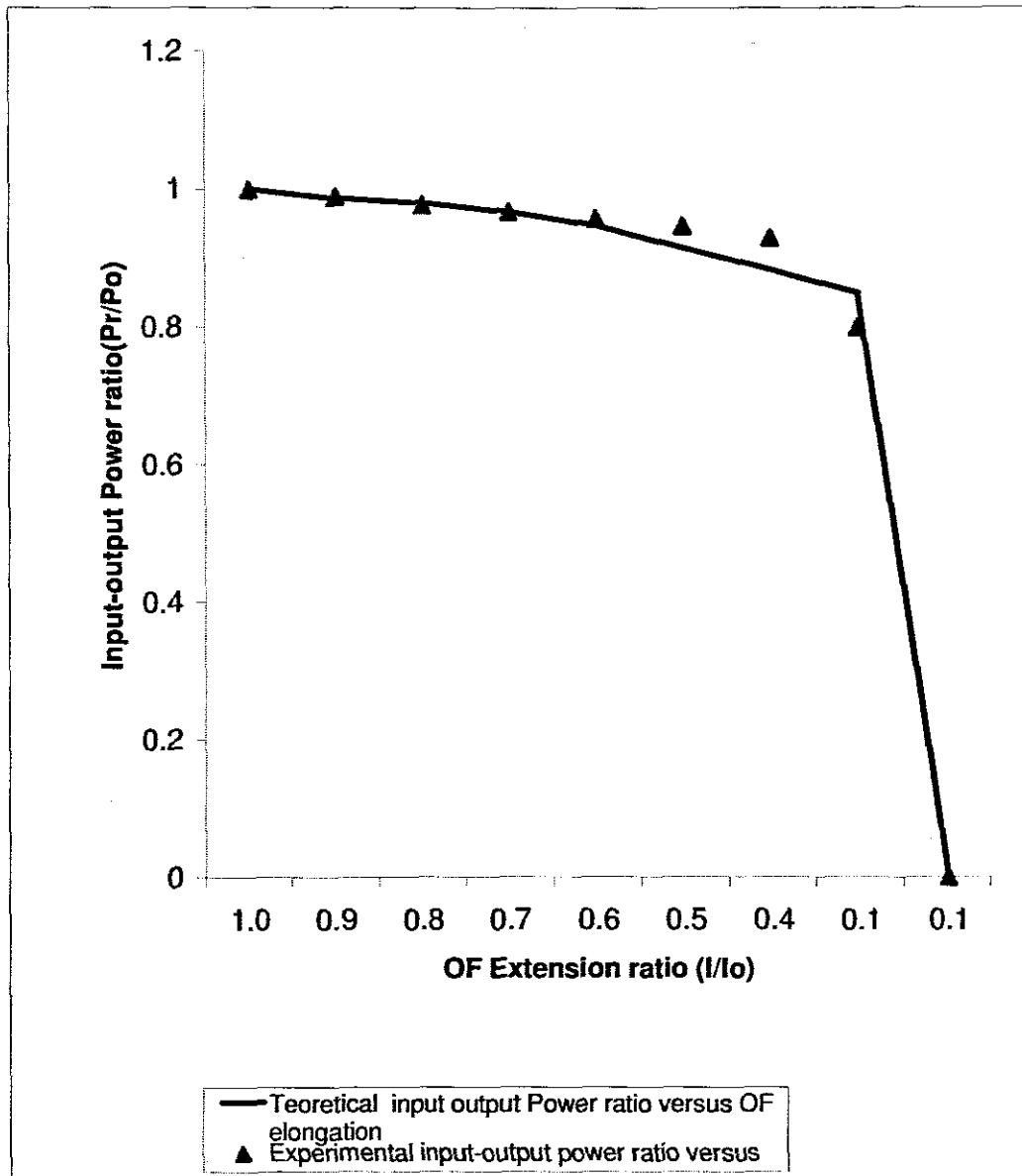


Figure 7.7: Comparison of theoretical and experimental results for the light intensity output, versus the optical fiber extension

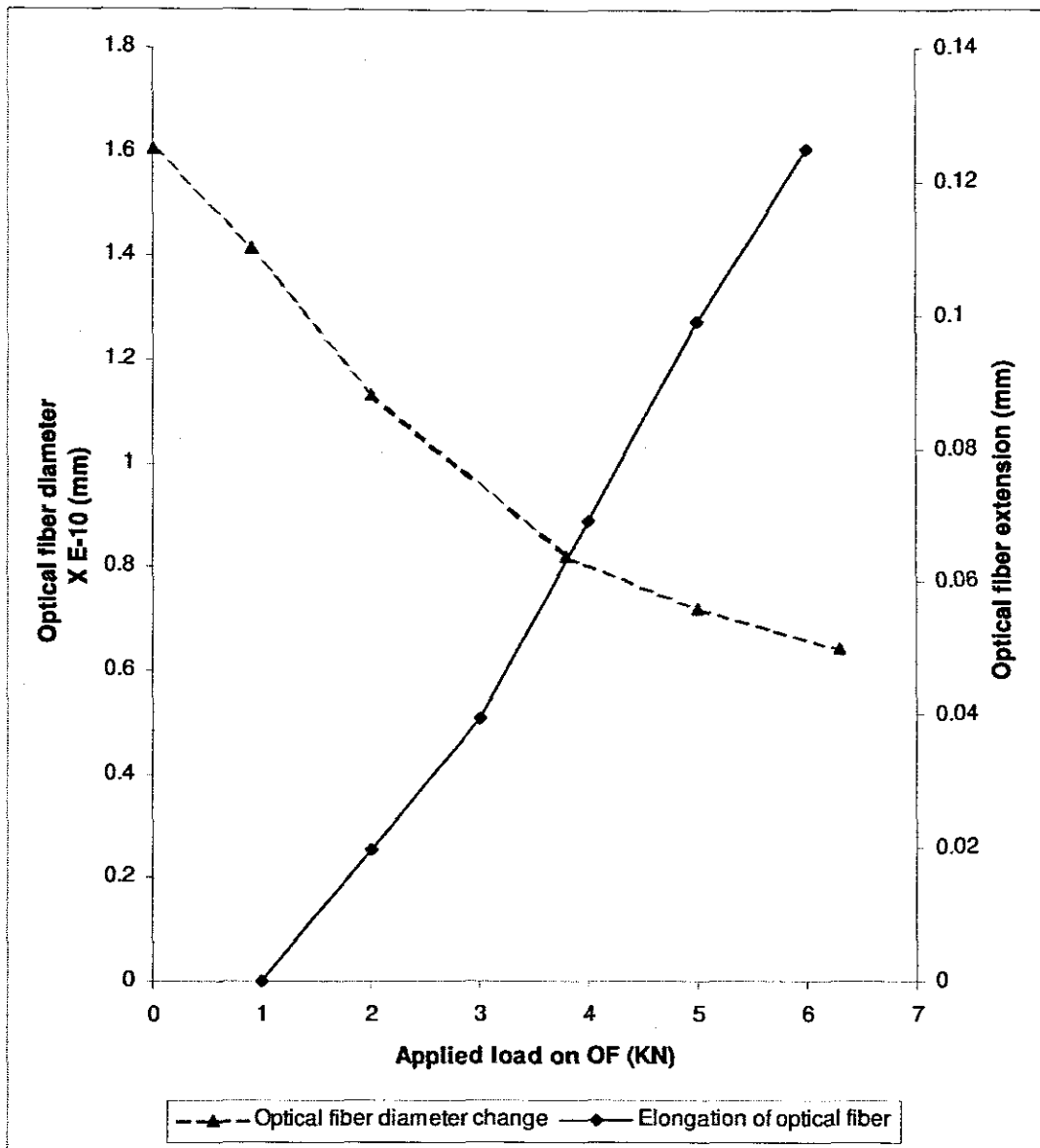


Figure 7.8: Optical fiber diameter change due to tensile loading and fiber elongation (as from equations (7.3)).

Chapter 8

8.0 The Performance of Fiber Optics as Displacement Sensors

8.1 Introduction

This chapter deals with the performance of commercially available Fiber optic sensor (FOS) employed as displacement transducers. They consist basically of a light source, normally a diode laser producing a single wavelength (monochromatic light), often in the visible range of $400 < \lambda < 700$ nm. The power supply, a fiber optical filament for the transmission of light and signal processing electronics from the diode laser to the test piece and return reflection, complete the assembly.

Manufacturers of such equipment often caution users of precautions to be taken with regard to rough texture surfaces affecting the reflection of rays of light from target surfaces and thus compromising the accuracy of these devices [49]. Similarly the manufacturers of such devices caution about mounting the sensor perpendicular to the target surface or about measurements on a moving surface, or the finish quality of a surface. The mentioned conditions contribute on the amount of reflectivity. In both cases of

surface texture and departure from normal angularity, manufacturers are apparently less specific about the effects of these parameters on the accuracy of the FOS devices [50]. Thus calibration procedures are required which often appear straight forward and operator friendly, however there are cases where considerable care and excessive precision requirements have been noted.

Our work here reports on the usage of a particular fiber optics displacement sensor with special emphasis on the procedures for calibration and the effects of variables that might affect FOS performance. For example the influence of the texture and reflectivity of the surface of the test piece; the effect of thickness of transparent material in front of the reflecting surface; the effect of angularity of the sensor with respect to the surface normal; and the combined effect of angularity induced from a surface displacement in an arc away or toward a stationary sensor [51].

8.2 Experiments

The schematic diagram in figure 8.1 depicts a typical experimental set-up for the measurement of proximity. In order to determine the affecting parameters for displacement measurement using FOS's, experiments were conducted using the basic components such as displacement sensor, displaying equipment (multimeter and oscilloscope), cantilever beam, an xyz micrometer stage for displacement control as well as reflective materials as targets for the sensor.

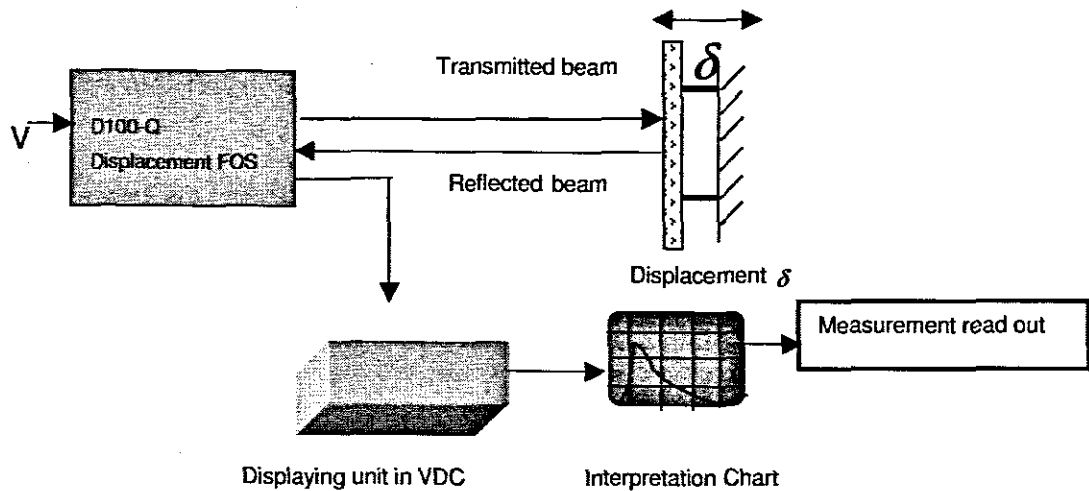


Figure 8.1. Schematic diagram for typical FOS displacement /proximity measurements

8.2.1 Calibration procedure

The sensor should be mounted perpendicular to the target surface and positioned flush against the surface. At worst, the output voltage of the sensor in this position should be close to zero or say less than 250 millivolts [49]. The sensor is then moved away from the target until maximum output voltage level is observed, of course still maintaining perpendicularity between the sensor and the test piece. At this position using the gain controls (coarse and fine) the output voltage must be adjusted to the level recommended by the manufacturer. Using this particular equipment the manufacturer recommended 5.0 volts, however this value is optional, as increased voltage facilitates greater sensitivity. Further movements of the sensor away from the target surface would result in reduced output voltage and thus data are obtained which enables one to construct the typical volts vs. displacement curve as shown in figure 8.2.

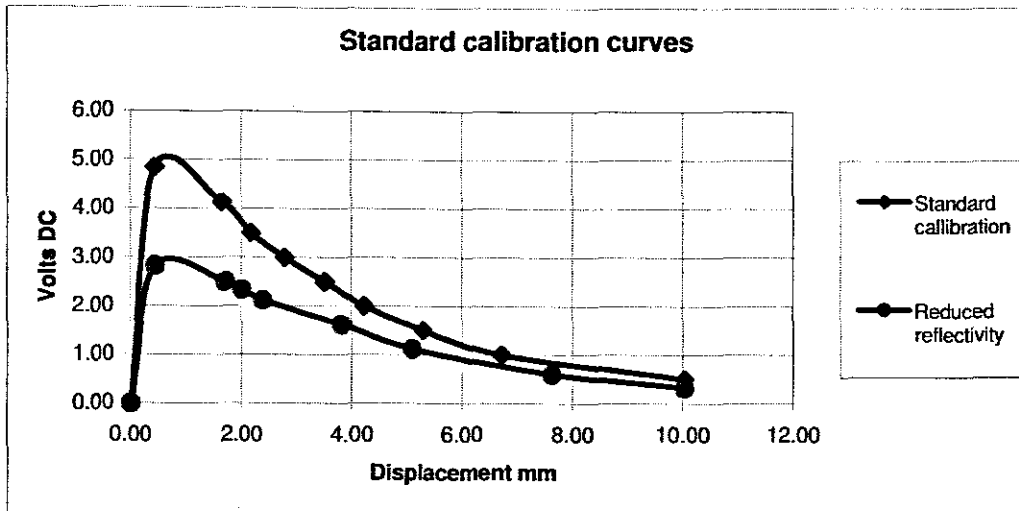


Figure 8.2. Typical calibration curves depending on surface reflectivity (top curve near perfect reflectivity, bottom as a result of reduced reflectivity).

8.2.2 Reflectivity

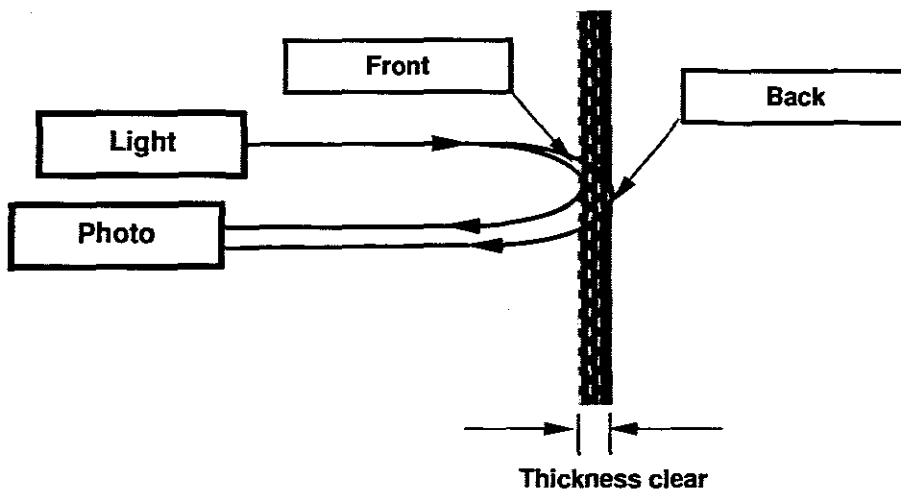
The voltage output from a fiber optical sensor is related to a) distance to a target surface and b) reflectivity of the target surface. If either the sensor or the target moves, in that a different area of the target falls under the sensor tip, or if the target surface changes say to a less reflective area, the effect will be to rescale the y-axis i.e. the voltage output of the sensor. As a result another curve will be obtained which is not equivalent to a fixed amount of voltage offset as shown in figure 8.2.

If there is a straight-line portion in the curves it is possible to apply the ratio of the voltages in the near and far side of the sensitivity and the conversion from voltage to distance or gap between sensor and target should account for the change proportionately. For example in figure 8.2 the sensitivity has decreased to 60% as a result of reduced reflectivity from the target, however it is advisable to resort to recalibration. There might be instances with poor reflective surfaces where it is impossible to obtain 5 volts output even with full gain on, in which case by attaching a small reflective target on the surface, such as polished metal, aluminium foil or a dab of reflective paint, the problem is solved.

8.2.3 The effect of thickness of transparent material

It was mentioned above that one way of overcoming the difficulty of obtaining reasonable peak voltage outputs from the surface under test, is to place on it a small reflecting target. For example by attaching on the surface, a small piece of glass mirror, the effect would be that the sensor's photo detector component would be subjected to two reflections returning from the front and the back surfaces of the target, [52] as shown in (repeated figure 1.1). This aspect was investigated using three different reflective targets comprising a front surfaced mirror, where of course the thickness of transparent material is zero, a 1.5 mm and a 3.0 mm thick ordinary glass mirrors. The fiber optical sensor was firmly mounted on an x-y-z axis micrometer stage perpendicularly above the target specimens as it is shown in figure 8.3.

The results of the calibration using the above-described reflective targets are shown in figure 8.4. Here it is noted that different gap magnitudes are indicated for the same voltage output from the sensor depending on the thickness of transparent material on the reflecting target. What is surprising is that the 1.5 mm thick glass mirror target repeatedly provided gaps or displacement less than those obtained from the front surfaced mirror!



(Repeated figure 1.1): Emitted and reflected signals using an ordinary mirror as target

It is suggested here that the front surface mirror was less than 100% reflective

and therefore a percentage of the light beam from the sensor tip was transmitted through and lost. As proof of this hypothesis a simple experiment was conducted. A laser beam was directed on to the front surfaced mirror get and when viewed from the back surface light could be detected thus proving transmittance through the target and therefore loss of intensity returning to the photodetector.

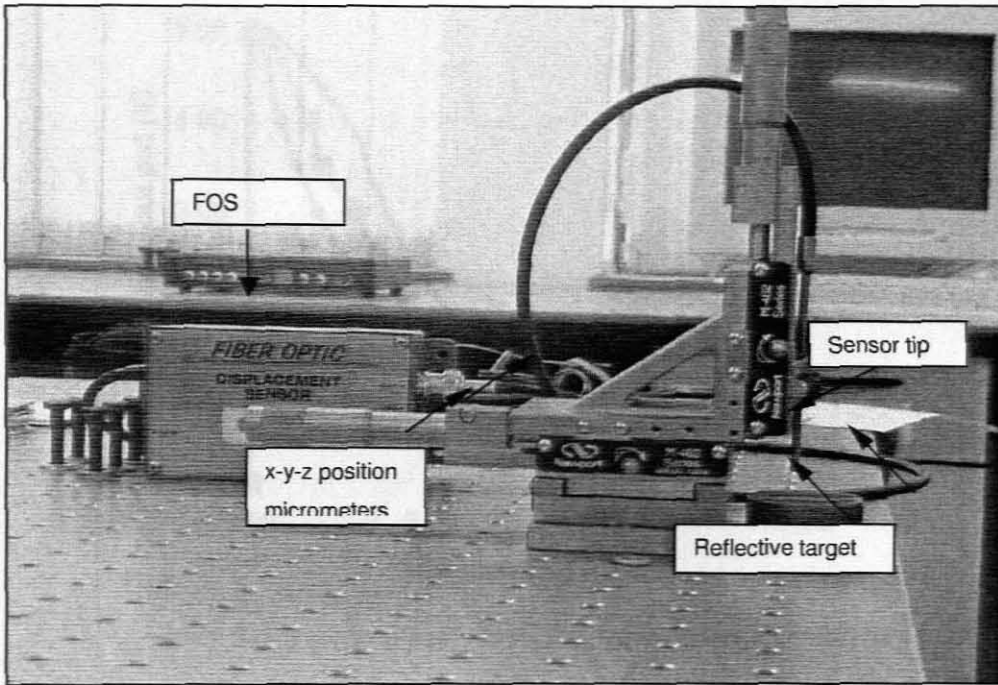


Figure 8.3: Effect of target plate misalignment on the reflective target

Figure 8.3: Experimental set-up with the FOS positioned above reflective targets

8.2.4 The effect of slight angular γ on a reflective target

There might be instances where the surface is moving away from a stationary sensor, such as by means of the use of a piezoelectric actuator. In such a case, the sensor tip would be deflected under load away from the sensor. It is assumed, however, that if the target is moving away from the sensor, there will be or should be an effect on the sensor's response such that the photo-detector part would not receive the full reflected light.

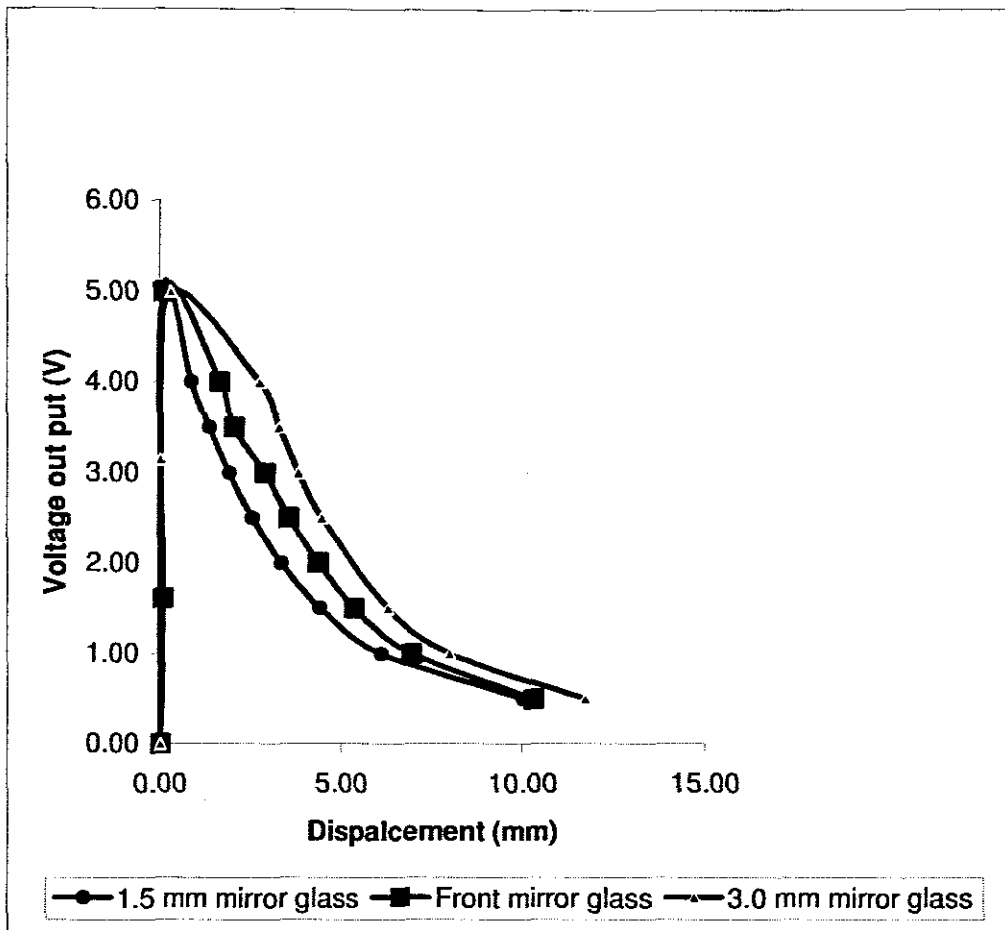


Figure 8.4: Effect of various glass mirror thicknesses and their reflective response

8.2.4 The effect of slight angularity on a moving target

There might be instances where the surface is moving away in an arc-path from a stationary sensor, such as for example the tip of a cantilever beam deflected under load away from the sensor. It is visualized that with such movement there will be or should be an effect on the sensor's voltage output in that the photo detector part would not receive the full reflection from the

reflective target's surface [53],[54]. This effect was investigated by an experiment where the tip of a cantilever beam with a target mounted on it, was depressed away using a micrometer, from an (initially perpendicular to it) optical fiber sensor.

The sensor was calibrated using the normal calibration procedure with its tip resting on the surface when the cantilever was horizontal or at zero position. By turning the micrometer against the cantilever surface the beam was forced away from the sensor in an arc path and hence it was possible to record the resulting gap versus voltage data. The results, which appear in figure 8.5, against expectations have not shown any detrimental effect on the sensor's performance. This can possibly be explained in that for the range of the experiment conducted, the induced angularity between the sensor tip and the reflective target surface was of insufficient magnitude to affect the fiber optic sensor's performance.

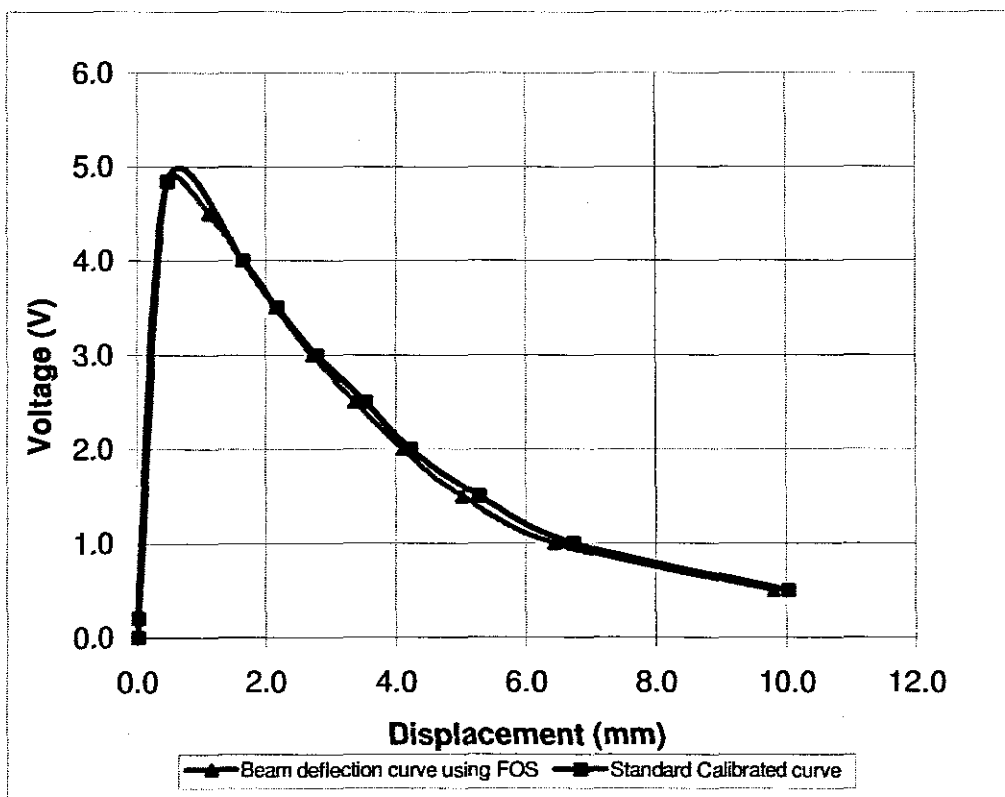


Figure 8.5: Cantilever beam deflection curve versus standard calibrated curve

8.2.5 The effect of angularity (target to sensor inclination)

The fiber optical sensor performance was investigated, by yet another experiment, attempting to show the effect of the reflective target surface being at an angle to the tip of the probe. The sensor was firmly attached to the micrometer stage in an inclined position of 0° , $\pm 2^\circ$, $\pm 10^\circ$ and $\pm 20^\circ$ respectively deviating from its perpendicularity. Going beyond the $\pm 20^\circ$ resulted in total loss of signal from the sensor. Calibration and data acquisition were performed in a similar manner as described previously and the results are shown in figure 8.6. The notable feature in this figure is the fact that the data for the 2.0 degree inclination coincided to that obtained from the normal or perpendicular orientation, while all other data indicated considerable sensor fall-off performance with increased angularity between sensor tip and reflective target surface. This experiment also served to explain the non-expected results from the cantilever experiment where obviously the surface of the cantilever did not deflect to more than 2.0 degrees away from perpendicularity to the sensor's tip.

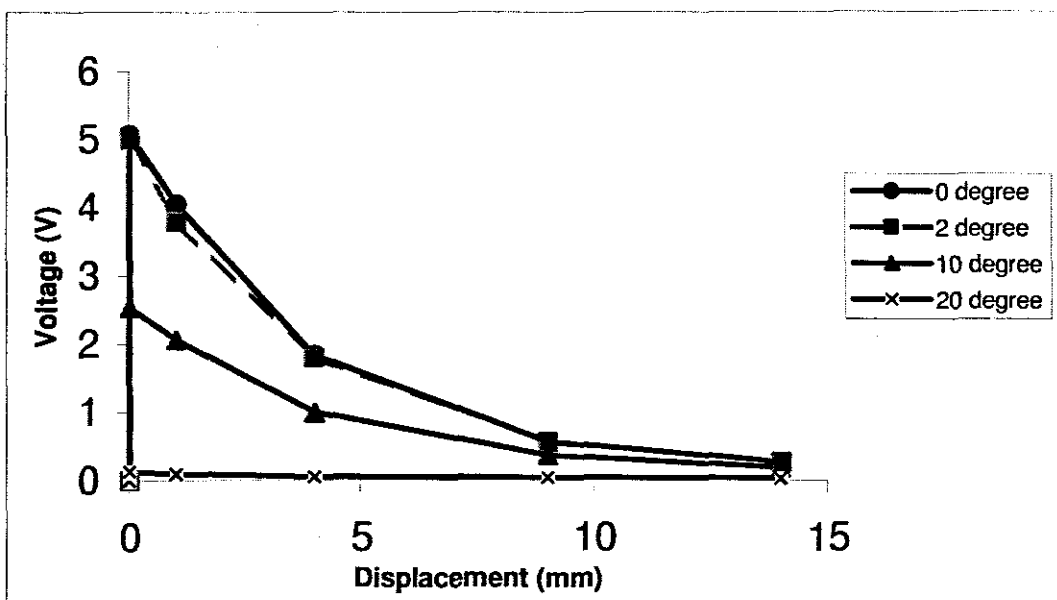


Figure 8.6: Results obtained with target inclination relative to the sensor's tip.

Chapter 9

9.0 Conclusions and Recommendation

9.1 Introductory comments.

This chapter summarizes the major findings in this work and presents concluding remarks and recommendations for future research on the subject.

The thesis presents a successful method of detecting a crack occurrence and the monitoring of the crack propagation by fiber optic sensors.

It is also presents information regarding the performance of FOS commercially available systems in their employment as displacement sensors.

From the theoretical point of view, we were able to establish and formulate an expression predicting the crack opening as well as the fiber optic elongation. From the physics of our system, crack opening is equal to measured fiber elongation; therefore the predicted results could be verified by experiment. With the aid of background of Linear Elastic Mechanics of Fracture (LEMF) we chose the sensor to resemble an individual fatigue test specimen, as the host for the optical fibers, in that we could be assured of the initiation and direction of propagation of a crack.

In order to build a sensor system to detect a crack occurrence and monitor its propagation, we employed optical fibers, which under elongation would transmit reduced light intensity. The inlet and outlet of the optical fibers require

proper connectors for the coupling to the light source and detectors. The process to manufacture the optical connectors was successfully conducted whereby quality fiber end connectors were achieved. The sensor system also required the equipment and instrumentation in order to produce the source of light (emitter) as well as a photo detector (receiver). This instrumentation was developed in our laboratory and proved adequate for our needs.

The experiments on stand-alone optical fibers regarding their mechanical and optical characteristics were carefully conducted, whereby the results were interpreted as important parameters to monitor, when the fibers were embedded into the host specimen.

The experimental part pertains the results of the major parameters that contribute to make a sensing system suitable for crack detection. The experimental results presented in the discussion part of chapter six, are adequately validated by comparison to the theoretical results.

It is to be noted that the adequate agreement between the theoretical and experimental results, assures us as being a good indicator of a viable crack detection system.

In fulfilling the obligation of this work, the following have been achieved.

- Able to associate the knowledge of the mechanics of deformation
- Able to use the theory behind the optical fiber and its mechanism of deformation
- Able to build up the instrumentation system that incorporates both the optical and mechanical sides of the experiment.
- Able to link all the system into an integrated component to form the fiber optic sensor for crack detection.
- Able to formulate a basic sensor equation that governs the conditions for designing the optical fiber sensor system.

9.1.1 Experimental outcomes

9.1.1.1 Fatigue test on a stand-alone host specimen

The aim for the fatigue test on a stand-alone host specimen was carried out in order to develop a crack using the ASTM standards. The crack type Model I was chosen to suit the experiment. According to the fatigue test results, the value of stress intensity factor K_{Ic} was $59.62 \text{ MPa}\sqrt{\text{m}}$, which satisfies the condition of the plane stress. The maximum fatigue loading was 15.2 kN just before the development of the crack. Subsequent to initiation of a crack the value of the load begins to decline as a result of crack propagation.

9.1.1.2 Experimental results on the embedded optical fiber in the host specimen

The knowledge and experience of the result of the test on the stand-alone optical fibers, assisted us greatly in incorporating three optical fibers into a host specimen. The light from the emitter passing through each of the optical fibers arriving at their respective photo detectors was affected by the fiber's elongation. This output measured as voltage drop showed a linearly decline from 2V to approximately 1.7V, before it dropped off to zero.

9.1.1.3 Experiments on the performance of the FOS as a displacement sensor.

We were able to show that parameters such as orientation between sensor tip and target surface i.e. angularity, the effect of varying reflectivity of targets' surfaces, the effect of various transparent material thickness over the target reflective surface and the displacement of a surface in an arc-path away from the stationary tip of a sensor. have an effect on the sensor's performance. It is hoped that the information in his work will be useful guidelines or criteria to experimenters attempting measurements of displacement, motion or speed.

9.2 Theoretical approach

Using the theoretical background discussed in chapter 2 for the crack development mechanism and optical fiber deformation, we were able to set the groundwork in formulating the sensor equation. Both, deformation of the host specimen and the embedded optical fiber gave us relationships for the light intensity through the fiber, with respect to the mechanical deformation parameters such as crack opening, fiber elongation, crack open to crack travel, and change of the optical fiber diameter.

9.3 Recommendation

It must be noted that this work has been conducted under laboratory conditions, which limits us as yet to consider real / industrial site applications. Although we were able to establish a system that is able to detect the crack occurrence, under mode I, further work must be done in order to establish crack propagation under modes II and III. Multi-directional crack propagation may also be considered in future investigations whereby an array of optical fibers is laid within a host structure.

In this work we were limited in fixing the optical fiber on the external surface of the host specimen.

It is suggested that true embedment of the optical fiber within the host specimen, be attempted, preferably with composite materials which are more compatible to host the optical fibers.

References:

- [1] Ghandi M.V and Thompson B.S (1992), "Smart Material and Structure"
Published by Chapman and Hall-London Chapter 7 pp 2,220
- [2] W.B Spillman Jr; J.S Sirkis and PT Gardiner, "Smart materials and Structures: What are they?" *Journals of Smart Materials and Structures Vol.5 pp. 247*
- [3] Xiao Chun Li, Fritz Prinz and John Seim, "Thermal behaviour of metal embedded fiber Bragg grating sensor", *Journals of Smart Materials and Structures (2000) Vol.10 pp. 575*
- [4] Udd E. Fiber Optic Smart Structures Blue Road Research (1994),
Chapter 4 pp61-103
- [5] B.S Jeon et el, "Low velocity impact and delaminating behaviour of composite laminated with fiber optic sensor", *Journals of Smart Materials and Structures (1998) vol. 8*
- [6] Rodney Allan and Gerard Franklyn, "An intensity –based optical fiber sensor for fatigue damage detection in advanced fiber-reinforced composites" *Journals of Smart Materials and Structures (1995) vol. 4 pp.223-229*

- [7] J.Gryzagoridis, "Safe-live Vs Damage tolerance" *1st National Non-Destructive Testing (NDT) Symposium (Pretoria) 2004.*
- [8] Z.L Yang, G R Liu and K Y Lam "An inverse procedure for crack detection using integral strain measured by optical fibers". (No 01 pp72). *Journals of Smart Materials and Structures (2002) vol. 11 pp.72-78*
- [9] Y.C Liang and C Hwu, "On line identification of holes/cracks in composite structures" *Journals of Smart Materials and Structures (2001) vol. 10 pp.599-609*
- [10] D. Rees, W. Chiu and R. Jones, "Numerical study of crack monitoring in patched structures, using piezoelectric sensors". *Journals of Smart Materials and Structures (1992) vol. 1 pp.202-205*
- [11] Yoji Okabe, Shigeki Yashiro, Tatsuro Kosaka, and Nabuo Takeda "Detection of transverse cracks in CFRP composites using embedded fiber Bragg grating sensors", *Journal of Smart Structure (2002) .*
- [12] H.K Kang et el "Development of fiber optic ingress/engress method for smart structure" *Journal of Smart Structures (1999) Vol. 9 pp 149-157*
- [13] Divyang R Shukla, Anthony J. Vizzini, Interlacing for improved performance of laminates with embedded devices. " *Journal of Smart Structure (1995) Vol. 5 pp 225-229.*
- [14] Udd E. Fiber Optic Smart Structures Blue Road Research (1994), Chapter 4 pp 61
- [15] David A. Krohn, Fiber Optic Sensors- Fundamental and Application, Second adition.(1992) pp 145-148
- [16] David A. Krohn, Fiber Optic Sensors- Fundamental and Application,

Second edition. (1992) pp 257

- [17] Armazov. B, "Composite Fiber Materials" *Material Science*, pp 284-292
- [18] Kin-tak Lau, Libo Yuan and Li-min Zhou, "Thermal effects on embedded grating sensor in an FRP structure" *Journal of Smart Structure* (2001) Vol. 10 pp 705-712.
- [19] A.K Green, M. Zaidman, E.Shafif et el, "Infrastructure development for incorporating fiber-optic sensors in composite materials, *Journal of Smart Structure* (2001) Vol. 9 pp 321.
- [20] William F. Smith. "Light refraction" *Materials Science and Engineering* (1990) pp....
- [21] David A. Krohn, *Fiber Optic Sensors- Fundamental and Application*, Second edition.(1992) pp 1-5
- [22] David A. Krohn, "Phase Modulated Sensors", *Fiber Optic Sensors- Fundamental and Application*, Second edition, (1992) pp 49
- [23] Ghandi M.V and Thompson B.S, "Fiber Optic Sensors" *Smart Materials and Structures Chap 2*, pp 220
- [24] E.E Gdoutos "Fracture Mechanics An Introduction." *Chapter 1* pp 7.
- [25] T.L Anderson "Fracture Mechanics. Fundamentals and Applications Second Edition, *Chapter 2* pp 72.
- [26] E Gdoutos, "Fracture Mechanics An Introduction." *Chapter 4* pp 81
- [27] Westergaad, H.M., "Bearing pressure and cracks". *Journal of Applied Mechanics*, Vol 6, 1939, pp 49-53.

- [28] Irwin, G.R., "Analysis of Stresses and Strains near the end of a crack traversing a plate". *Journal of Applied Mechanics*, Vol. 24, 1957, pp 361-364.
- [29] Sneddon, I.N., "The distribution of Stress in the neighbourhood of a crack in an elastic Solid." *Proceeding, Royal society of London*, Vol A-187, 1946, pp 229-260
- [30] William, M.L., "On the Stress distribution at the Base of Stationary Crack". *Journal of Applied Mechanics*, Vol 24, 1957, pp 109-114.
- [31] T.L Anderson "Fracture Mechanics. Fundamentals and Applications Second Edition, Chapter 2, pp52.
- [32] T.L Anderson "Fracture Mechanics. Fundamentals and Applications Second Edition, Chapter 2 pp 41
- [33] T.L Anderson "Fracture Mechanics. Fundamentals and Applications Second Edition, Chapter 2 pp 82-83.
- [34] E.E Gdoutos "Fracture Mechanics An Introduction." Chapter 1 pp 16.
- [35] T.L Anderson "Fracture Mechanics. Fundamentals and Applications Second Edition, Chapter 2 pp 54.
- [36] E.E Gdoutos "Fracture Mechanics an Introduction." Chapter 2 pp 24.
- [37] American Society for Testing and Materials (ASTM) Standards (1997), *Plane-Strain Fracture Toughness of Metallic Materials, Series E-399-90*.
- [38] American Society for Testing and Materials (ASTM) Standards (1997), *Plane-Strain Fracture Toughness of Metallic Materials, Series E-1820*.

- [39] E.E Gdoutos "Fracture Mechanics an Introduction." *Chapter 2 pp 123-127.*
- [40] E.E Gdoutos "Fracture Mechanics an Introduction." *Chapter 5 pp 117-119.*
- [41] David A. Krohn, *Fiber Optic Sensors- Fundamental and Application, Second adition.(1992) pp 127*
- [42] David A. Krohn, *Fiber Optic Sensors- Fundamental and Application, Second adition. (1992) pp 13*
- [43] David A. Krohn, *Fiber Optic Sensors- Fundamental and Application, Second adition. (1992) pp 19*
- [44] ThorLabs Inc, *Guide to Connectorization and Polishing Optical Fiber (1997)*
- [45] Takeda Nobuo; Kosaka Tatsuro; Ichiyama Takayuki, *Detection of transverse cracks by embedded plastic optical fiber in FRP laminates; Proc. SPIE Vol.3670, p. 248-255, Smart Structures and Materials 1999:*
- [46] A.V. Srivinasan, Michael Mc Farland, *Smart Structures Analysis and Design Book, pp 151, Published by Cambridge University Press pp 151-152.*
- [47] Thomas P. Pearsall, *Photonics Essentials an Introduction with experiments, Published by Mc Graw-Hill Professional Engineering.*
- [48] Peter K.Cheo "Fiber Optics Devices and Systems Prentice Hall Series in Solid State PHYSICAL Electrons Nick Nonyak Jr Series pp 103
- [49] *Fiber Optic displacement sensors " Manual of Instruction" Type D-100*

reflectance Dependant, supplied by the Phitech, Inc.

- [50] David A. Krohn (1992), "Fiber optic sensor –Fundamental and application second edition", pp.89-107.
- [51] Eric Udd (1995), "Fiber optic smart structure" Chapter 12 pp. 319, 571.
- [52] Kathryn Booth and Steven Hill (1998) "Essence of Opto-electronics, chapter 10 pp 251.
- [53] Virkam Bhatia, Kent A.Murphy et al, "Recent development in optical fiber based extrinsic Fabry-Perot Interferometric strain sensing technology", Journal of Smart Materials and Structure (Dec 1995) Vol. 4 pp240; 246.
- [54] C.F Than and KC Tee, et al", "Optical measurement of slope, thickness and velocity in liquid film flow." Journal of Smart Materials and Structure (Mar 1993), Vol. 2 pp.13.

Figure A.1: Si-PLAN window for the fatigue test control

Appendix A

Crack Propagation using Fatigue Test as discussed in chapters 2 and 5

Si-Plan windows

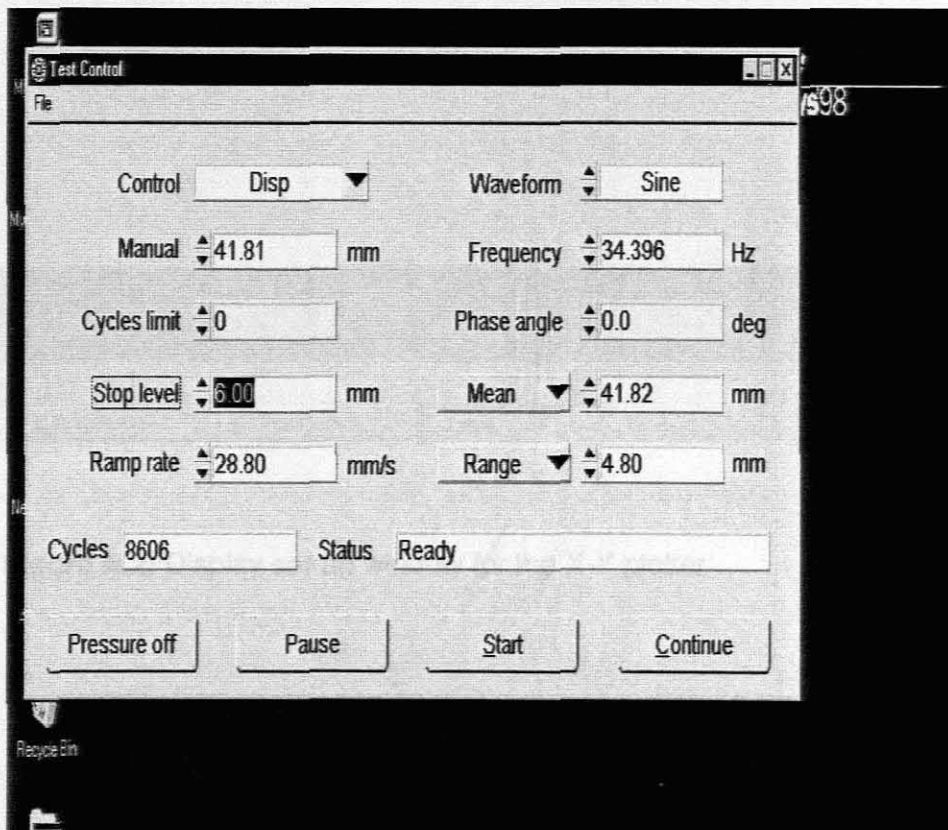


Figure A.1: SI PLAN window for the fatigue test control

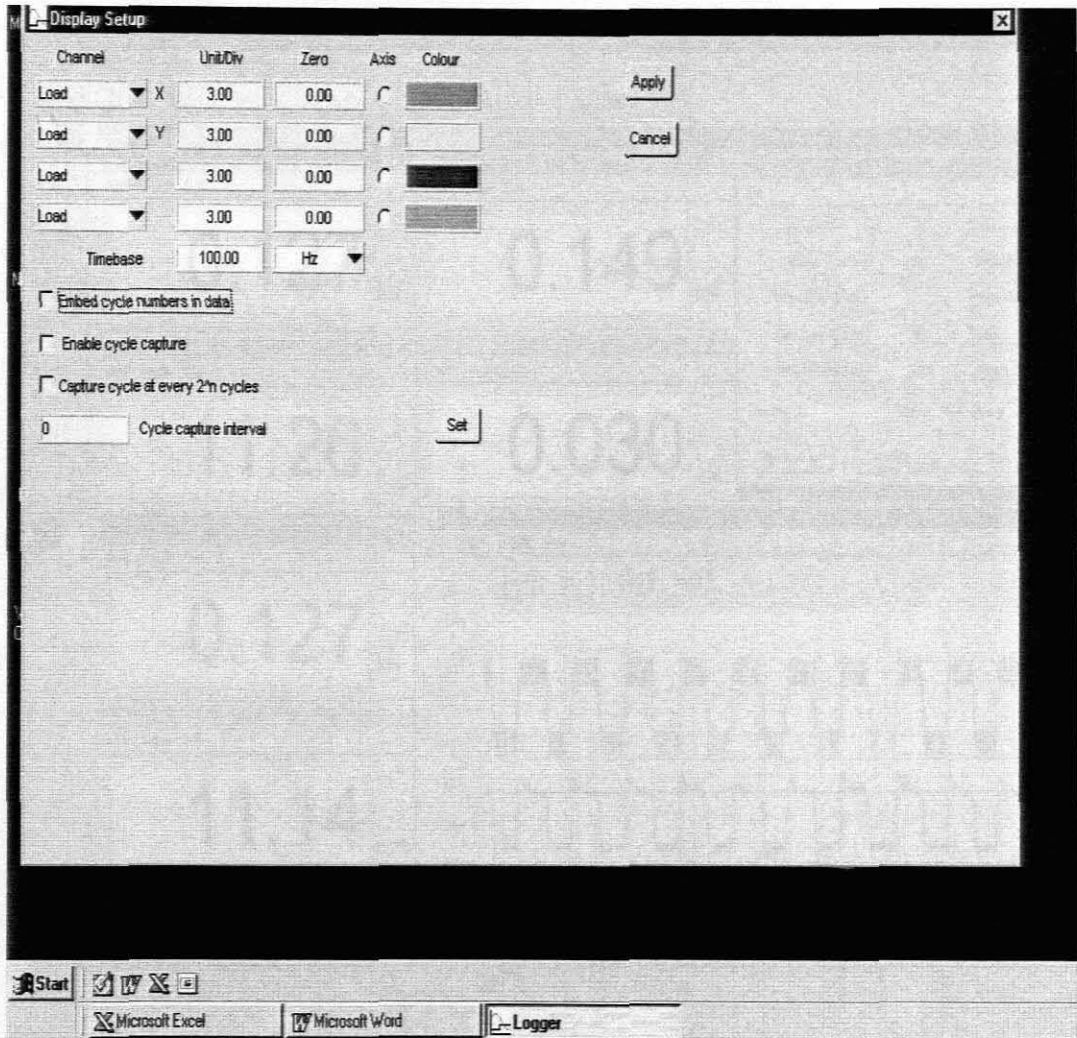


Figure A.3: Digital panel meter (DPM) with Data Logger windows

Figure A.2: Display set-up window for the X-Y plotter

Some results from fatigue test by SI Plan

SI Plan Data Logger

Date: 7/3/2007

Time: 11:47:02

Interval: 0.005

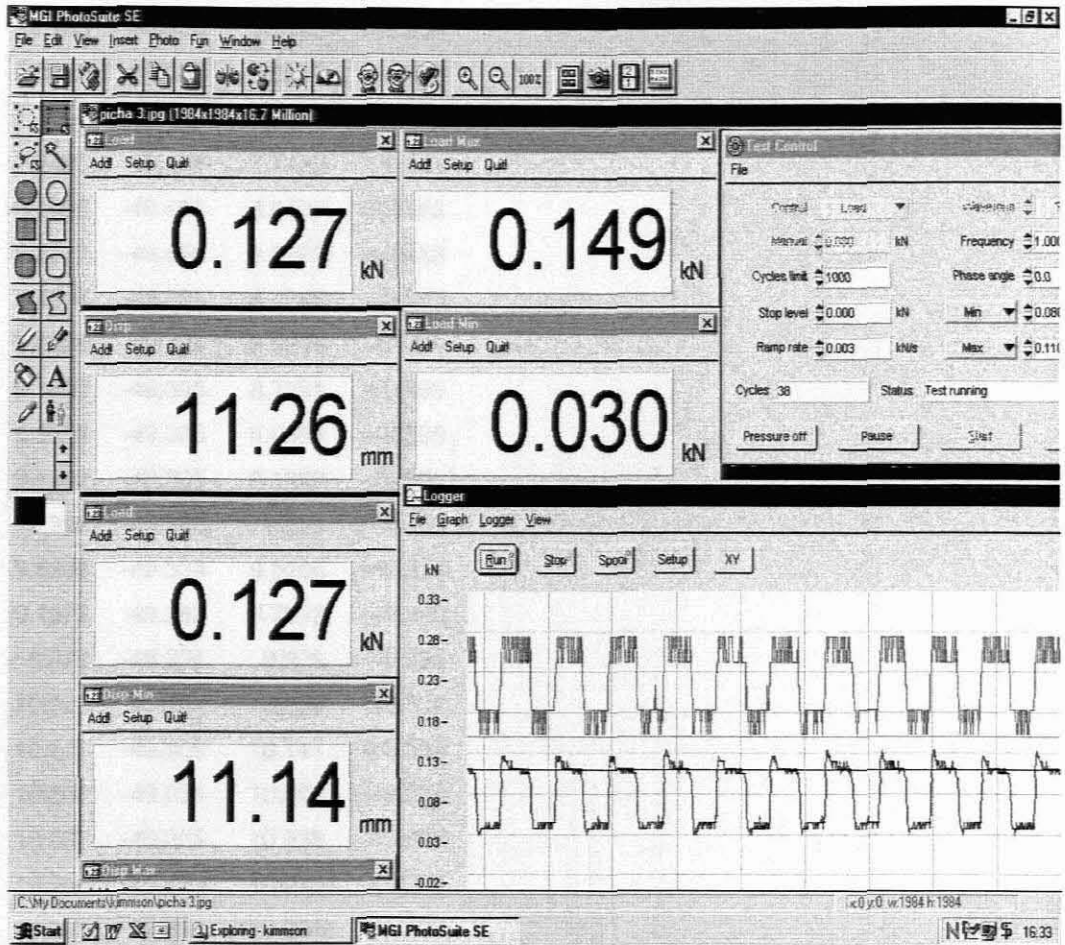


Figure A.3: Digital panel meter (DPM_s) with Data Logger windows

Some results from fatigue test by Si Plan

'Si-Plan Data Logger'

'Date' '7/5/2003'

'Time' '11:45:22'

'Interval' 0.005

'Channels'		4	
'kN'	'mm'	'kN'	'mm'
'Load'	'Disp'	'Load'	'Disp'
10.178	-49.305	10.178	-49.305
10.148	-49.276	10.148	-49.276
10.103	-49.305	10.103	-49.305
9.9985	-49.305	9.9985	-49.305
7.4057	-49.453	7.4057	-49.453
7.7495	-49.484	7.7495	-49.484
8.0406	-49.453	8.0406	-49.453
8.2727	-49.453	8.2727	-49.453
8.4595	-49.395	8.4595	-49.395
8.6238	-49.424	8.6238	-49.424
8.7881	-49.395	8.7881	-49.395
8.9598	-49.395	8.9598	-49.395
9.1393	-49.395	9.1393	-49.395
9.326	-49.363	9.326	-49.363
9.5206	-49.334	9.5206	-49.334
9.7073	-49.363	9.7073	-49.363
9.879	-49.334	9.879	-49.334
10.029	-49.334	10.029	-49.334
10.141	-49.305	10.141	-49.305
10.208	-49.334	10.208	-49.334
10.238	-49.305	10.238	-49.305
10.245	-49.305	10.245	-49.305
10.231	-49.305	10.231	-49.305
10.215	-49.305	10.215	-49.305
10.193	-49.276	10.193	-49.276
10.171	-49.305	10.171	-49.305
10.148	-49.305	10.148	-49.305
10.103	-49.305	10.103	-49.305
10.006	-49.305	10.006	-49.305
9.7668	-49.305	9.7668	-49.305
9.5128	-49.276	9.5128	-49.276
9.2514	-49.305	9.2514	-49.305
9.0047	-49.305	9.0047	-49.305
8.8257	-49.334	8.8257	-49.334
8.6911	-49.334	8.6911	-49.334

8.5565	-49.334	8.5565	-49.334
8.3995	-49.363	8.3995	-49.363
8.1903	-49.363	8.1903	-49.363
7.8841	-49.395	7.8841	-49.395
7.5179	-49.363	7.5179	-49.363
7.1292	-49.395	7.1292	-49.395
6.7479	-49.395	6.7479	-49.395
6.4192	-49.395	6.4192	-49.395
6.1427	-49.424	6.1427	-49.424
5.896	-49.453	5.896	-49.453
5.6721	-49.424	5.6721	-49.424
5.4254	-49.453	5.4254	-49.453
5.1265	-49.453	5.1265	-49.453
4.7827	-49.484	4.7827	-49.484
4.3941	-49.514	4.3941	-49.514
4.0132	-49.543	4.0132	-49.543
3.647	-49.514	3.647	-49.514
3.3032	-49.543	3.3032	-49.543
3.019	-49.572	3.019	-49.572
2.78	-49.572	2.78	-49.572
2.5708	-49.603	2.5708	-49.603
2.3543	-49.633	2.3543	-49.633
2.1222	-49.633	2.1222	-49.633
1.8759	-49.662	1.8759	-49.662
1.6141	-49.662	1.6141	-49.662
1.3454	-49.662	1.3454	-49.662
1.0835	-49.691	1.0835	-49.691
0.8519	-49.691	0.8519	-49.691
0.67291	-49.691	0.67291	-49.691
0.53833	-49.781	0.53833	-49.781
0.4335	-49.752	0.4335	-49.752
0.35156	-49.752	0.35156	-49.752
0.2916	-49.781	0.2916	-49.781
0.2243	-49.781	0.2243	-49.781
0.17212	-49.781	0.17212	-49.781
0.13458	-49.81	0.13458	-49.81
0.11215	-49.81	0.11215	-49.81
0.10483	-49.841	0.10483	-49.841

0.10483	-49.841	0.10483	-49.841
0.08972	-49.841	0.08972	-49.841
0.10483	-49.871	0.10483	-49.871
0.10483	-49.841	0.10483	-49.841
0.10483	-49.841	0.10483	-49.841
0.0975	-49.871	0.0975	-49.871
0.10483	-49.871	0.10483	-49.871
0.23163	-49.871	0.23163	-49.871
0.47836	-49.841	0.47836	-49.841
0.9494	-49.81	0.9494	-49.81
1.4497	-49.781	1.4497	-49.781
1.8681	-49.752	1.8681	-49.752
2.1671	-49.781	2.1671	-49.781
2.3016	-49.722	2.3016	-49.722
2.3016	-49.722	2.3016	-49.722
2.3016	-49.691	2.3016	-49.691
2.3392	-49.691	2.3392	-49.691
2.623	-49.691	2.623	-49.691
3.0267	-49.662	3.0267	-49.662
3.5349	-49.662	3.5349	-49.662
4.08	-49.662	4.08	-49.662
4.5438	-49.633	4.5438	-49.633
4.9095	-49.633	4.9095	-49.633
5.1714	-49.572	5.1714	-49.572
5.3357	-49.572	5.3357	-49.572
5.4552	-49.572	5.4552	-49.572
5.6195	-49.543	5.6195	-49.543
5.8813	-49.543	5.8813	-49.543
6.2173	-49.514	6.2173	-49.514
6.5987	-49.484	6.5987	-49.484
7.0097	-49.484	7.0097	-49.484
7.4057	-49.453	7.4057	-49.453
7.7417	-49.484	7.7417	-49.484
8.0333	-49.453	8.0333	-49.453
8.2649	-49.453	8.2649	-49.453
8.4595	-49.424	8.4595	-49.424
8.6238	-49.424	8.6238	-49.424
8.7881	-49.395	8.7881	-49.395

8.9676	-49.363	8.9676	-49.363
9.1466	-49.395	9.1466	-49.395
9.326	-49.363	9.326	-49.363
9.5206	-49.334	9.5206	-49.334
9.6996	-49.363	9.6996	-49.363
9.879	-49.363	9.879	-49.363
10.029	-49.334	10.029	-49.334
10.141	-49.334	10.141	-49.334
10.208	-49.334	10.208	-49.334
10.238	-49.305	10.238	-49.305
10.238	-49.305	10.238	-49.305
10.231	-49.305	10.231	-49.305
10.223	-49.305	10.223	-49.305
10.2	-49.305	10.2	-49.305
10.178	-49.305	10.178	-49.305
10.148	-49.305	10.148	-49.305
10.103	-49.305	10.103	-49.305
10.006	-49.305	10.006	-49.305
9.7746	-49.305	9.7746	-49.305
9.5128	-49.276	9.5128	-49.276
9.2441	-49.305	9.2441	-49.305
9.0125	-49.334	9.0125	-49.334
8.833	-49.334	8.833	-49.334
8.6911	-49.363	8.6911	-49.363
8.5638	-49.334	8.5638	-49.334
8.4146	-49.363	8.4146	-49.363
8.183	-49.363	8.183	-49.363
7.8763	-49.395	7.8763	-49.395
7.5252	-49.363	7.5252	-49.363
7.1292	-49.363	7.1292	-49.363
6.7479	-49.424	6.7479	-49.424
6.4265	-49.395	6.4265	-49.395

Appendix B

List of Auxiliary Apparatus, and Tools employed for the Sensor Making as discussed in chapters 3 and 4


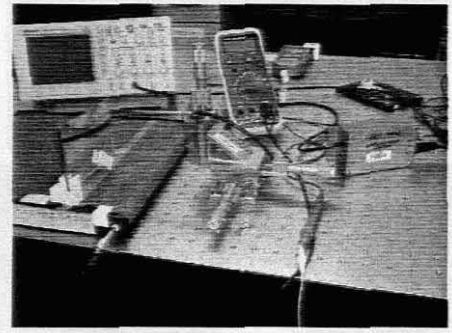
Fig No	Photo	Equipment /Item	Use	Manufacturer
1		Fusion device	Splicing and terminating of OF	Compact Inc
2		Oscilloscope ¹ and multimeter ²	Measuring the voltage signal output	Tetronix ¹ Fluke ²

Figure A.4: Experimental setup for the proposed sensor


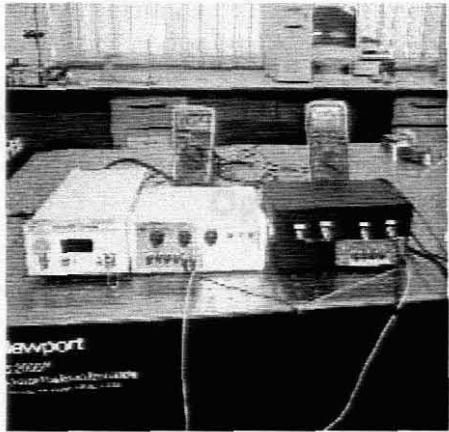
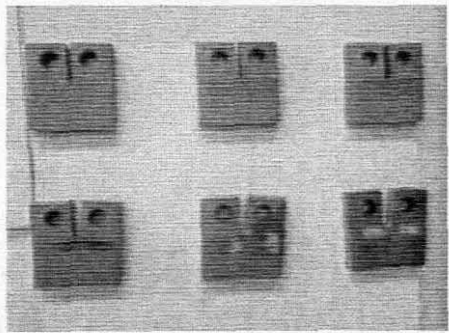
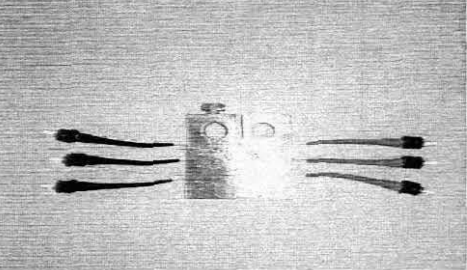
3		Universal tensile machine	Testing of the optical fiber tensile strength	
4		Light source; Photo-detector apparatus	Light emitting, Optical light conversion into voltage read out	Thorlabs Inc. CPUT
5		Samples from fatigue test with before optical fibers embedded	Specimen Preparation before embedding optical fibers	CRATECH LAB CPUT
		Host test specimen with embedded optical fibers	Determination of of the crack propagation versus light out put intensity in volts	CRATECH LAB CPUT

Figure A.4: Experimental setup for the product manufacturing and testing

Appendix C

Opto-electrical circuitry

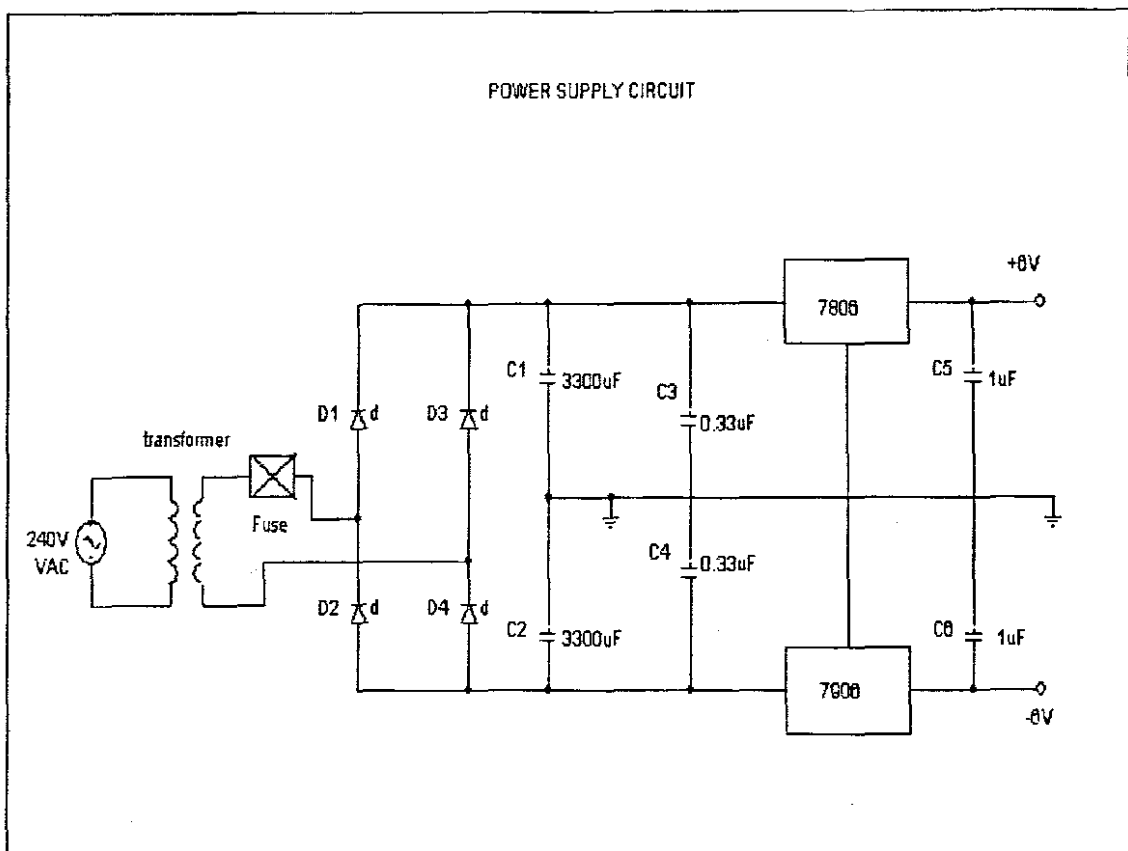


Figure A.5: Power supply circuit

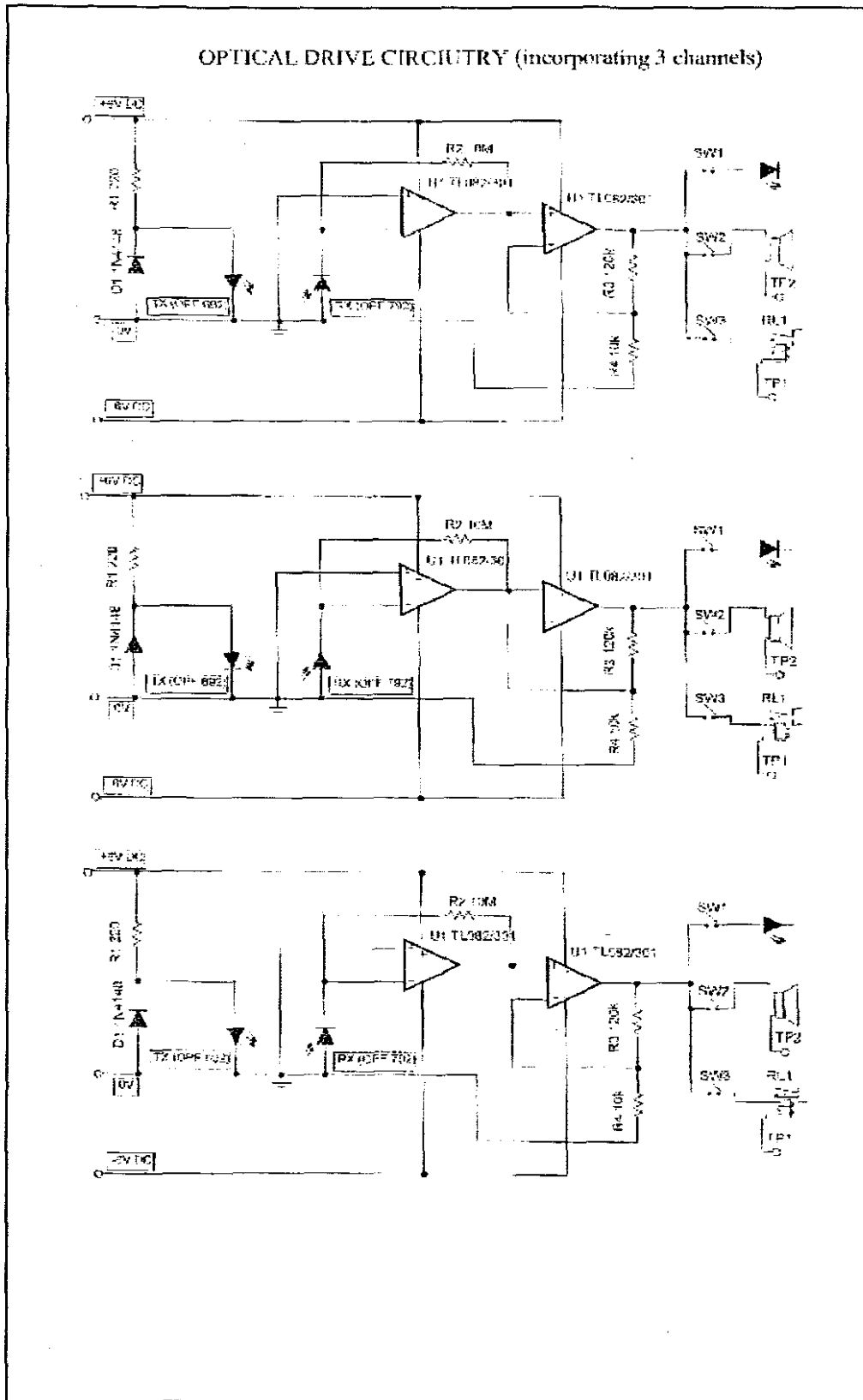


Figure A.6: Optical drive circuit

